AUBURN UNIVERSITY

SCHOOL OF ENGINEERING
Department of Mechanical Engineering
Thermoscience Group

REPORT X
(Final Report)

SATURATED SYSTEM BEHAVIOR—SURFACE BOILING AND CONTROLLED BLOWDOWN

G. H. Nix and R. I. Vachon

Under Contract NAS8-11234 With
NATIONAL AERONAUTICS AND SPACE ADMINISTRATION
George C. Marshall Space Flight Center

Administered Through
Engineering Experiment Station
Auburn, Alabama 36830

March 1969

CR 102345

AUBURN UNIVERSITY

SCHOOL OF ENGINEERING
Department of Mechanical Engineering
Thermoscience Group

REPORT X
(Final Report)

SATURATED SYSTEM BEHAVIOR—SURFACE BOILING AND CONTROLLED BLOWDOWN

G. H. Nix and R. I. Vachon

Under Contract NAS8-11234 With
NATIONAL AERONAUTICS AND SPACE ADMINISTRATION
George C. Marshall Space Flight Center

Administered Through
Engineering Experiment Station
Auburn, Alabama 36830

March 1969

CONTRACT SUMMARY

The following information briefly summarizes the activities connected with Contract NAS8-11234 between Auburn University and George C. Marshall Space Flight Center.

1. Contract History

4/25/64 to 4/24/65	Funded First Year
4/25/65 to 4/24/66	Funded Second Year
4/25/66 to 5/25/66	No Cost Extension
5/26/66 to 8/31/66	Funded Extension
9/01/66 to 10/20/66	No Cost Extension
10/20/66 to 8/31/67	Funded Extension
9/01/67 to 12/03/68	No Cost Extension

2. Total Expended to Date — $100,381.00

3. Contract Personnel

D. M. Vestal, Jr.	7/64 to 8/31/66
G. E. Tanger	4/64 to 9/15/66
R. I. Vachon	4/64 to 6/15/64
	9/64 to 6/15/65
	9/65 to 6/15/66
G. H. Nix	4/64 to 8/31/64
	6/65 to 9/15/65
	6/66 to 9/15/66
	12/66 to 8/31/67
J. H. Lytle	4/64 to 9/15/64
R. B. Pollard	4/64 to 6/30/65
B. J. Fluker	6/64 to 9/15/65
J. D. Hornsby	11/65 to 8/31/66

4. Progress Reports

Tanger, G. E., Nix, G. H., and Davis, D. L. *Preliminary Investigation of Surface Roughness Influence on Multiphase Heat Transfer* (Report I), September 1964.

Vachon, R. I., Tanger, G. E., Pollard, R. B., and Davis, D. L. *Preliminary Investigation of Pressure Influence on Multiphase Heat Transfer* (Report II), November 1964.

Tanger, G. E., Vachon, R. I., Pollard, R. B., and Nix, G. H. *Pressure Influence on Multiphase Heat Transfer from Stainless Steel Surfaces* (Report III), July 1965.

Vachon, R. I., Tanger, G. E., Nix, G. H., and Davis, D. L. *Pool Boiling of Water from Mechanically Polished and Chemically Etched Stainless Steel Surfaces* (Report IV), December 1965.

Vachon, R. I., Tanger, G. E., Nix, G. H., and Cobb, R. O. *Pool Boiling Heat Transfer from Teflon Coated Stainless Steel to Water* (Report V), February 1966.

Vachon, R. I., Tanger, G. E., Nix, G. H., and Goree, L. H. *Pool Boiling of Water on 304 Stainless Steel Etched with Hydrochloric Acid* (Report VI), August 1966.

Vachon, R. I., Nix, G. H., Hare, J. F., and Anderson, W. C. *The Rohsenow Pool Boiling Correlation--Examination of the Equation and a Tabulation of Data* (Report VII), December 1966.

Nix, G. H., Vachon, R. I., and Brenneman, B. F. *Pool Boiling Heat Transfer Response of Chemically Etched Surfaces to Varying System Pressures* (Report VIII), July 1967.

Nix, G. H., Vachon, R. I., and Respess, W. S. *Preliminary Analysis of Rapid and Controlled Venting of Saturated Systems* (Report IX), January 1968.

5. Publications

Tanger, G. E., Vachon, R. I., and Pollard, R. B. "Pool Boiling Response to Pressure Decay," *Proceedings of the Third International Heat Transfer Conference*. Volume IV. Ephrata, Pennsylvania: The Science Press, Inc. (for American Institute of Chemical Engineers), August 1966, pp. 38-43.

Vachon, R. I., Tanger, G. E., Davis, D. L., and Nix, G. H. "Pool Boiling on Polished and Chemically Etched Stainless-Steel Surfaces," *Transactions of the ASME, Journal of Heat Transfer*, 90, C, 2 (May 1968), 231-238.

Vachon, R. I., Nix, G. H., and Tanger, G. E. "Evaluation of Constants for the Rohsenow Pool-Boiling Correlation," *Transactions of the ASME, Journal of Heat Transfer*, 90, C, 2 (May 1968), 239-246.

Vachon, R. I., Nix, G. H., Tanger, G. E., and Cobb, R. O. "Pool Boiling Heat Transfer from Teflon-Coated Stainless Steel," Presented at the ASME Winter Annual Meeting, New York, December 1-5, 1968, and to be Published in *Transactions of the ASME, Journal of Heat Transfer.*

6. Papers Submitted to Fourth International Heat Transfer Conference

Nix, G. H., Vachon, R. I., and Hall, David M. "A Scanning and Transmission Electron Microscopy Study of Pool Boiling Surfaces," Paper 69-IC-99.

Nix, G. H., and Vachon, R. I. "Surface and Pressure Effects on Pool Boiling from Chemically Etched Surfaces," Paper 69-IC-104.

Nix, G. H., and Vachon, R. I. "Analysis and Test Results for Blowdown of a Saturated System," Paper 69-IC-105.

7. Requests for Reports and Publications

Report II, November 1964	
J. Lielmezs	University of British Columbia

Report IV, December 1965	
J. Lielmezs	University of British Columbia
Aluf Orell	Israel Institute of Technology
Russell B. Mesler	University of Kansas

Proceedings of Third International Heat Transfer Conference, Volume IV, August 1966, pp. 38-43	
Aluf Orell	Israel Institute of Technology

Journal of Heat Transfer, 90, C, 2 (May 1968), 231-238, 239-246	
M. Akiyama	University of Tokyo
S. William Gouse, Jr.	Carnegie-Mellon University
Takehiro Ito	Kyushu University
Aluf Orell	Israel Institute of Technology
L. W. Florschuetz	Arizona State University
R. Nagarajan	University of Windsor
A. Spyridonos	Nuclear Research Center "Democritus"
George W. Preckshot	University of Missouri
Stanley S. Grossel	Chemical Engineer
K. K. Nangia	McGill University
Monroe Alter	Iliffe-NTP Incorporated

ABSTRACT

Two separate but related studies are reported on areas pertinent to an understanding of the behavior of saturated systems. The first is an experimental investigation of surface and static pressure effects on nucleate pool boiling. The second is an analysis of saturated system response to rapid and controlled depressurization.

Pool boiling data were collected, at various system pressures, for chemically etched 304 stainless steel surfaces in contact with distilled water. Results show the changes in heat transfer with varying rms surface roughness and preparation techniques. Several correlation equations for predicting wall superheat were examined, but most were not satisfactory. However, the Rohsenow equation, because of its flexibility, was applied satisfactorily to the present data and to data from the literature.

Results of transient discharge tests are compared to a model developed for analysis and with results obtained by other investigators. The model agrees well with system pressures and temperatures, and predicts local time-dependent liquid and vapor properties within the vessel. Other models considered did not produce satisfactory agreement with the data of the present investigation. An explanation is given for pressure fluctuations that have been observed in discharging saturated systems.

ACKNOWLEDGMENTS

The project personnel express their appreciation to the National Aeronautics and Space Administration for sponsoring this work under Contract NAS8-11234. The support and suggestions of the following personnel at the George C. Marshall Space Flight Center contributed to the success of this project:

Mr. H. Paul, Chief, Propulsion Division
Propulsion and Vehicle Engineering Laboratory
Dr. R. R. Head, Chief, Applied Mechanics Research Branch
Propulsion and Vehicle Engineering Laboratory
Mr. C. G. Fritz, Contract Supervisor, Applied Mechanics Research Branch, Propulsion and Vehicle Engineering Laboratory

In addition to the above, the services of Mr. J. D. Hornsby, Mr. C. T. Moore, and Mr. J. F. Young, Mechanicians, Auburn University Mechanical Engineering Laboratories, Mrs. Helen N. Martin, Editorial Assistant, Engineering Experiment Station, and Mr. John Pozadzides, Draftsman, as well as the 26 undergraduates who supported the graduate students and staff on the project, insured the success of this research.

The results of this effort demonstrate the desirability of the NASA/University team approach to the pursuit of knowledge in engineering and the sciences.

TABLE OF CONTENTS

LIST OF FIGURES

LIST OF TABLES

NOMENCLATURE

A. Roman Letters

Symbols		Dimensional Units
A	Area, Eq. (II-6)*	ft^2
A	Parameter representing $\frac{2\sigma T_s}{h_{\ell v}\rho_v}$, Eq. (II-1)	
$B(r)$	Constant in Eq. (II-5)	
C_ℓ	Specific heat of saturated liquid, Eq. (II-17)	$Btu/lb_m°F$
C_p	Specific heat at constant pressure, Eq. (VI-8)	$Btu/lb_m°F$
C_{sf}	Coefficient in Eq. (II-17)	
C_1	$\frac{1 + \cos \phi}{\sin \phi}$, Eq. (II-1)	
C_3	$1 + \cos \phi$, Eq. (II-1)	
C_4	Constant C_3 used by Kurihara and Myers [29], Eq. (II-5)	
D	Hydraulic diameter, Eq. (II-22)	ft
D_f	Diameter of bubble leaving surface, Eq. (II-15)	in
E	Characteristic term in Eq. (II-5)	
f	Frequency of bubble formation, Eq. (II-15)	

*The table or equation number immediately following the description indicates where the symbol first appears in the text.

Symbols		Dimensional Units
$\bar{f}$	Average Darcy friction factor, Eq. (II-22)	
G	Mass velocity per unit area, Eq. (II-12)	$lb_m/sec\text{-}ft^2$
g	Acceleration due to gravity, Eq. (II-15)	ft/sec^2
g_c	Gravitational constant, Eq. (II-15)	$lb_m ft/lb_f sec^2$
h	Convective heat transfer coefficient, Eq. (II-7)	$Btu/hr\ ft^2 °F$
h	Specific enthalpy, Eq. (II-10)	Btu/lb_m
I	Current, Eq. (B-1)	amps
k	Thermal conductivity, Eq. (II-4)	$Btu/hr\ ft °F$
L	Length, Eq. (II-22)	ft
M	Mass in system, Eq. (II-19)	lb_m
n	Number of sites, Eq. (II-5)	
n/A	Site density, Eq. (II-6)	ft^{-2}
P	Pressure, Eq. (II-18)	lb_f/in^2
ΔP	Excess bubble pressure, Eq. (II-9)	lb_f/in^2
Q	Heat, Eq. (II-6)	Btu
q	Rate of heat flow, Eq. (II-4)	Btu/hr
R	Resistance, Eq. (B-1)	ohm
r	Exponent in Eq. (II-17)	
r	Radius of cavity mouth, Eq. (II-1)	in
rms	Root mean square, Table 4	
s	Exponent in Eq. (II-17)	

Symbols		Dimensional Units
T	Temperature, Eq. (II-1)	°F
t	Time, Eq. (II-21)	sec
t*	Dimensional time defined by $\frac{A}{M_i}$ t, Eq. (II-19)	ft^2-sec/lb_m
U	Internal energy, Eq. (II-19)	Btu
u	Specific internal energy, Eq. (II-19)	Btu/lb_m
V	Volume, Eq. (VI-2)	ft^3
v	Specific volume, Eq. (II-10)	ft^3/lb_m

B. Greek Letters

$\beta^\circ(y)$	Number of grooves of depth between y and y + 1 units over a distance of 1/16 inch, Eq. (II-5)	
Δ	Difference in quantity, Eq. (II-5)	
δ	Limiting thermal layer thickness, Eq. (II-1)	in
μ_ℓ	Viscosity of liquid, Eq. (II-12)	lb_m/ft hr
ϕ	Conical angle of cavity, Eq. (II-18)	degrees
ρ	Resistivity, Eq. (B-2)	ohm-ft
ρ_ℓ	Density of liquid phase, Eq. (II-15)	lb_m/ft^3
ρ_v	Density of vapor phase, Eq. (II-15)	lb_m/ft^3
σ	Interfacial surface tension, Eq. (II-9)	lb_f/ft
θ	Contact angle, Eq. (II-15)	degrees

C. Dimensionless Groups

Nu	Nusselt number, Eq. (II-13)
Pr	Prandtl number, Eq. (II-13)
Re	Reynolds number, Eq. (II-12)

D. Subscripts

b	Bubble
E	Blowdown escape value
e	Exit condition
ext	External
i	Initial value
ℓ	Liquid phase
ℓv	Liquid-vapor
max	Maximum
min	Minimum
o	Incipience of boiling
s	Saturated
u	Bottom surface of test strip
v	Vapor phase
vp	Vapor pressure
w	Wall
∞	Conditions in bulk of liquid
$( )^{\cdot}$	Time derivative of quantity
$( )'$	Derivative with respect to pressure
$( )^{*}$	Ratio of quantity to initial value

I. INTRODUCTION

The analysis of pool boiling heat transfer and two-phase flow is the subject of numerous investigations conducted in the past two decades. The increasing importance of nucleate boiling has prompted many fundamental studies of the various processes. However, these studies are complicated by the fact that a dimensional analysis of all variables associated with boiling yields 38 dimensionless groupings [1, 2]. Thus, although several design correlations [3-6] for various aspects of the phenomenon have been advanced in recent years, no equation correlating the general case of boiling is available.

An important problem associated with any pool boiling correlation is incurred in accounting for the change in heat flux as a function of static pressure and surface effects. Attempts to predict the effect of static pressure have attained little success. This is owed in part to the interaction of pressure effects with surface effects. These surface effects are a result of 1) the method of surface preparation, 2) the surface-liquid combination, and 3) the effective surface roughness. There is no accurate description of pool boiling surfaces which accounts for surface variables. Nevertheless, surface effects must be considered.

Another separate but inter-related problem of current interest is the transient pressure decay of a saturated system. The analysis

of such systems has applications to nuclear reactor safety, space venting of cryogenic systems and space vehicle propellant loss caused by meteroid puncture. Rapid depressurization of a boiling system may be initiated as a result of boiling vessel rupture or pump failure. The general area of rapidly depressurizing systems at saturation conditions is relatively unexplored [7-13]. No satisfactory explanation exists for pressure spikes observed during depressurization [9, 11-13]. Thus, a systematic investigation of the pressure decay of saturated systems is necessary for a more complete understanding of the phenomena involved.

The present investigation is concerned with two separate but related areas pertinent to an understanding of the behavior of saturated systems. These are:

1. Investigation of the effects of static pressure and surface condition on nucleate pool boiling;

2. Analysis of rapid and controlled depressurization on saturated system response.

Results of the study should be relevant to NASA programs concerned with simultaneous surface boiling and periodic venting of stored cryogens in space as well as a number of nonspace related applications.

The first phase of the study is an attempt to clarify the effects of surface characteristics and static pressure on nucleate pool boiling. Data will be obtained from stainless steel surfaces which have been etched chemically. These data will be utilized along with data from the literature in a study of present pool boiling design correlations.

The part of the investigation concerned with static pressure effects was initiated as a result of observing a phenomenon associated with pool boiling from chemically etched surfaces operated at successively higher pressures. The data indicated an increase in wall superheat with an increase in pressure. This is contrary to expectation and heretofore unreported in the literature. Additional test data and analysis are presented to confirm and clarify this situation.

The second part of the study is concerned with the effects of rapid and controlled depressurization on an initially saturated pool boiling system. Parameters to be examined include dynamic liquid/vapor temperature response and fluid behavior during depressurization. An explanation will be presented for the pressure fluctuations observed in discharging saturated systems.

A test facility has been constructed which will allow basic experimental studies on surface and static pressure effects and will permit determination of the effects of various system parameters on depressurization. The facility has the flexibility such that basic boiling studies can be conducted on the same apparatus used for discharge tests. Results of transient discharge tests will be compared to a model developed for analysis and with results obtained by other investigators. Other predictive models will be examined for their applicability to the present study. During the course of the investigation, an attempt will be made to relate the results of model studies such as the present to the behavior of large-scale systems in current use.

II. LITERATURE SURVEY

The goal of the present study is to analyze the behavior of a saturated pool boiling system under static and dynamic pressure conditions. Closely connected with this goal is the task of predicting boiling heat transfer fluxes with varying pressure and surface conditions. Discharge may be considered a macroscopic phenomenon where surface conditions are of secondary importance. However, surface effects are of major importance in nucleate pool boiling and must be analyzed in microscopic detail. Analysis of steady-state boiling characteristics is necessary to obtain the initial input variables for the discharge analysis. The first portion of the literature review focuses attention on prior analyses and experiments which concern surface and pressure effects on nucleate pool boiling heat transfer. The latter portion of the review is devoted to an analysis of the current status of knowledge concerning saturated discharge.

A. Pool Boiling Surface Studies

The importance of surface conditions was recognized early in the study of nucleate boiling heat transfer. Jakob and Fritz [14] discovered that, for a given superheat, the rate of heat transfer increased as the surface roughness increased. The observed increase in roughness was primarily macroscopic in nature since the authors did not attempt quantitative surface measurements. Other investigations have established the

role of microscopic roughness in boiling heat transfer [15-19]. Clark, Strenge, and Westwater [15], in a microscopic study of surfaces, identified photographically 20 separate nucleation sites during boiling of ether and pentane on zinc- and aluminum-alloy surfaces. The size of the active pits ranged from 0.0003 to 0.003 inch. Grain boundaries, as observed from electron micrographs, were found to have little or no effect on boiling nucleation. The smallest scratches which were observed as active sites were roughly 0.0005 inch in width.

Quantitative surface roughness measurements were made by Corty and Foust [16] with various techniques. The roughness ranged from 2.2 to 23 μ-inches rms. Varying degrees of surface roughness were obtained by using 4/0, 2/0, 0, 1, and 3 emery polishing paper. Corty and Foust found that roughness changed the slope, as well as the position of the curve of the heat transfer coefficient. Their investigation indicated much steeper slopes than have been found experimentally in previous studies. They attributed these differences to the wide range of effective nucleation sites which may occur in two systems which appear to be similar. Extensive data were taken which included: heat transfer data; shape, contact angle, and number of bubbles; surface conditions; and boiling history. In conclusion, the authors postulated that the number of bubbles existing on a surface at any given superheat depends on the physical properties of the fluid, the shape and sizes of the microscopic surface cavities, and the contact angle in the cavity.

Other attempts at surface preparation have consisted of mechanical polishing, artificial scoring, and lapping. Polished surfaces were used by Gaertner and Westwater [18] and Griffith and Wallis [19].

Gaertner and Westwater [18] conducted 51 experimental tests with an aqueous solution of nickel salts on copper in an attempt to determine the relationship between q/A, $T_w - T_s$, and the site density, n/A. A two inch diameter surface polished with seven grades of emery through 4/0, with all visible scratches removed from the surface, was employed in the tests. A larger number of bubble columns were observed as the surface roughness increased, coinciding with an increase in film coefficient and the rate of heat transfer. The active sites were noted to be distributed randomly over the surface. A special electroplating technique was utilized which allowed visual counts of the active sites up to a maximum of $1130/in^2$ at a heat flux of 317,000 Btu/hr^2ft. This number far exceeded the previous site count which was possible using ordinary means.

Methanol, ethanol, and water solutions were boiled on copper in the investigation of Griffith and Wallis [19]. Surfaces were prepared with 3/0 emery, and all strokes were in the same direction. The authors prepared a special surface for their studies by pricking 37 holes--uniform in size and shape--in the 3/0 surface. The holes were uniformly spaced over the surface. Comparative tests were conducted on a similar surface without the holes to demonstrate the increase in heat flux for increased roughness.

Berenson [20] used lapped surfaces. Lapping is usually thought of as producing a very smooth surface finish; however, grit which is suspended in the oil actually saturates the surface with cavities. Mechanical polishing of the copper surface with various grades of emery cloth was also employed as a means of preparation. The boiling heat

transfer coefficient varied as much as 600 percent as a result of the variations in surface finish. The lapped surface required less superheat than the mechanically polished surfaces. Berenson thus demonstrated that the rms roughness is not the significant roughness parameter for use in correlations. Clark, Strenge, and Westwater [15] determined visually that, regardless of the overall rms value, the "rougher" surface is the one which has the greatest number of cavities in a size range appropriate for activity.

Berenson explained the increase in film coefficient and heat transfer for a lapped surface as follows: The lapped surface, which is smooth in a macroscopic sense, produced the highest values of h and q/A in the study. This was attributed to a large number of very small cavity sites rather than to an rms value, which actually measured only the statistical mean of surface variance. This is similar to the conclusion reached by Clark, Strenge, and Westwater [15].

Artificial scoring was employed by Bonilla, Grady, and Avery [21]. Copper surfaces were prepared with parallel scratches of known depth, geometry, and length. The scratches were spaced at distances of 1.0, 0.5, 0.25, and 0.125 inch on four plates. A Brush Surface Analyzer was used to measure surface roughness. In the study, water was boiled from copper surfaces, and mercury was boiled from a similarly prepared low-carbon steel surface. The results indicated that the heat flux was dependent upon the spacing widths. The higher values of heat flux were obtained for scratches 2 to 2.5 bubble diameters apart. The data for water indicated that the influence of the scratches on heat transfer for large values of q/A was less pronounced than for small values. On the

other hand, the data for mercury boiling from low-carbon steel indicated that the effect of the scratches was more pronounced for high q/A than for low fluxes. The authors did not offer an explanation for the increase in film coefficient with the mercury surface. They did point out that the results will not confirm nor deny the location of a maximum h at 2 to 2.5 bubble diameters for the liquid metal. In conclusion, the authors indicate the scratches should be spaced approximately $2.5\sigma/(\rho_v-\rho_\ell)$ inches apart for maximum effectiveness. The scratches should be sharp and at least 0.001 inch in depth.

The effect of surface roughness on the rate of heat transfer has received considerable attention in past investigations. Various surface preparation techniques have been employed in attempts to reveal the relationship involved. Nucleation sites are of major importance to an understanding of boiling heat transfer and have received considerable analysis. Westwater [2] has discussed the necessity of nucleation sites and given the necessary criterion that there must be a good gas trap. Therefore, the surface flaws must be microscopic in nature. The necessity of sites has been demonstrated by Hsu and Graham [22] and Otterman [23], who investigated the heating of pure, degassed water on a clean mercury surface. No boiling was observed other than the explosive formations resulting from cavitation, thus demonstrating the importance of surface irregularities.

Westwater [24] confirmed that the phenomenon which he called "bumping" occurs when liquids are boiled from cavity-free surfaces. The superheat requirements were reported to be quite large with respect to ordinary nucleate boiling. Further evidence of the high superheats

required to initiate boiling from smooth surfaces has been presented by Lottes and Viskanta [25]. The superheats obtained were higher than those reported for boiling from solid surfaces but not as high as those reported by Gordon, et al.[26] and Mead, et al.[27].

A cavity must fall within a given size range if it is to be active during a boiling process. Hsu [28] developed a mathematical model from which he predicted the minimum and maximum radii required for activity and the criterion for incipience of boiling. The model employed was the same as that used by Hsu and Graham [22] to predict the waiting period in the ebullition cycle. Hsu assumed a limiting thermal layer, δ, outside of which the bulk temperature remained constant and considered the process to be similar to the case of transient conduction. Two cases were investigated. The first, a constant temperature case, is approximated by the use of a thick heater block of high thermal conductivity. The constant heat flux case approximates the conditions encountered with a thin strip heater. Equations were developed for the maximum and minimum radii required for an active cavity. These parameters were found to be functions of the amount of subcooling, system pressure, physical properties, and thickness of the superheated liquid layer. The equations developed for the constant-temperature case were

$$r_{max} = \frac{\delta}{2C_1}\left[1 - \frac{(T_S - T_\infty)}{(T_W - T_\infty)} + \sqrt{\left(1 - \frac{(T_S - T_\infty)}{(T_W - T_\infty)}\right)^2 - \frac{4AC_3}{(T_W - T_\infty)}}\right] \quad \text{(II-1)}$$

$$r_{min} = \frac{\delta}{2C_1}\left[1 - \frac{(T_S - T_\infty)}{(T_W - T_\infty)} - \sqrt{\left(1 - \frac{(T_S - T_\infty)}{(T_W - T_\infty)}\right)^2 - \frac{4AC_3}{(T_W - T_\infty)}}\right] \quad \text{(II-2)}$$

and the criterion for the incipience of boiling was given as

$$T_{wo} - T_{\infty o} = T_s - T_\infty + \frac{2AC_3}{\delta} + \sqrt{\left(2(T_s - T_\infty) + \frac{2AC_3}{\delta}\right)\left(\frac{2AC_3}{\delta}\right)} \quad \text{(II-3)}$$

Therefore, if δ is known, the incipience of boiling may be determined for a given pressure and subcooling. Similarly, for the constant heat flux case, the incipience of boiling was predicted by the equation

$$q_o = \frac{k}{\delta}\left[T_s - T_\infty + \frac{2AC_3}{\delta} + \sqrt{\left(2(T_s - T_\infty) + \frac{2AC_3}{\delta}\right)\left(\frac{2AC_3}{\delta}\right)}\right] \quad \text{(II-4)}$$

In each case, the thickness of the superheated liquid layer, δ, must be known or measured.

Data by Clark, et al. [15] are correlated with the curves predicted by Eqs. (II-3) and (II-4) in Fig. 1. Since the surfaces used in the investigation were well polished, the equations developed may be assumed to predict cavity radii for well polished surfaces. Hsu concluded that the theory was successful for predicting boiling incipience and the size range of active cavities. However, he pointed out that more experimental studies were needed to fully understand the limiting thermal layer thickness and its behavior as determined by the various parameters. Experimentation is also necessary to determine the correct values of the constants in the equations.

Using cavity radius as one parameter, Kurihara and Myers [29] related the number of cavities on a surface to the average cavity radius through the work of Frenkel [30]. A model consisting of a cone and a

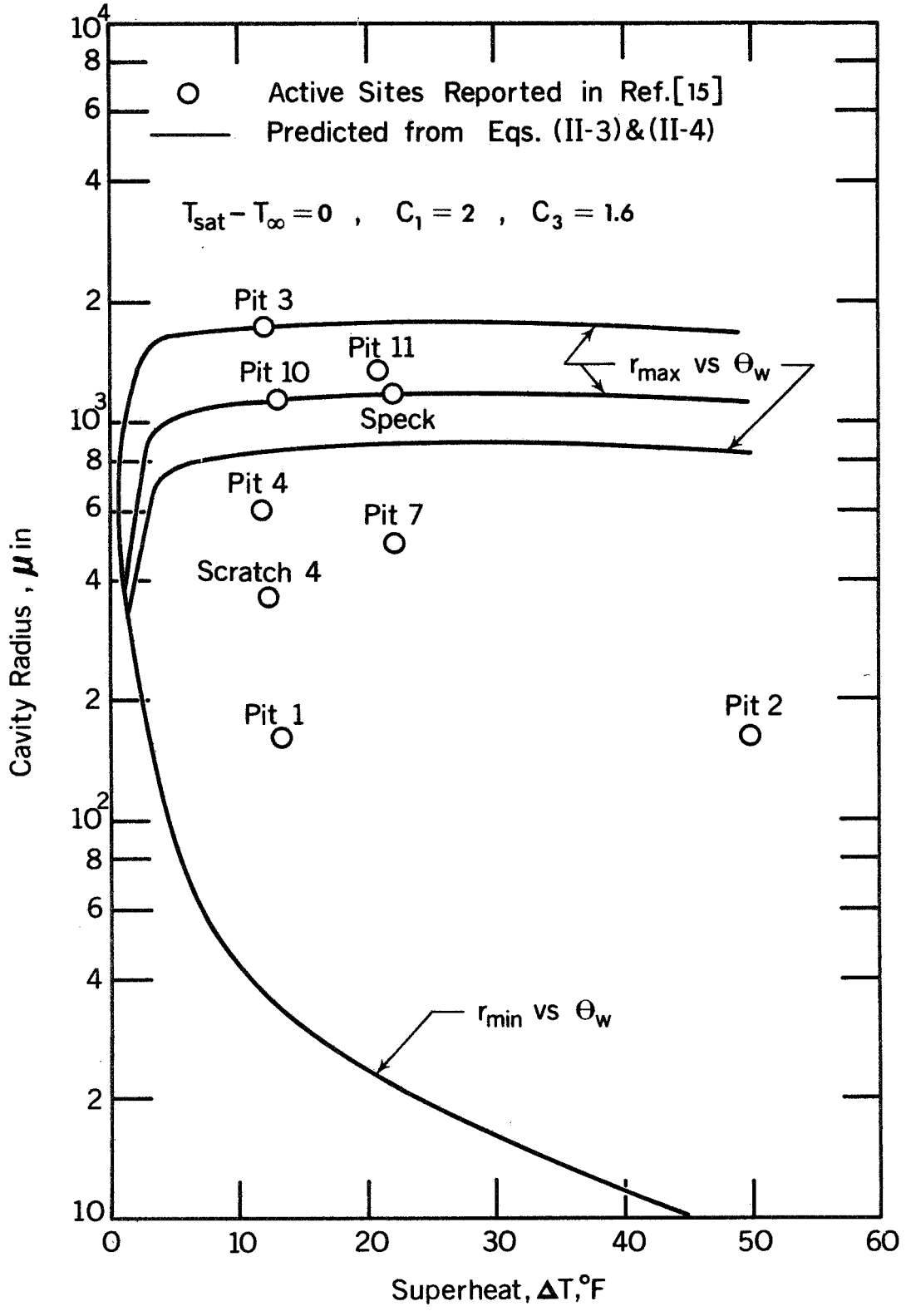

FIG. 1 SIZES OF EFFECTIVE CAVITIES AS FUNCTION OF SUPERHEAT FOR N-PENTANE BOILING ON ALUMINUM

groove of depth y was used to develop the equation.

$$n_2 - n_1 = \int_{\Delta T_1}^{\Delta T_2} r^2 \beta^{o}(y) \exp\left(\frac{-E}{r}\right) d(\Delta T) \qquad \text{(II-5)}$$

If one set of measurements for a given fluid-surface roughness combination is used, the number of nucleating sites for any ΔT may be obtained from Eq. (II-5). The values of B(r) and E used in Eq. (II-5) are presented in Table 1.

TABLE 1

VALUES OF B AND E IN EQUATION (II-5)

Term	Water	Acetone	n-Hexane	Carbon Tetrachloride	Carbon Disulfide
B(μ-Inches) (°R)	2330.0	790.0	620.0	960.0	1280.0
E(μ-Inches)	3.8	5.7	7.3	7.8	8.1

A typical correlation predicted by Eq. (II-5) compared to experimental data is shown in Fig. 2. The data presented include measurements with acetone, n-hexane, carbon tetrachloride, and carbon disulfide boiling on 4/0, 1/0, and number two polished surfaces. No calculations were presented for water because the size of the term B indicates a valley depth of 20 micro-inches or more. No indication of this depth on the 4/0 surface could be found. The authors postulated that the bubbles form over

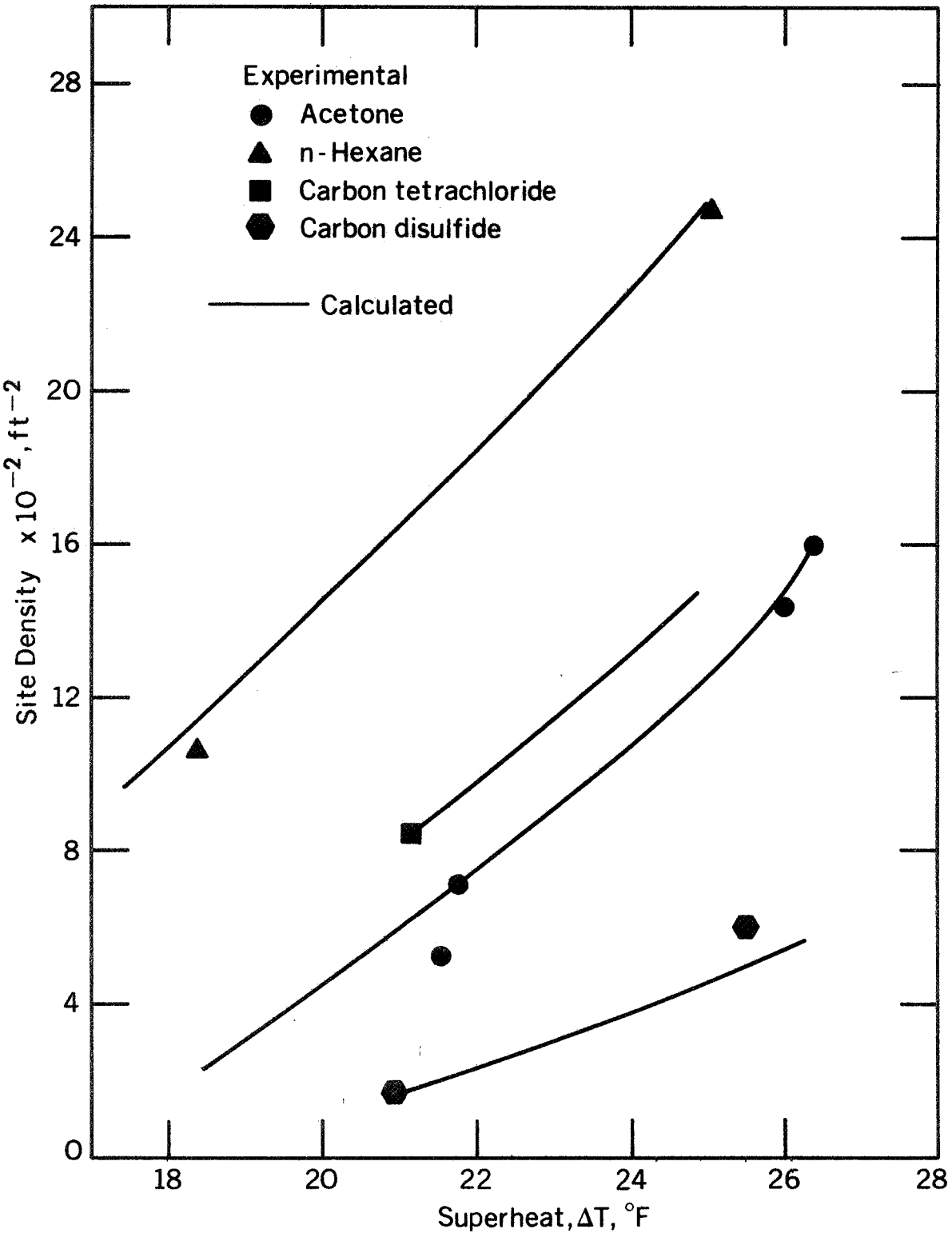

FIG. 2 COMPARISON OF SITE DENSITY CALCULATED BY EQ. (II-5) WITH EXPERIMENTAL DATA FOR 4/0 POLISHED COPPER

several adjacent sites; consequently, the value of B(r) cannot be predicted for this case.

Several investigators have related the site density to the heat flux and film coefficient through empirical equations. Gaertner and Westwater [18] found that the heat flux is proportional to the square root of the site density and proposed the following equation.

$$Q/A = 1400\ (n/A)^{0.47} \tag{II-6}$$

This differs from the linear relationship proposed by Jakob [31]. For site densities greater than $500/ft^2$, the relation

$$h = 49\ (n/A)^{0.43} \tag{II-7}$$

was found to be within the range found by Nishikawa [17] and Kurihara and Myers [29].

Gaertner [32], in another investigation, found the relationship between site population and heat flux to be given by

$$Q/A = 181\ (n/A)^{0.66} \tag{II-8}$$

This equation is similar to the equations given by Kurihara and Myers [29] and by Gaertner and Westwater [18]. The exponent of the n/A term varies in the following manner: 0.66, 0.55, and 0.49. The variation is attributed to minor surface-finish differences. The comparison demonstrates the difficulty in reproducing results of other investigators. It also points out the inadequacy of empirical approaches in surface boiling heat transfer.

The numerous investigations that have been reported point out the importance of the bubble-generation process in determining the total heat transfer rate. The number of sites and, therefore, the number of vapor columns are very important in this regard. Rohsenow and Clark [33], in an early paper, pointed out that the latent heat actually carried from the surface by the bubbles does not account for the increased rate of heat transfer observed during boiling. They proposed that the agitation of surrounding fluid, resulting in relatively high induced velocities within the quiescent layer, was the primary mechanism. However, there is disagreement among the various investigators on this point. The idea that agitation of the liquid causes the excellent heat transfer was also held by Jakob [34]. Forster and Grief [35] favor a vapor-liquid exchange action for the mechanism of nucleate boiling. They visualize vapor bubbles as displacing superheated liquid from the surface. The authors interpret their viewpoint as a case of bubbles agitating the liquid. Many other investigators have written along similar lines.

Closely connected with the idea of bubbles furnishing the agitation is the concept that when a bubble departs it allows cooler liquid to contact the surface. The cold liquid readily carries the heat away from the hot surface.

Another hypothesis is that liquid at the base of the bubble is vaporized into the bubble. However, Moore and Mesler [36] postulated a model which they substantially demonstrated with experiments. Their microlayer evaporation theory proposes vaporization in a thin microlayer at the base of the bubble.

The need for an analytical model describing bubble evolution is evident. Some investigators [16,19] have developed mathematical models to represent bubble formation. A representative model is that used by Griffith and Wallis [19]. A conical cavity was chosen to represent the nucleation site since it may closely approximate an actual site and lends itself to mathematical formulation. Figure 3 illustrates the physical model used by the authors. The radius of curvature of a curved surface which is a segment of a sphere and the liquid superheat at static, mechanical equilibrium may be related through the Gibbs equation as follows:

$$\Delta P = 2\sigma/r \tag{II-9}$$

When the bubble is at equilibrium, vapor within the bubble must be at the saturation temperature corresponding to the interior pressure, and the liquid must be at the same temperature. Consequently, the liquid must be superheated. The Clausius-Clapeyron equation, Eq. (II-10), relates excess temperature in the liquid to excess pressure in the bubble.

$$\frac{\Delta P}{(T_w - T_s)} = \frac{h_{\ell v}}{T_w v_{\ell v}} \tag{II-10}$$

Substitution of the above relation for ΔP in Eq. (II-9) yields the following relation between liquid superheat and radius of curvature.

$$r = \frac{2T_w v_{\ell v}}{(T_w - T_s)h_{\ell v}} \tag{II-11}$$

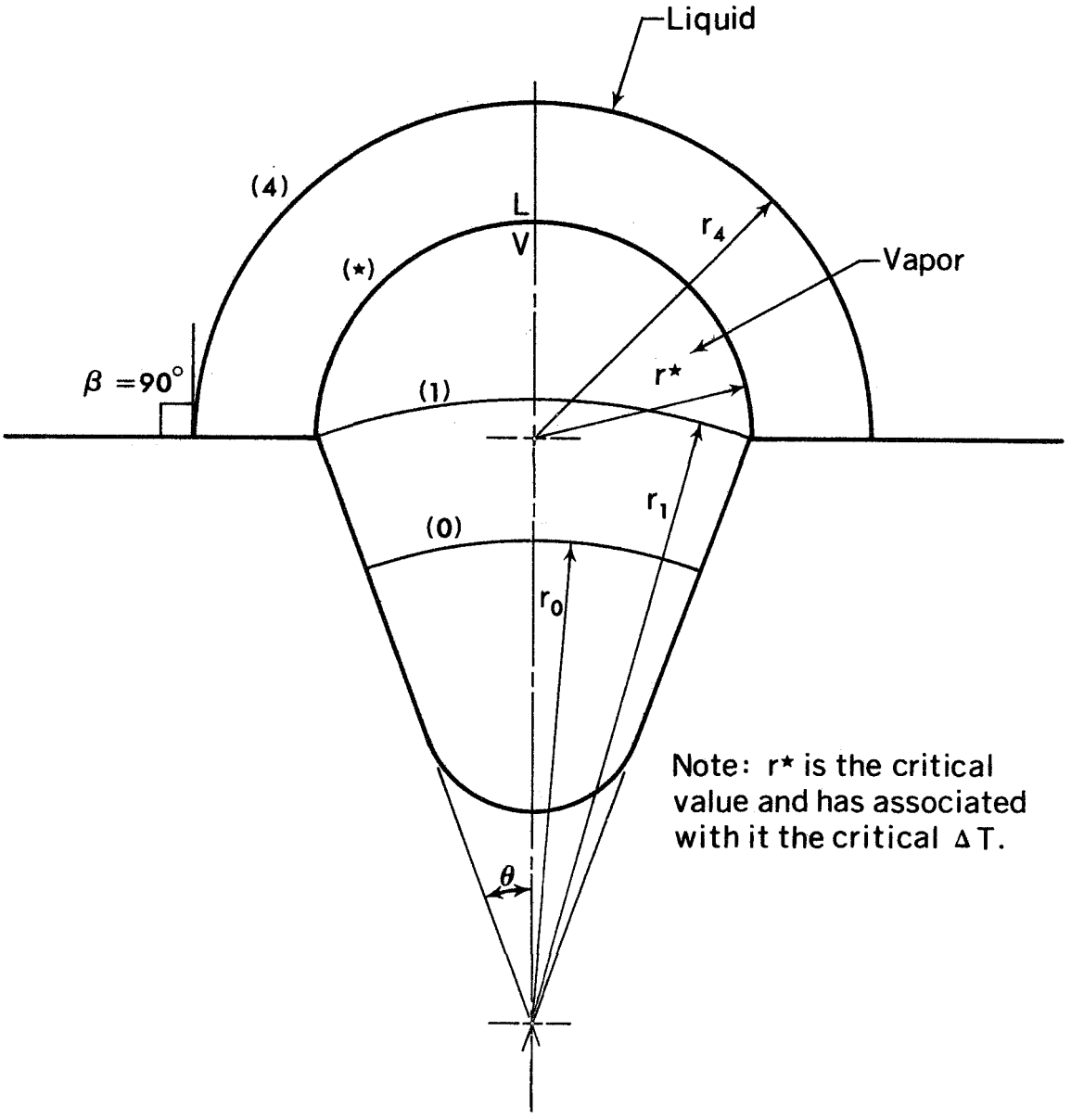

FIG. 3 MODEL OF CONICAL CAVITY WITH A 90-DEGREE CONTACT ANGLE

When the critical radius, i.e., the radius of the cavity, is substituted into Eq. (II-11), the minimum temperature difference needed to initiate bubble growth may be obtained.

There have been numerous correlation equations proposed by different investigators. A method established by Rohsenow [9] for nucleate pool boiling employs a bubble Reynolds number which measures the effect of increased agitation resulting from the bubbles on heat transfer. This dimensionless parameter was formed by combining the average bubble diameter D_b, the mass velocity of the bubbles per unit area G_b, and the liquid viscosity M_ℓ to obtain

$$Re_b = \frac{D_b G_b}{M_\ell} \tag{II-12}$$

Then, by similarity with single-phase forced-convection correlations,

$$Nu_b = \psi(Re_b, Pr_\ell) \tag{II-13}$$

where

$$Nu_b = \frac{(q/A)_b D_b}{(T_w - T_s)k_\ell} \tag{II-14}$$

and Pr_ℓ is the Prandtl number based on the fluid properties. Rohsenow used the expression developed by Fritz [37]

$$D_f = 0.0209\theta\sqrt{\frac{g_c\sigma}{g(\rho_\ell - \rho_v)}} \tag{II-15}$$

and the relation developed by Jakob [34]

$$(q/A)_b = h_{\ell v}\rho_v n \frac{\pi}{6} D_f{}^3 f \tag{II-16}$$

for the heat transfer to the bubble while attached to the surface to

develop his correlation. The final form of the correlation is

$$\frac{C_\ell(T_W - T_S)}{h_{\ell V}} = C_{sf}\left[\frac{q/A}{M_\ell h_{\ell V}}\sqrt{\frac{g_c\sigma}{g_\ell(\rho_\ell - \rho_V)}}\right]^r\left(\frac{C_\ell\mu_\ell}{k_\ell}\right)^s \qquad \text{(II-17)}$$

where C_{sf} is a coefficient which depends upon the nature of the heating surface-fluid combination. Rohsenow pointed out that the correlation is valid for liquids boiling on a clean surface, and further study must be undertaken to determine the effect of liquid-surface combinations on the coefficient, C_{sf}.

Other correlations have been forwarded [29,38,39], but most are limited in scope since they do not account for the nature of the surface. The correlation equations may be classed as:

1. Equations with site density as a parameter.
2. Equations developed from hydrodynamic theory.
3. Equations containing experimentally determined coefficients.

The large number of physical variables associated with boiling heat transfer greatly complicates the procedure for describing any system analytically. Also, duplication of previous data is extremely difficult as a result of the large effect associated with small variations in surface preparation.

Another factor which must be accounted for in any general correlation is pressure. Early work concerned with the effect of pressure on boiling systems was performed by Cichelli and Bonilla [40] who showed the displacement of the boiling curve (q/A versus ΔT) with pressure. Corty and Foust [16] presented the equation

$$P_{vp} - P_{ext} = \frac{2\sigma}{r} \cos\left(\frac{\phi}{2} - \theta\right) \qquad \text{(II-18)}$$

for the radius of curvature of an idealized nucleating cavity. Since surface tension decreases with increasing temperature and the contact angle probably increases, Corty and Foust assumed the right-hand term did not change greatly with increasing temperature. However, the slope of the vapor pressure-temperature curve becomes greater as the temperature is increased. Thus, they explained that less superheat would be required for the necessary excess vapor pressure $P_{vp} - P_{ext}$ and the boiling curve would be shifted toward a lower wall superheat by increasing system pressure. Similarly, Griffith and Wallis [19] developed a relation between the cavity radius and the wall superheat. An inverse relationship was predicted between system pressure and wall superheat necessary to sustain nucleation of a given size cavity. This conclusion was also obtained by Corty and Foust.

Bankoff [41] presents an equation which predicts the minimum wall superheat for pressures less than the critical pressure. Bankoff [42] also proposes that the increase in heat transfer with pressure for a given wall superheat is caused by the increase in the number of active sites.

Other investigators [43-45] postulate that the wall superheat for a given heat flux is primarily a function of system pressure. Cryder and Finalborgo [43] found that for a given liquid-surface combination, increased wall superheat is required when the system pressure is reduced at constant heat flux. Kreith and Summerfield [44], in an experimental study, found that the wall superheat at constant heat flux varies as the

reciprocal of the absolute pressure to the three-fourths power. Raben et al. [45] conducted an investigation of nucleate boiling at pressures below the atmospheric pressure. They concluded that the mechanisms of heat transfer become less effective with reduced pressure because of

1. Decreased number of active sites.
2. Reduced contribution of convective transfer.
3. Reduced vapor density.

The reduced effectiveness of heat transfer dictates an increase in wall superheat with reduced pressure to maintain a constant heat flux.

Critical heat flux data for benzene, diphenyl, and benzene-diphenyl mixtures boiling under pressures from 13.5 to 488.5 psia were obtained by Huber and Hoehne [46]. Lienhard and Schrock [47] correlated the peak and minimum heat fluxes with pressure for a variety of fluids. They showed that variations in pressure and geometry have a significant effect on the peak and minimum flux. A later investigation by Lienhard and Watanabe [48] concluded that the effects of geometry and pressure on the peak and minimum nucleate boiling heat fluxes are separable.

More recently, Lienhard and Schrock [4] proposed a generalized correlation for the displacement of the nucleate boiling heat flux curve with pressure. The basis of their correlation is the hypothesis that the superheat for any configuration and heat flux is directly proportional to the van der Waal maximum superheat. Justification for the hypothesis is by comparison with experimental data.

Clearly, pressure is a parameter which must be considered in nucleate boiling although a general correlation must account for the effect of surface variables as well. Numerous investigations [49-55]

have shown the effects of surface material, method of preparation, surface roughness, and cleanliness on pool boiling. Berenson [20] points out that no method is available for proper description of pool boiling surfaces. Some investigators specify preparation technique [20,29] and others use rms surface roughness as determined with a profilometer [16,52]. Surface variations account for the wide discrepancies in boiling experiments obtained under seemingly similar conditions.

Thus, additional knowledge is needed to complete and integrate what is known about the basic boiling process. Specifically, studies are needed concerning the effect of pressure on heat transfer from prepared surfaces. Tests conducted on chemically etched stainless steel surfaces at various pressures will be presented and analyzed in Chapters IV and V.

B. Saturated Discharge

Two-phase vapor-liquid flow can develop from single-phase flow by:

1. Addition of heat from external sources.
2. Decrease in system pressure.
3. Combination of heat addition and pressure drops.

Regardless of the method by which two-phase flow develops, a precise knowledge of its behavior is necessary to adequately predict system response. Analysis of any system is made more complicated with the occurrence of two-phase flow.

The final objective of a two-phase flow analysis is the determination of heat transfer and pressure drop characteristics of a given flow. The analysis is, in general, that of a coupled thermal-hydrodynamic

problem, with heat addition influencing the flow pattern and phase distribution and with the hydrodynamics (pressure drop) affecting the heat transfer characteristics. These interactions fundamentally affect the changes in flow velocities, pressures, temperatures, and thermal and diffusion fluxes transferring across the various flow interfaces.

Despite the complexities, many simplified studies--of both analytical and experimental origins--have met with some measure of success in dealing with the general problem. However, simplifying assumptions have decreased the utility of many of the investigations. To date, any single analysis of two-phase flow is limited to a small area of the overall spectrum of flow conditions.

A considerable amount of published material is available for two-phase flow. It is beyond the current scope of work to conduct a survey which encompasses the many aspects of two-phase flow. The reader is instead referred to the comprehensive reviews of Tong [56] and Kepple and Tung [57] for this purpose. This investigation will be concerned mainly with discharging analyses as opposed to the general case of flow in a pipe.

Numerous investigators have studied the discharging of a single-phase fluid from tanks and vessels. These efforts will be discussed briefly before the more general and difficult problem of two-phase discharge is considered.

The quasi-steady analysis of rapid discharge from a vessel is a classical problem in thermodynamics. However, many discrepancies arise which may not be treated by the strict classical thermodynamic approach. Giffen [58] analyzed the rate of pressure decrease of a vessel discharging

to the atmosphere through a rapidly opened port. Using a numerical technique, Giffen found that the internal pressure change did not decrease in a continuous fashion, as predicted by the classical methods, but varied in a step-wise fashion. He concluded that the speed of sound within the gas is the controlling parameter. When the orifice or port diameter is small with respect to the vessel, the rate of pressure variation within the vessel is negligible compared to the rate at which disturbances are propagated throughout the vessel. Thus, the pressure can be assumed to be constant throughout the vessel, and the velocity of the approach to the discharge port can be neglected.

Numerous other authors [59-62] considered the problem of non-steady discharge of a gas, basing their calculations on the method of characteristics. Progelhof [62] found that the mass-versus-time relationship for sonic discharge through a nozzle can be approximated by application of the velocity-of-approach correction factor to the quasi-steady result. However, for sonic discharge through a nozzle, accuracy depends on the estimated average discharge coefficient for the process. For a subsonic discharge, Progelhof found that the pressure in the vessel may fall below the pressure of the surroundings. This is a further discrepancy not predicted by the classical quasi-steady approach.

Giffen [58] gives some general conclusions concerning the nature of the discharge process:

1. The extent of pressure variation in a vessel is determined by a) the rate of change of pressure near the port, and b) the time required for changes at the port to be propagated throughout the vessel.

2. Unless the port opens with a speed greater than the sonic velocity, area variations of the port will be accompanied by instantaneous variations in the rate of discharge.

3. Resistance to the pressure waves by the surrounding medium is most important when a pipe is connected to the discharge port.

4. A pressure depression will usually occur when a vessel is discharged rapidly to the atmosphere.

The previous analyses consider only a single-phase flow, which is somewhat simpler than the case of one-component, two-phase flow. Two-phase (vapor-liquid) discharge is complicated by the flashing of liquid to vapor as a result of a pressure decrease. However, certain aspects of the single-phase problem may be carried over into the investigation of two-phase discharge. For instances, it is likely that the sonic velocity explanation of discharge rate variations, offered by Giffen [58], may be used to help explain the pressure spikes [9,11-13] noticed for a two-phase pressure decay.

Recently, a number of investigators have been concerned with the problem of two-phase flow through various apertures [63-66] and with the mechanisms and interface relations [67-70] involved with boiling and two-phase flow. Also, emphasis was placed on the prediction of the critical flow rate in two-phase flow. The models of Fauske [8], Levy [71], and Moody [72] are perhaps the best known of these analyses.

The problem of two-phase discharge is currently being investigated by a number of laboratories [9,12,13,73-78]. Pollard [12,81], in a previous investigation, studied the history of liquid superheat in a pool boiling system subjected to a sudden pressure release. A 304

stainless steel heater surface in contact with distilled, degassed water was monitored during system pressure decay through a one-inch orifice to the atmosphere. The data indicated that the liquid superheat reached a maximum during the initial transient pressure phase and became negative during the final phase with a release time of approximately 12 seconds. The phenomenon found by Pollard has not received extensive publication in the literature but is quite probable in cryogenic systems.

Pollard also found a "spike" in the pressure-versus-time trace during the initial phase. The spike was similar to those observed by Howell and Bell [11], Ordin, Weiss and Christenson [13], and Moody [9]. Ordin et al. [13] presented results of an experimental investigation concerning temperature stratification and pressure rise of liquid hydrogen contained in an aircraft-type tank exposed to atmospheric turbulence conditions during flight. Pressures and temperatures were monitored at various positions in the tank during pressurization and venting conditions. They found--as did Pollard--that immediately after venting, the liquids are superheated and very little boiling takes place during the initial drop in pressure. This initial period is marked by a sharp drop in pressure with gas outflow from the tank. The authors found that the decay in tank pressure is a function of liquid temperature, vapor temperature, vaporization rate, ullage, and line and valve size.

Nuclear reactor containment and emergency cooling systems are designed to cope with the transient and maximum pressure buildups arising from loss of coolant accidents [82]. The expulsion of the coolant from pipe and vessel breaks in high pressure water systems involves metastable and two-phase flow phenomena (including what is called the maximum,

critical, or choking, two-phase flow rate). Adequate predictive models have not been developed for the discharge of saturated water through short length apertures. Current experimental studies are attempting to characterize the important parameters. One such study is the large scale LOFT (Loss of Fluid Test) program [76-80] being conducted by Phillips Petroleum Company at the National Reactor Testing Station in Idaho Falls, Idaho.

Current objectives of the LOFT program, similar to this investigation, include the generation of data for verification of analytical models and scaling considerations used to predict and extrapolate the LOFT behavior [76,83]. Detailed information will be provided for:

1. The overall thermal behavior of the coolant in the subcooled region (where acoustic effects predominate), through the two-phase saturated region, and in the post-blowdown convection region.

2. The transient and semi-steady-state hydraulic loading applied to various system components and structures.

3. The importance of system configuration and initial conditions; i.e., break size and location, hot and cold leg temperature differences, initial flow, and break duration.

4. The downstream shock pressure generation.

5. The amount and location of water remaining in the system after the break.

Future plans include simulation of core heat input to determine its influence on blowdown behavior. The blowdown program consists of three phases. Phase I includes tests using an unscaled empty vessel; Phase II includes tests using a quarter-scale model of the LOFT vessel with a simulated reactor core and internal components; and Phase III includes

tests using a quarter-scale model of the integral LOFT reactor and coolant system.

The LOFT Phase I blowdown facility is shown in Fig. 4. The vessel is attached to an I-beam frame through thrust load cells and weight-loss cells and can be utilized for top or bottom blowdowns. Initial tests [76] were performed at subcooled conditions with test pressures ranging from 600 to 1600 psi and at room temperature to investigate the behavior of the subcooled fluid in the semiscale vessel when subjected to rapid decompression. Several tests were performed using a liquid-full vessel to obtain data which should be similar to the subcooled portion of decompression during LOFT blowdowns.

The second series of tests [77] in the LOFT program are concerned with bottom blowdown tests at elevated pressure and temperature conditions. Tests were conducted at fluid temperatures of 400, 445, 495, and 540 degrees Fahrenheit with corresponding pressures of 600, 1270, 1700, and 2300 psi. The enthalpy stored in the vessels was varied to investigate enthalpy effects on blowdown phenomena. It was found that the durations of the subcooled portions of the decompression were essentially identical to the duration of a comparable subcooled test at ambient temperature. This implied that over the temperature range considered the acoustic relaxation of the system was primarily dependent upon the disturbance propagation time in the exit nozzle. The blowdown time was observed to decrease with an increase in the stored enthalpy of the fluid.

The facility shown in Fig. 4 was also utilized for top blowdown tests [78,79]. Partial pipe breaks were simulated by using a sharp-edged

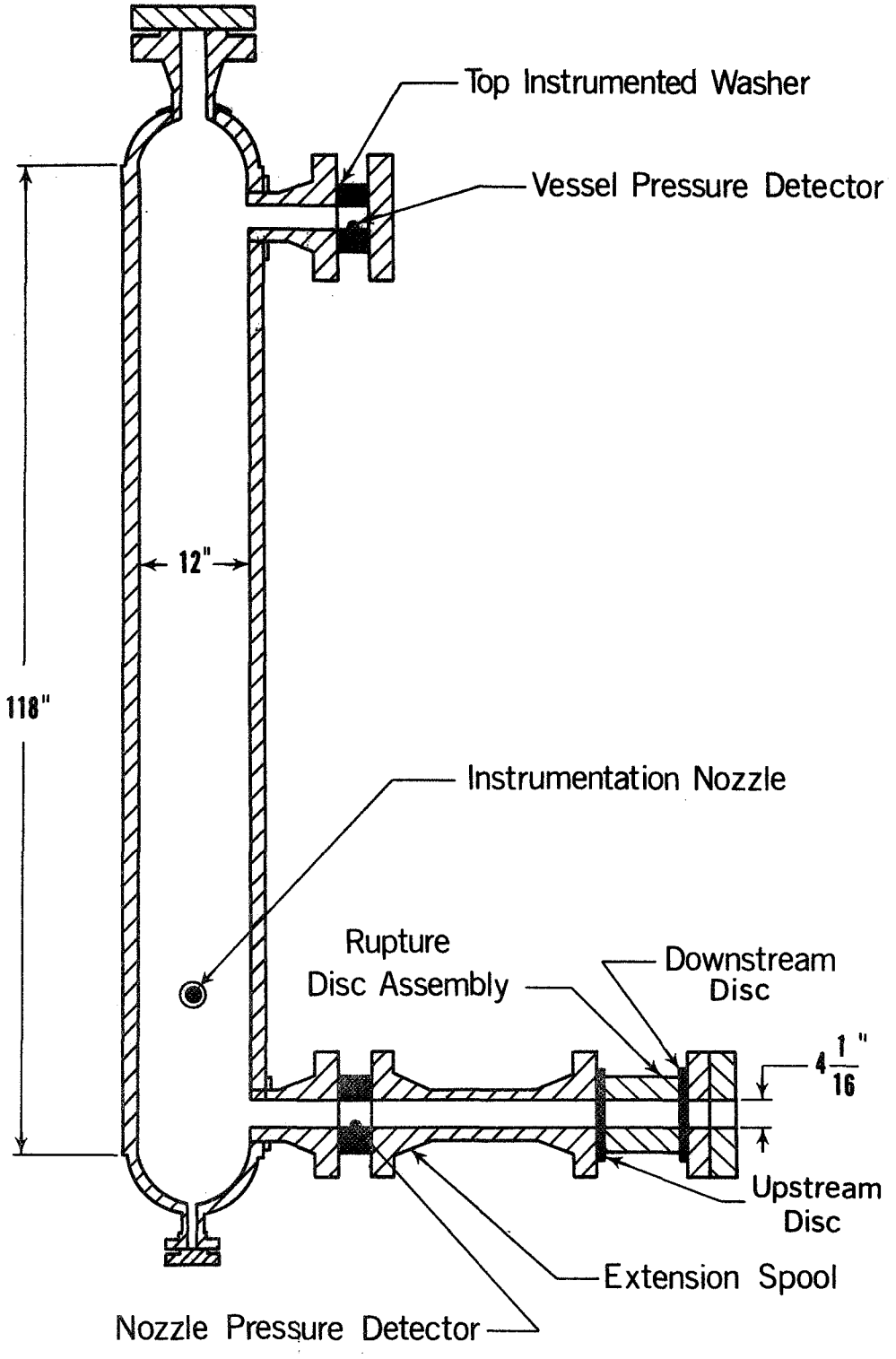

FIG. 4 LOFT PHASE I BLOWDOWN FACILITY [76]

orifice in the top blowdown nozzle to determine the effect of break size on such phenomena as subcooled decompression, blowdown time, and fluid remaining in the vessel. Separation of the fluid phase was enhanced by the top blowdown, and liquid entrainment was reduced. Separation of the fluid phases was promoted by a reduction in break size, and the increased blowdown time allowed more time for the fluid to reach thermodynamic equilibrium. The break size markedly affected the subcooled decompression, as shown in Fig. 5. Smaller break sizes increased the subcooled decompression and could result in oscillatory pressure forces coincident to the natural frequency of a reactor core.

Top blowdown tests at elevated temperature and pressure conditions were conducted with break sizes corresponding to 2, 6, 10, 30, 60, and 100 percent of the full pipe area [79]. It was found that the residual water in the vessel depended not only on break size but also on the location of the blowdown nozzle. Also, it was found that the steam exiting from the top nozzle was of a higher quality than that of comparable bottom blowdown tests. The conclusion was reached that the elevation difference between the nozzles accounted for the difference in quality. In the top blowdown configuration, the enthalpy stored in the fluid was dissipated by expanding or flashing the fluid to high quality steam which escaped through the blowdown nozzle. In the bottom blowdown, the expanding fluid in the vessel maintained a fluid pressure which forced a fluid mixture out the bottom nozzle. Results of the top blowdown with small simulated breaks indicated that an appreciable amount of residual water might remain in the vessel.

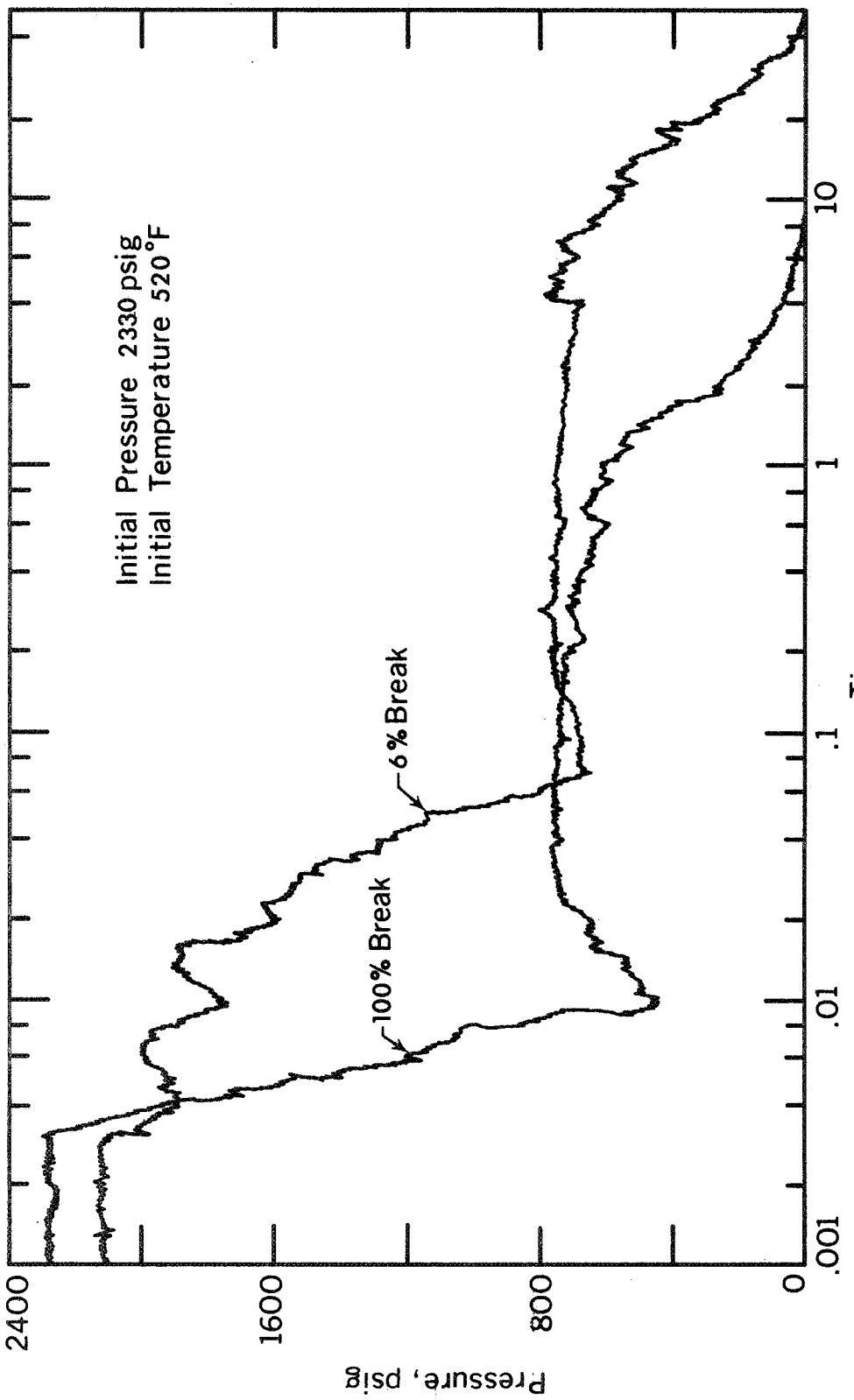

FIG. 5 LOFT VESSEL PRESSURE FOR TOP BLOWDOWN TEST-EFFECT OF BREAK SIZE ON SUBCOOLED DECOMPRESSION BEHAVIOR [78]

Coolant blowdown studies similar to the LOFT program are being conducted at the Pacific Northwest Laboratory by Battelle Memorial Institute as part of their containment systems experiments [74,75]. The experimental phase of the program is just beginning. The test vessel is designed to permit both top and bottom blowdown series. A schematic of the vessel simulating a top or steam-outlet break is shown in Fig. 6. The blowdown series will start as simple no-core blowdowns of the contained liquid through various sizes of orifices under different initial conditions. Subsequently, a simple orifice plate will be installed within the vessel to provide a controllable flow resistance. Pressures, flow rates, and other measured data will be compared to the values obtained from mathematical models. These results will determine the need for inclusion of further details in the model.

Results and test conditions of three initial blowdown tests in the CSE series are presented in Table 2 [75]. All of these tests were conducted with a blowdown nozzle near the bottom of the cylindrical vessel. Rough comparisons of the initial data have been made with the blowdown prediction model of Johnson [84], but further information on the nature of the flow and the flow conditions at the nozzle will be required to resolve the questions raised by the data.

Moody [9,85] developed a theoretical blowdown model to predict two-phase blowdown for various steam-water reference systems. The saturated system blowdown model used in developing the analysis is shown in Fig. 7. The model consisted of an adiabatic, constant volume system which contained an equilibrium mixture of liquid and vapor. Mass and energy escape through a single pipe at rates W and $h_E W$, respectively,

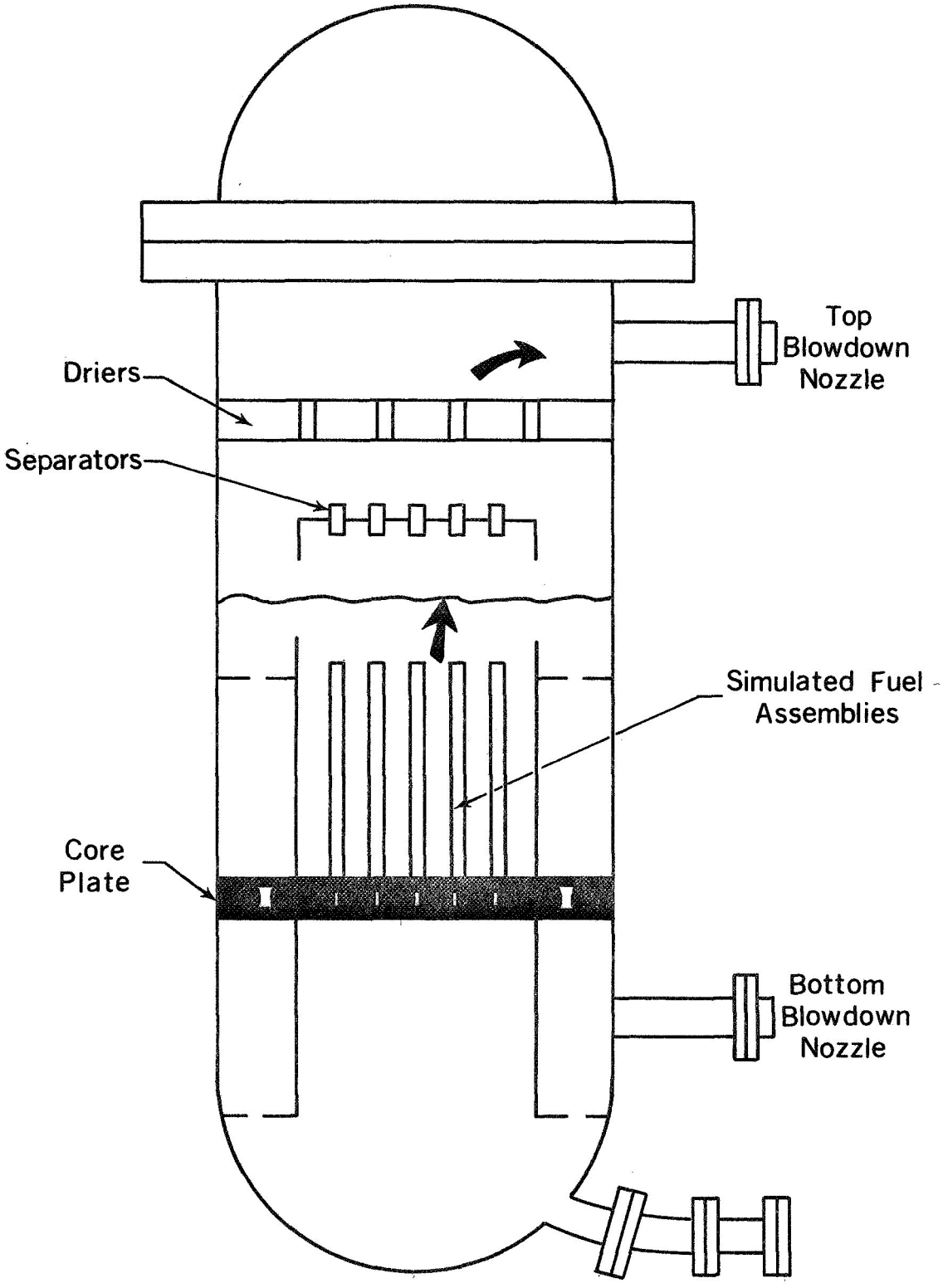

FIG. 6 CONTAINMENT SYSTEMS EXPERIMENT REACTOR SIMULATOR VESSEL: STEAM-OUTLET BREAK SIMULATION [74]

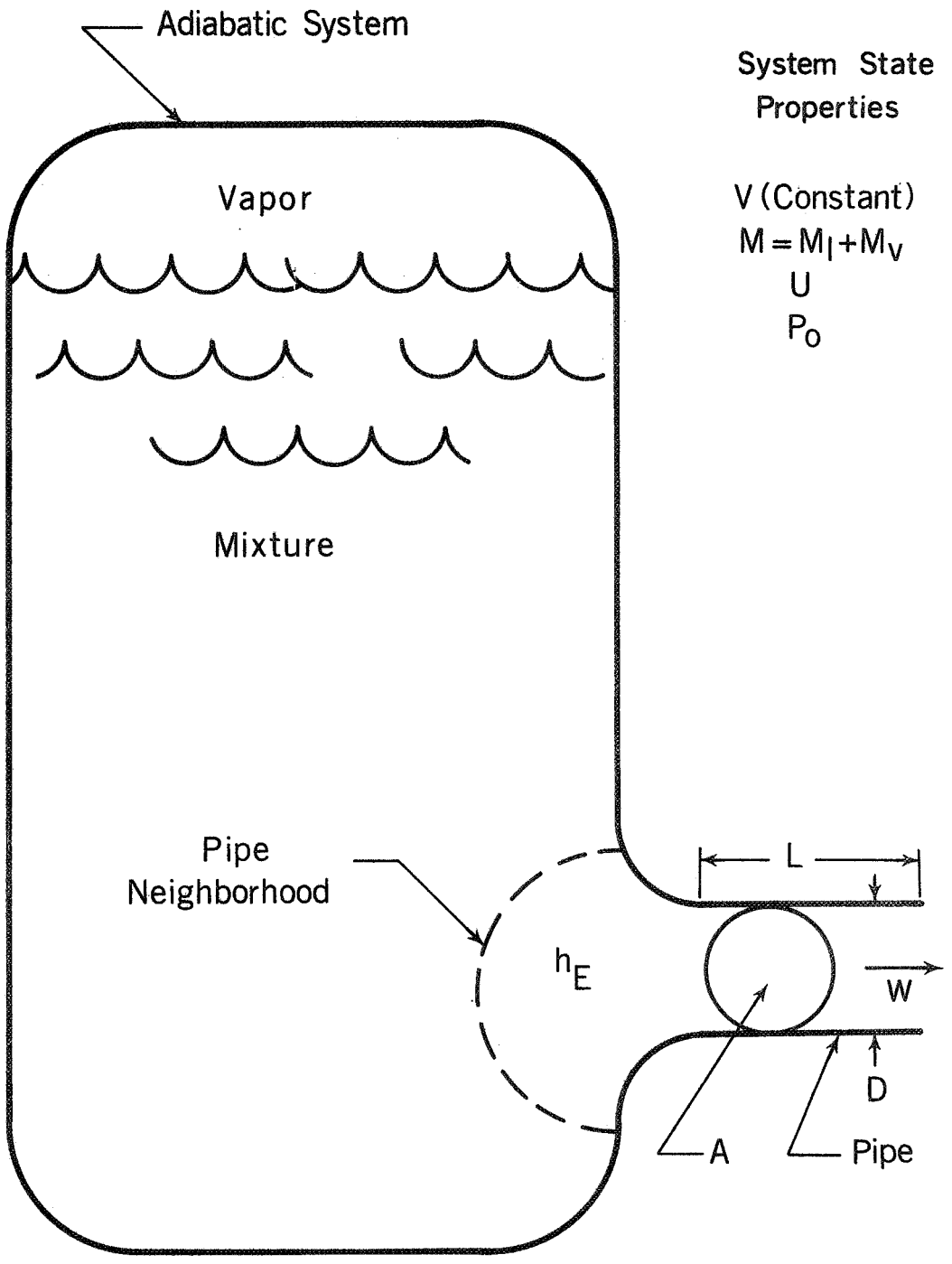

FIG. 7 SATURATED SYSTEM BLOWDOWN MODEL OF MOODY [85]

TABLE 2

SUMMARY OF HIGH TEMPERATURE BLOWDOWN RUNS FOR THE CSE REACTOR [75]

Description	Run B-7 Saturated	Run B-8 Saturated	Subcooled
Pressure (psia)	665.0	665.0	1565.0
Temperature (°F)	490.0	495.0	400.0
Orifice Area (ft^2)	0.0643	0.253	0.0643
Initial Mass of Water (lb_m)	7300.0	7100.0	6600.0
Time to Water Exhaustion (sec)	27.0	8.0	12.0
Time to End of Run (sec)	39.0	19.0	27.0
Initial Volume of Water (ft^3)	147.5	145.0	122.0
Initial Volume of Steam-Nitrogen (ft^3)	5.0	7.5	30.0

where h_E is the stagnation enthalpy of the fluid in the immediate pipe neighborhood. Moody obtained the following for system mass, energy, and pressure rates:

$$\frac{dM^*}{dt^*} = - G$$

$$\frac{dU^*}{dt^*} = - \frac{h_e}{u_i} G \qquad \text{(II-20)}$$

and

$$\frac{dP_o}{dt} = - \frac{\left(h_E + \frac{u_{\ell v}}{v_{\ell v}} v_\ell - u_\ell\right) G}{\left[\frac{v_i}{M^*}\left(\frac{u_{\ell v}}{v_{\ell v}}\right)' - \left(\frac{u_{\ell v}}{v_{\ell v}} v_\ell\right)' + u_\ell'\right] M^*} \qquad \text{(II-21)}$$

The value of G is determined as a function of stagnation pressure, enthalpy, and the quantity $\overline{f}L/D$. Moody presents a series of graphs giving G_M in the form:

$$G_M\left(P_o,\ h_o,\ \frac{\overline{f}L}{D}\right) = 0 \qquad \text{(II-22)}$$

The theory requires an estimation of $\overline{f}L/D$ to predict the blowdown rates.

The value of h_E depends on P_o and on the liquid-vapor action in the system. Moody considers three characteristic types of blowdowns:

1. Saturated liquid blowdown, characterized by

$$h_E = h_\ell(P_o) \qquad \text{(II-23)}$$

2. Homogenized mixture blowdown, characterized by

$$h_E = h_\ell(P_o) + \frac{h_{\ell v}(P_o)}{v_{\ell v}(P_o)}\left[\frac{v_i}{M^*} - v_\ell(P_o)\right] \qquad \text{(II-24)}$$

3. Saturated vapor blowdown, characterized by

$$h_E = h_v(P_o) \qquad \text{(II-25)}$$

Integration of Eqs. (II-19), (II-20), and (II-21) yields P_o, M^*, and U^* in terms of t^*. Sample results are shown in Figs. 8 and 9 for an initially saturated system at 1000 psia. The three characteristic blowdowns are shown for $\overline{f}L/D$ values from 0 to 100. The results in Figs. 8 and 9 can be used to estimate system pressure, mass, and energy at various times during blowdown.

Liquid blowdown corresponds to mass loss from a low point on the system if vapor entrainment is minor. Mixture blowdown applies to rapid mass loss from the system when vapor is formed faster than it can

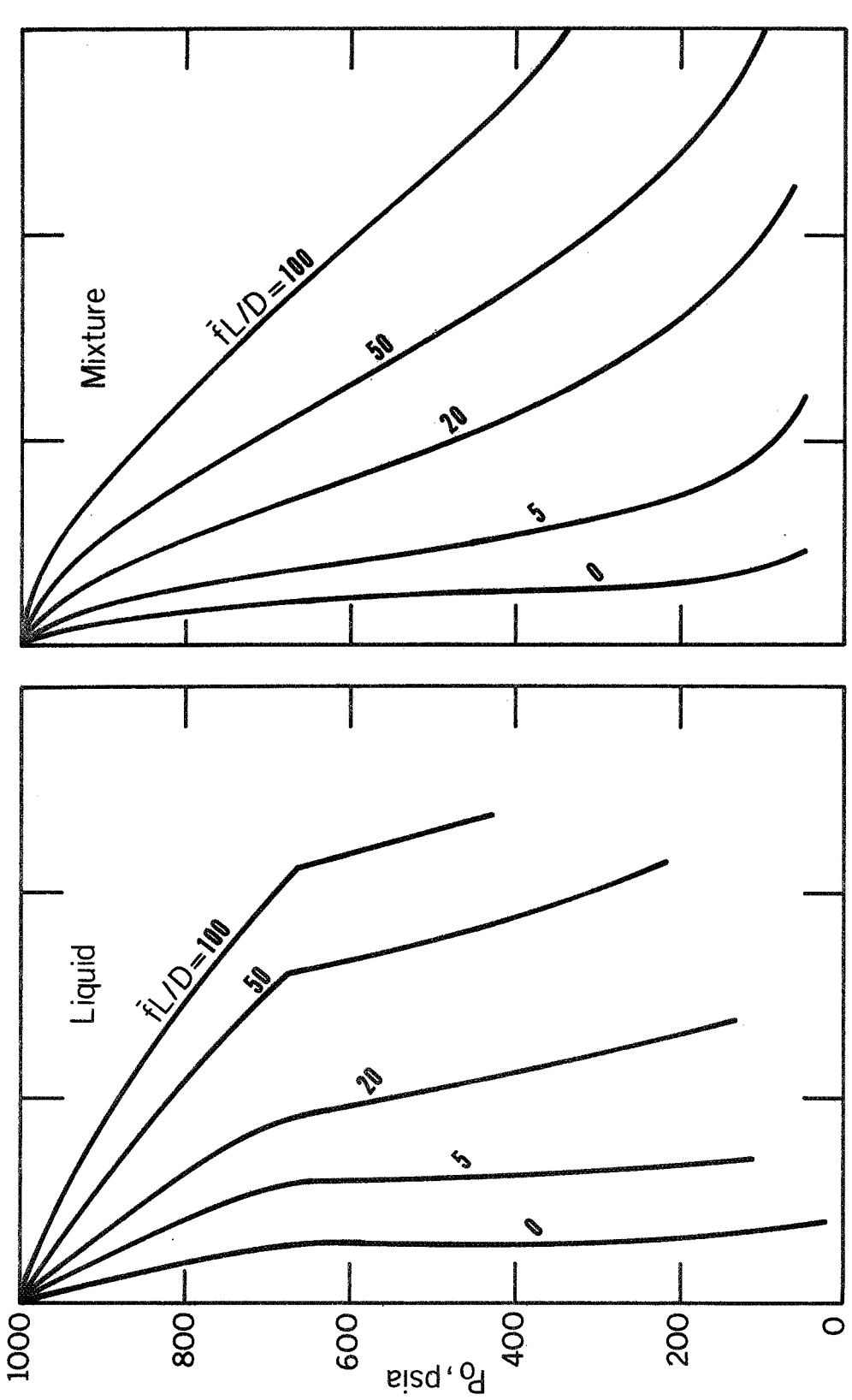

FIG. 8 BLOWDOWN FROM 1000 psia STEAM/WATER REFERENCE SYSTEM [85]

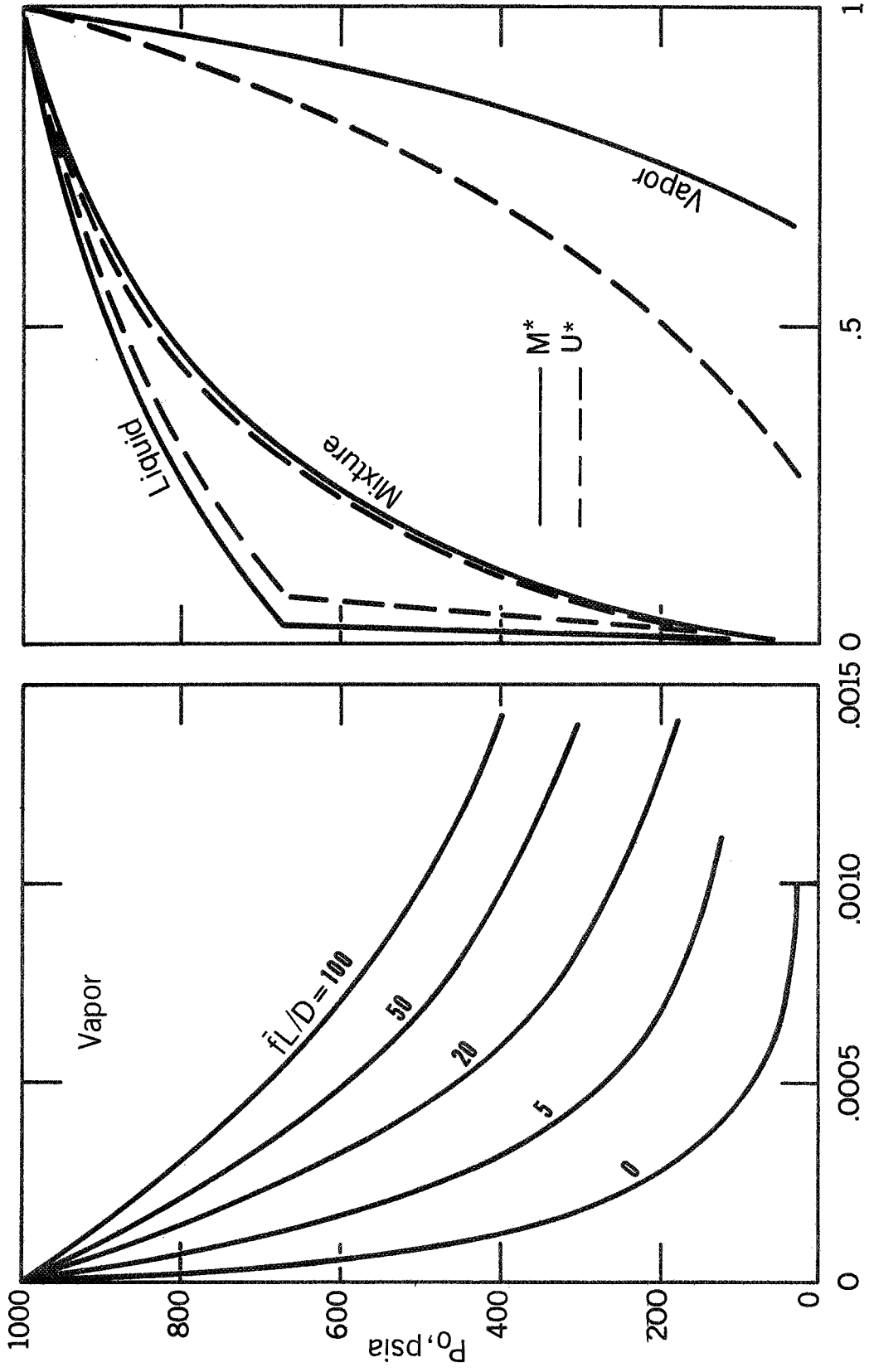

FIG. 9 BLOWDOWN FROM 1000 psia STEAM/WATER REFERENCE SYSTEM [85]

separate from the liquid. Vapor blowdown occurs from a high point on the physical system, which is slow enough for vapor separation without liquid entrainment.

The model results were compared with blowdown test data from a full-scale, 1/112 segment of the Bodega Bay atomic power plant [86] and a full-scale, 1/48 segment of the Humboldt Bay plant [87]. A list of conditions for these tests is given in Table 3. The vessel initially contained saturated steam-water at 1250 psia. The test results are shown in Figs. 10 and 11. As pointed out earlier, the value of $\overline{f}L/D$ must be estimated for a meaningful comparison with the theory. This estimation can be made by either of two methods: summation of standard single-phase geometric loss coefficients plus the actual $\overline{f}L/D$ components associated with the system tested, or calculation of an equivalent $\overline{f}L/D$ from measured irreversible pressure drop at a known cold-water flow rate. Moody chose the latter method for his comparison.

The theory with $\overline{f}L/D = 1.0$ is compared with Bodega Test 21 in Fig. 10. A sharp initial dip in test pressure which essentially recovers in one second appears in all saturated blowdown tests. This phenomenon, not explained, by the model, is similar to that noticed by other investigators [5-7]. Moody explains the characteristic as a combination of two effects: initial discharge of slightly subcooled liquid which is not restricted by the two-phase mechanism and the delay time for vapor bubbles to form and expand in the liquid.

Also evident in the test data of Figs. 10 and 11 is a "knee" or sudden increase in the rate of pressure drop. This is predicted by the theory, as shown in Figs. 8 and 9, when saturated water blowdown is

TABLE 3

SYSTEM DATA FOR BLOWDOWN TESTS USED BY MOODY [85]

Description	Bodega - 40	Bodega - 22	Bodega - 16	Humboldt - 22
Vessel Initial Pressure (psia)	1250.0	1250.0	1250.0	1250.0
Saturation Temperature (°F)	572.4	572.4	572.4	572.4
Saturation Enthalpy (btu/lb_m)	578.6	578.6	578.6	578.6
Initial Water Temperature (°F)	537.4	572.4	572.4	572.4
Initial Water Enthalpy (btu/lb_m)	532.5	578.6	578.6	578.6
Initial Water Subcooling (btu/lb_m)	46.1	0	0	0
Flashing Pressure (psia)	940.0	1250.0	1250.0	1250.0
Nozzle Throat Area (in^2)	8.25	8.25	--	--
Orifice Throat Area (in^2)	--	--	20.6	0.95
Back Pressure (atm)	1.0	1.0	1.0	1.0
Upstream Pipe Area (in^2)	115.0	115.0	115.0	26.0

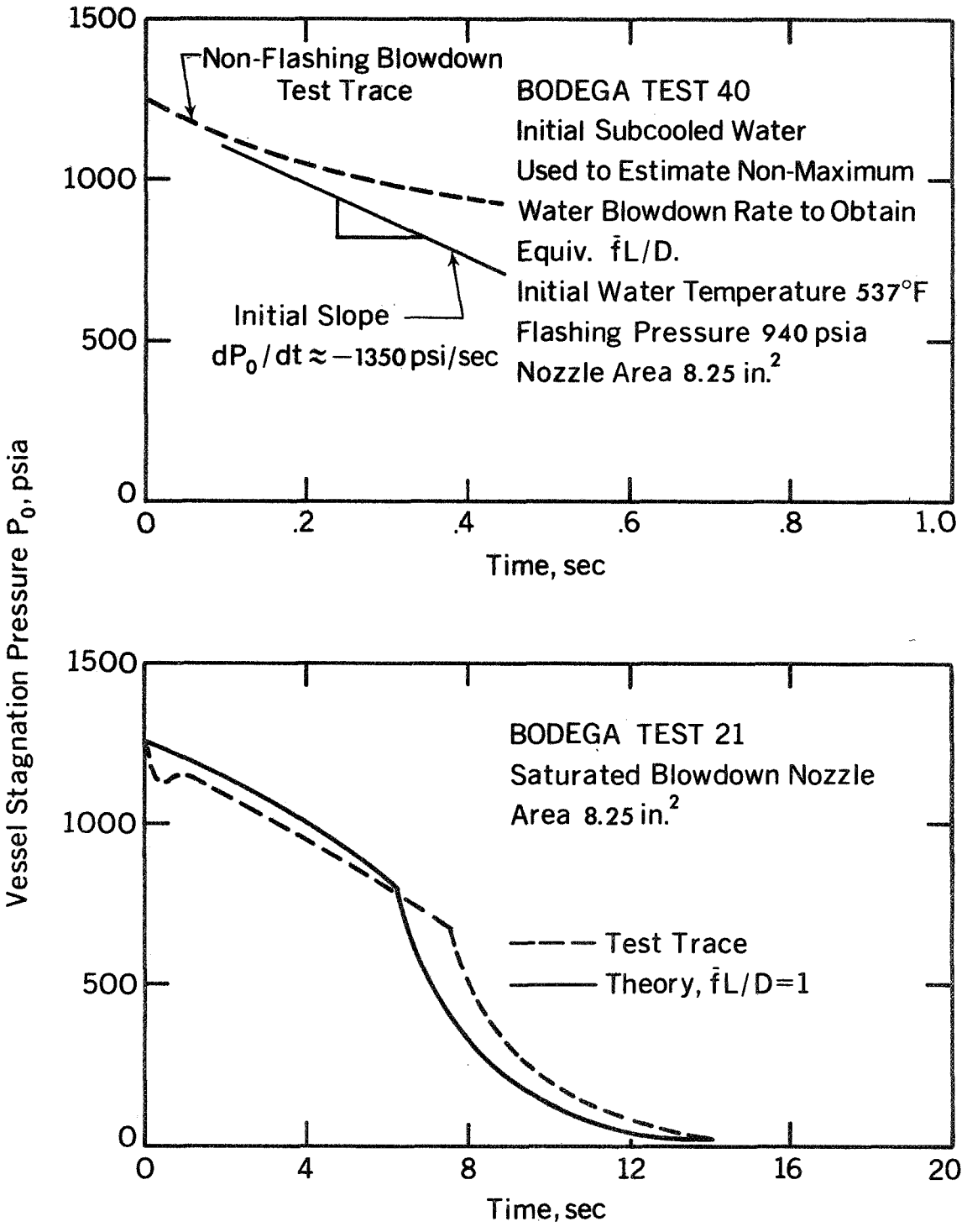

FIG. 10 COMPARISON OF MOODY'S THEORY WITH EXPERIMENTAL BLOWDOWN RESULTS [85]

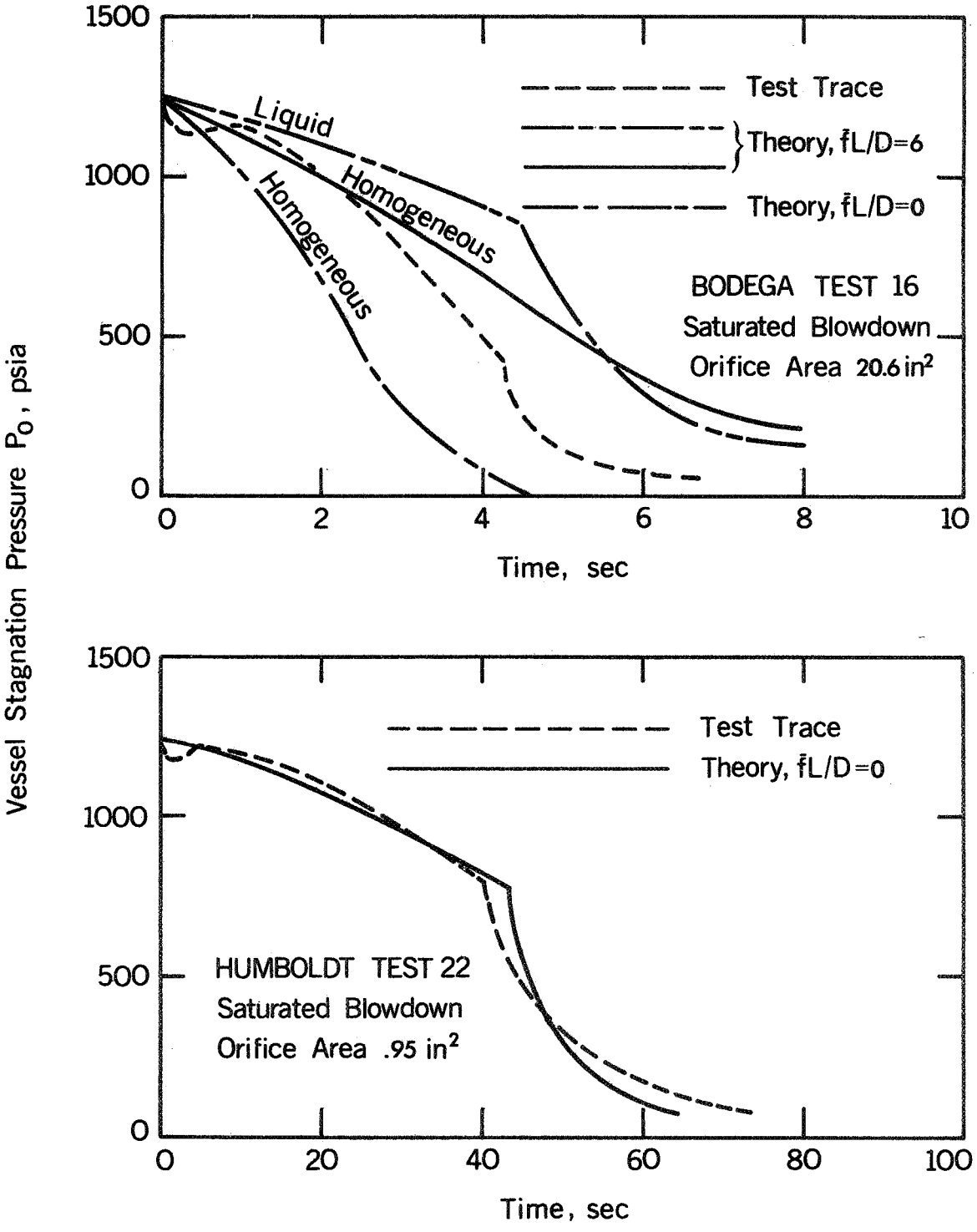

FIG. 11 COMPARISON OF MOODY'S THEORY WITH BLOWDOWN RESULTS ILLUSTRATING EFFECT OF BLOWDOWN AREA [85]

followed by saturated vapor blowdown. The much larger blowdown area of Test 16 (Fig. 11) nearly caused the disappearance of the knee. A large nozzle might cause such rapid vapor formation that a nearly homogeneous mixture would fill the vessel and the knee would disappear completely.

Moody discussed the reason for the estimation of $\overline{f}L/D = 6$, used for comparison with Bodega Test 16. He observed that Bodega Test 17 (not shown) was nearly identical to Bodega Test 21 except that an orifice was used instead of a nozzle. Blowdown area was the same in each case, and the pressure-time characteristics were nearly identical. It was concluded that exchanging an orifice for a nozzle caused negligible effects on flow rates for these blowdown tests, with upstream irreversibilities being unaffected. It is clear that blowdown area is evidently the important variable.

Further, it was concluded that it is unlikely that a high concentration of vapor would occupy the vessel lower region during blowdown while liquid was still present. Therefore, steam/water action in the vessel for all Bodega and Humboldt tests should lie somewhere between a homogeneous mixture filling the vessel and completely separated phases with water occupying the vessel lower region until fully expelled.

The problem of two-phase discharge is receiving extensive study, as evidenced by the preceding discussion. The corresponding analytical and experimental studies have been reviewed. The investigation satisfactorily explains certain aspects of the overall problem. However, several difficulties remain. It appears that a satisfactory predictive

model has not been developed for system response during pressure decay. The model developed by Moody [9,85] is restrictive in that friction loss factors must be estimated before a comparison can be made. However, Moody's model does seem to be the most promising analysis forwarded at this time, and it will be compared to the data from the facility reported herein and from the writer's model, as shown in Chapters VI and VII.

III. SYSTEM DESCRIPTION

An overall view of the pool boiling heat transfer and depressurization facility is given in Fig. 12. An attempt was made in the design of the basic components to provide maximum flexibility, consistent with present requirements for future investigations. The main components of the apparatus are:

A. Boiler

B. Orifice and Quick Release Valve

C. Fluid Purification Loop

D. Power Supply and Control

E. Test Strip Support Block

F. Instrumentation

A. Boiler

Incorporated in the boiler design are provisions for conducting both phases of the study. The boiler was designed for an ultimate working pressure of 300 pounds per square inch to permit elevated pressure work. A schematic diagram of the boiler is shown in Fig. 13. The boiler is constructed of one-half-inch thick, type 316, stainless steel plate and is 12 inches long, 12 inches deep and 8 inches wide. All joints of the boiler were welded with a heliarc welder on the exterior to prevent the formation of voids on the interior surface,

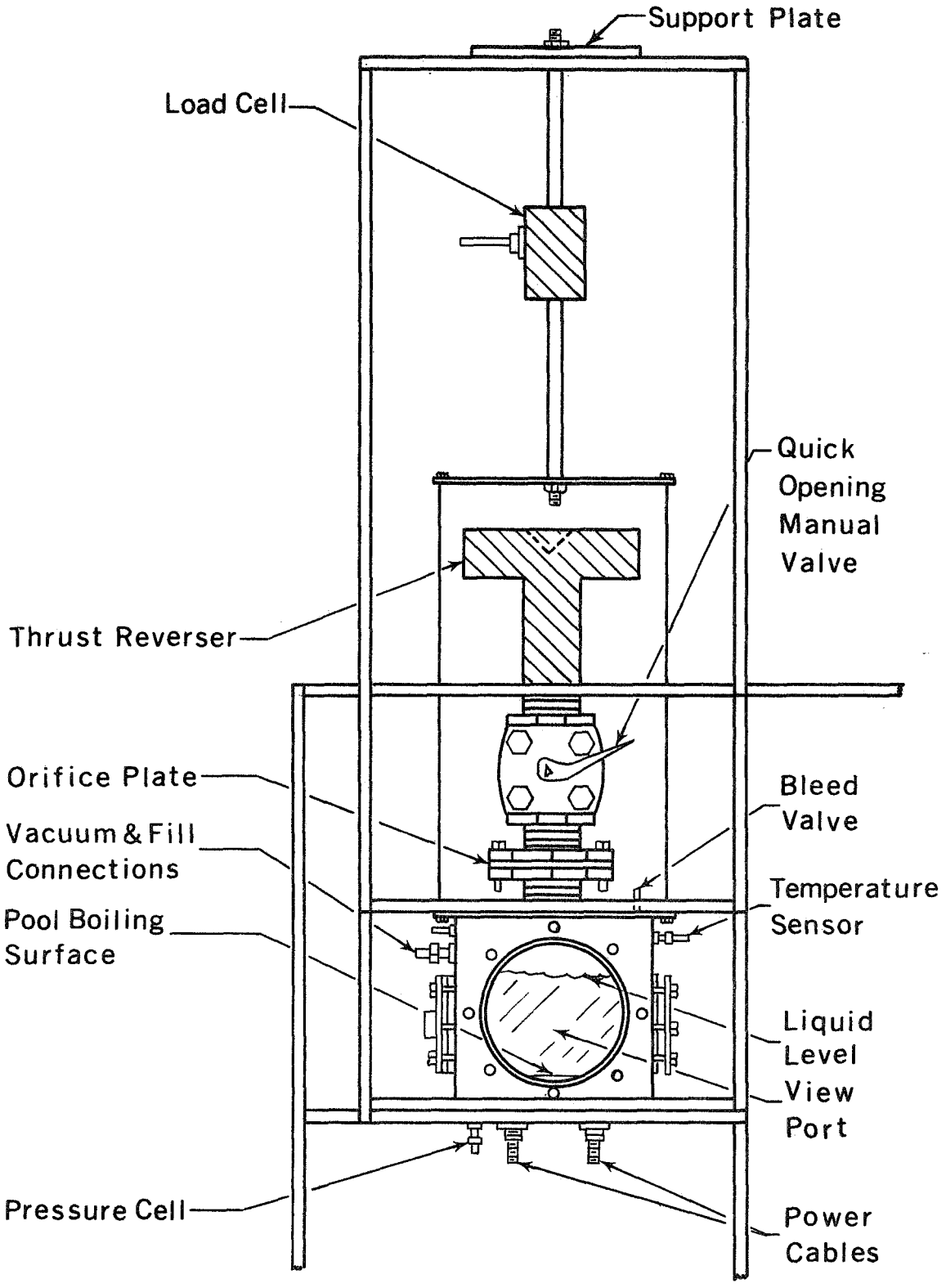

FIG. 12 POOL BOILING HEAT TRANSFER AND DEPRESSURIZATION FACILITY

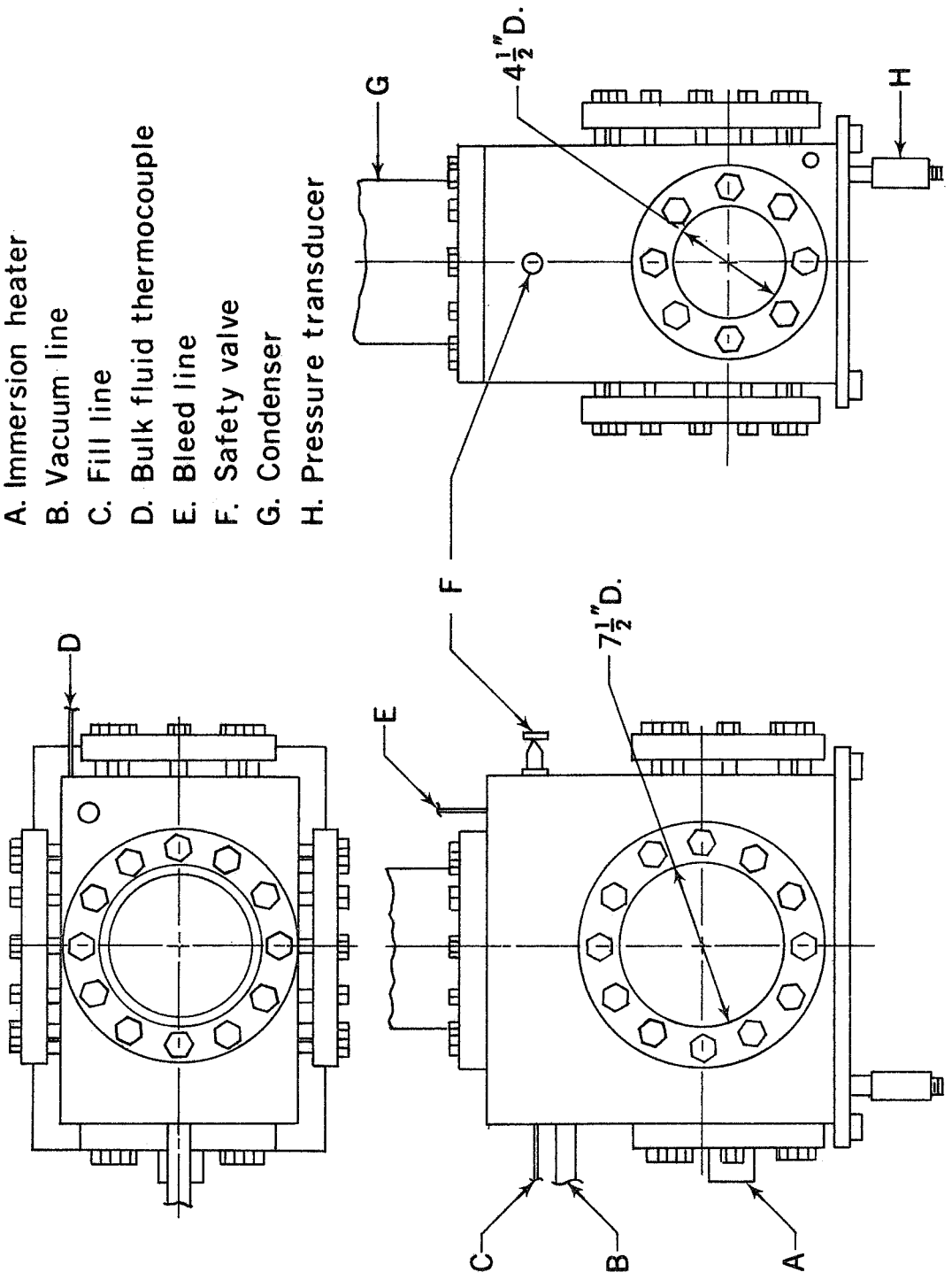

FIG. 13 BOILER ASSEMBLY

thereby reducing the test fluid contamination and pump down time. Openings are provided on three sides of the boiler for visual observation and auxiliary equipment. View ports are an optically clear pyrex glass, 1.25 inches thick, capable of withstanding pressures to 150 psia and temperatures of 450 degrees Fahrenheit. A side view of the boiler showing the test strip is given in Fig. 14. The various connections and instrumentation leading from the boiler are shown in Figs. 12 through 14.

The boiler was coupled to a vacuum system designed to maintain a pressure of 10-4 mm Hg. in a dry, tight enclosure of 2.5 cubic feet. A packless valve isolated the vacuum system from the boiler, thereby preventing damage to the vacuum pump when the boiler was under high pressure. The vacuum tank consists of a stainless steel cylindrical shell capped with 0.5 inch plates. A 9 KW heater extended into the tank from the bottom for use as a preheater and to facilitate the degassing process.

B. Orifice and Quick Release Valve

The rate of discharge from the boiler was controlled with various sizes of orifices installed in the outlet line. A variety of sharp edge orifices were investigated, ranging in diameter from 0.25 to 1 inch. A 3 inch, pipe size, McCannoseal quick-opening ball valve was installed above the orifice to produce a rapid depressurization. The ball valve, made of type 316 stainless steel, gives an obstruction-free flow with rapid opening speeds.

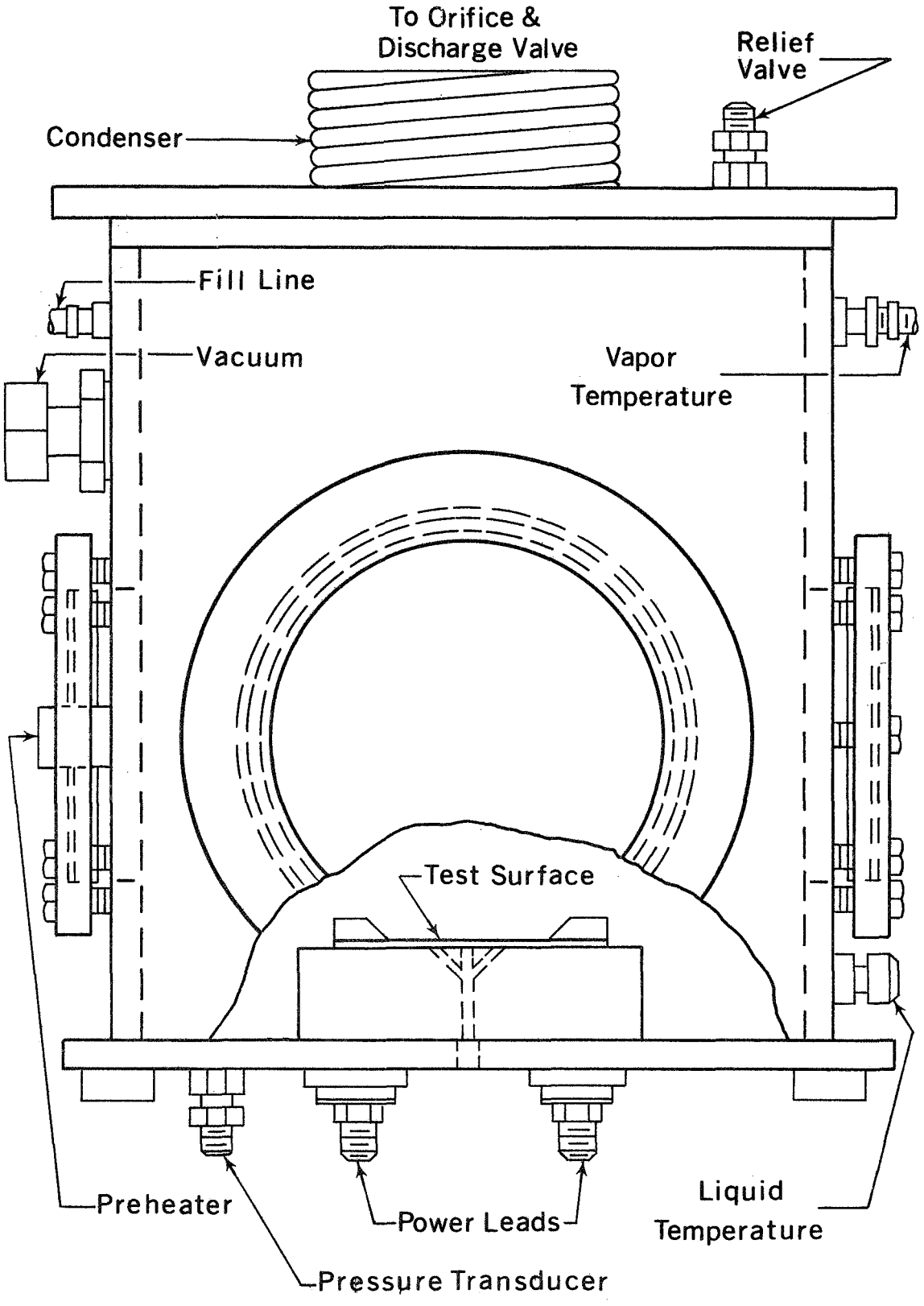

FIG. 14 VIEW OF BOILER WITH TEST SPECIMEN LOCATION

C. Fluid Purification Loop

The water purification facility supplies and maintains distilled, deionized water for the boiler. Degassed, distilled water was used in an attempt to minimize the effects of dissolved gas on the test results and to maintain constant fluid conditions. Once the storage tank was filled, the water was continuously treated by circulation through an Elgin Junior 120 deionizer. Water was admitted into the boiler by applying a small differential pressure between the supply tank and the boiler vessel.

D. Power Supply and Control

A low voltage, high amperage alternating current was used to heat the test specimen. The current was supplied to the test strip by a saturable reactor through a stepdown transformer. The reactor and transformer are capable of delivering alternating current power over a wide range with smooth adjustment to the test specimen. By controlling the direct current voltage to the saturable reactor, secondary outputs to the test strip ranging from 0 to 2.5 volts and 0 to 900 amperes, respectively, were possible.

E. Test Strip Support Block

The test strip support facility is an important aspect of the boiler. It consists of a high temperature resistant block of glass-phenolic which was machined to accommodate conductor electrodes and

thermocouple outlets. When installed, the support block and test strip are located in the center of the boiler base. Extra care was taken to insure that the copper conductor electrodes did not contact any part of the boiler surface. The test strip served as a heater - resistance element. A known current was applied to the element which, in turn, dissipated energy into the surrounding fluid. The test apparatus was designed to allow heat flow primarily to the fluid.

F. Instrumentation

The main parameters of interest to the present study include system pressure and temperature and heat flux. Instrumentation can therefore be divided into the following categories: pressure, temperature and electrical. Also, most of the instrumentation was used for both the steady-state investigation and for the transient discharge study.

Pressure is an important variable and accurate measurement was necessary in both parts of the investigation. An indication of the boiler static pressure was taken from a Bourdon tube gage installed in the control panel. The gage has a range of 0-100 psig, with an accuracy of $\pm$0.1 percent of full scale deflection or $\pm$0.5 psig. A valve was placed in the line between the boiler and gage to protect the gage during depressurization. A 1/8-inch O. D. stainless steel tube from the valve to the gage was coiled several times to serve as a heat exchanger. This protected the gage from excessive temperature damage. Swagelok stainless steel tube fittings were used

for all connections.

System pressure was continuously recorded during a transient by a recorder and pressure transducer system. The transducer, a BLH general purpose pressure cell, 0 to 100 psig, was located in the bottom of the boiler, as shown in Fig. 14. The connection was made through a 3 inch by 0.25 inch stainless steel pipe. By locating the pressure transducer where its cavity was filled with liquid, recorded fluctuations in pressure were minimized. The transducer was also placed in the vapor space at the top of the boiler during certain tests in order to determine the magnitude of fluctuations occurring during a transient.

Honeywell, 28 gage iron-constantan Megopak units were used to continuously monitor vapor and liquid temperatures, before, during, and after a discharge. One Megopak unit was located one-half-inch above the center of the test block and measured the liquid saturation temperature. The other was in the center of the vapor space above the boiling pool. A Leeds and Northrup type K-3 potentiometer and a Honeywell Model 1108 Visicorder were used to monitor the liquid and vapor temperatures.

Three thermocouples were employed on the test strip itself, as shown in Fig. 14. The 30 gage iron-constantan thermocouples were spot welded to the back of the test strip prior to installing the strip on the support block. A condenser type welder was used to attach the thermocouples to the test strip.

Recorded electrical data during a test were obtained from precision meters connected through panel mounted jacks. Voltage

across the test strip was measured by a Ballantine Model 300 G Vacuum Tube Voltmeter with a six position switch which gave a total range of 1 mv to 1000 v rms. The rated accuracy of the voltmeter was $\pm$3 percent of full scale deflection. Current through the test strip was measured with a Weston Model 370 ammeter with ranges 0-5 and 0-10 amperes, with rated accuracy of 0.25 percent of full scale deflection. A general Electric model 9JP1 current transformer with a ratio of 160 to 1 amperes was employed to reduce the current to a value readable on the meter.

A BLH precision load cell was installed to give a continuous reading of system weight during a test. Special precautions were necessary to insure correct operation of the load cell. A special frame and support plate were provided for suspending the vessel in tension beneath the cell. All couplings to the boiler were made flexible, and lateral restraints were provided to restrict the vessel to vertical movement only. Leveling screws beneath the boiler and vertical stiffeners in the support frame were included to suppress vibrations and motion resulting from the action of the quick opening valve and fluid sloshing during a discharge. The load cell itself is a precision instrument and is generally well suited for dynamic measurements. However, the thrust of the discharge will be measured unless proper precautions are taken. For this reason, a thrust reverser was constructed, as shown in Fig. 12. The reverser consisted of a 3 inch tee with a solid triangular insert (shown by the dotted lines in Fig. 12) to change the flow from vertical to horizontal, thus

negating the downward thrust force on the load cell. A few tests were conducted using the load cell. However, erratic behavior was encountered, and all attempts to correct this were to no avail. Subsequent tests were conducted without the load cell in the system.

Continuous recordings of system pressure and weight were obtained on Honeywell and Mosley two-channel strip chart recorders. A full recording of each variable was obtained. Also, an amplified trace of pressure was obtained during the initial period of the discharge. The purpose of the amplified recording was to make possible the detection of any pulsations in pressure during the initial phases of depressurization.

IV. SURFACE BOILING INVESTIGATIONS

The data presented in the present chapter were collected in an attempt to define the effects of surface condition and pressure on nucleate pool boiling. All of the data are for degassed, distilled water boiling from chemically etched 304 stainless-steel surfaces. The initial data at atmospheric pressure were collected as an aid in the study of existing correlation equations. Data were subsequently collected at various elevated pressures to illustrate the changes in wall superheat as a function of pressure.

A. Atmospheric Pressure Data

A description of the specimen preparation and test procedure is given in Appendix A. A summary of the specimen and test conditions is presented in Table 4.

The dilemma of any investigator studying pool boiling from prepared surfaces is the proper description of the surface. Some investigators specify preparation technique [20], and others use rms surface roughness as determined with a Profilometer [16,52]. The rms roughness does not adequately describe the surface if it is interpreted as an indication of microscopic roughness directly related to nucleation sites. The rms roughness does indicate macroscopically similar surfaces where the surface preparation is the same. Caution must be exercised when considering rms values. Chemically etched surfaces might indicate simi-

TABLE 4

SPECIMENS ETCHED WITH THIRTY-SEVEN PERCENT HYDROCHLORIC ACID

Specimen and Run	rms Roughness		Average rms Value	Etching Time (Hours)
	Transverse	Parallel		
76	31.5	32.0	32	6
77	25.0	27.6	27	4
78	30.2	30.8	30	5
79	41.8	42.5	42	7
80	16.3	15.8	16	2
82	41.7	42.3	42	7
83	30.4	30.5	30	5
84	27.8	28.3	27	4

lar rms values for different etching times. These surfaces, as can be seen from the data, may not give the same pool boiling results. Similar rms values for a fixed etching time can be used with some certainty to predict pool boiling performance from a surface. The same is generally true if other surface preparation techniques such as polishing or grinding are used.

It is not, however, realistic to compare surfaces with similar rms values which are prepared differently. A better comparison of boiling data can be made using the two surface descriptors--preparation technique and rms roughness. Both methods are employed in this study. Thus, the data presented in Figs. 15-17 must be considered in terms of surface preparation as well as rms surface roughness.

The Rohsenow equation

$$\frac{C_\ell\ (T_w - T_s)}{h_{\ell v}} = C_{sf}\left(\frac{q/A}{\mu_\ell h_{\ell v}}\sqrt{\frac{g_c\sigma}{g(\rho_\ell - \rho_v)}}\right)^r\left(\frac{C_\ell\mu_\ell}{k_\ell}\right)^s \qquad \text{(II-17)}$$

is used to correlate the data and determine values of C_{sf} and the exponent r. The coefficient C_{sf} accounts for the surface-liquid combination. The exponent of the heat flux term is the reciprocal of the slope of the least-squares fit correlation curve. The Prandtl number exponent s accounts to some degree for surface contamination. Rohsenow [88] suggested recently a value of 1.0 for the Prandtl exponent for boiling water. Previously a value of 0.8 to 2.0 was chosen arbitrarily. The use of the equation for boiling water by engineers to predict pool boiling heat transfer rates is limited by a scarcity of C_{sf} values. In addition it is observed from this study that there is a value for the heat flux exponent r concomitant with

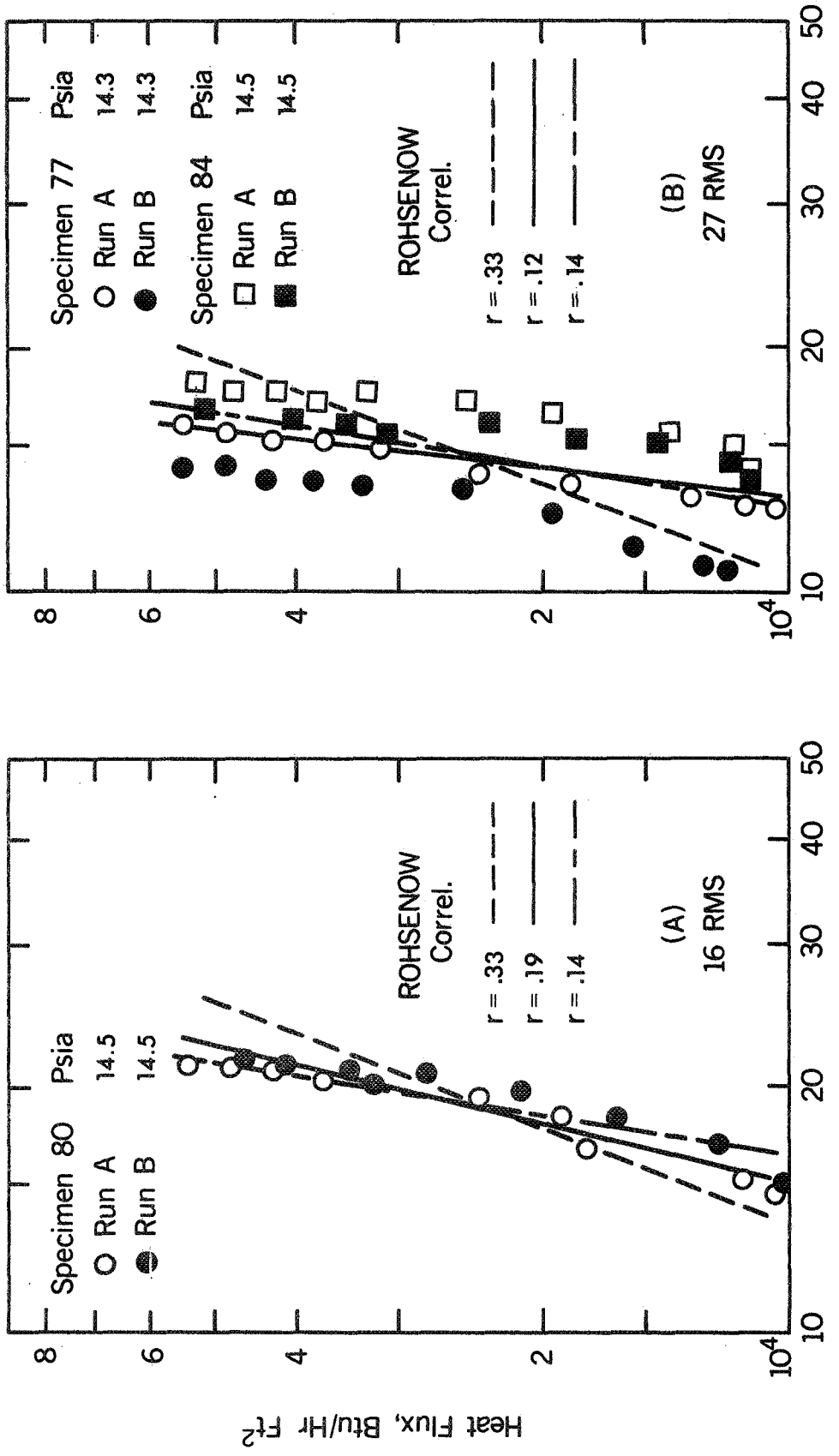

FIG. 15 HEAT FLUX VERSUS SUPERHEAT: ETCHED SURFACES [16 AND 27 RMS]

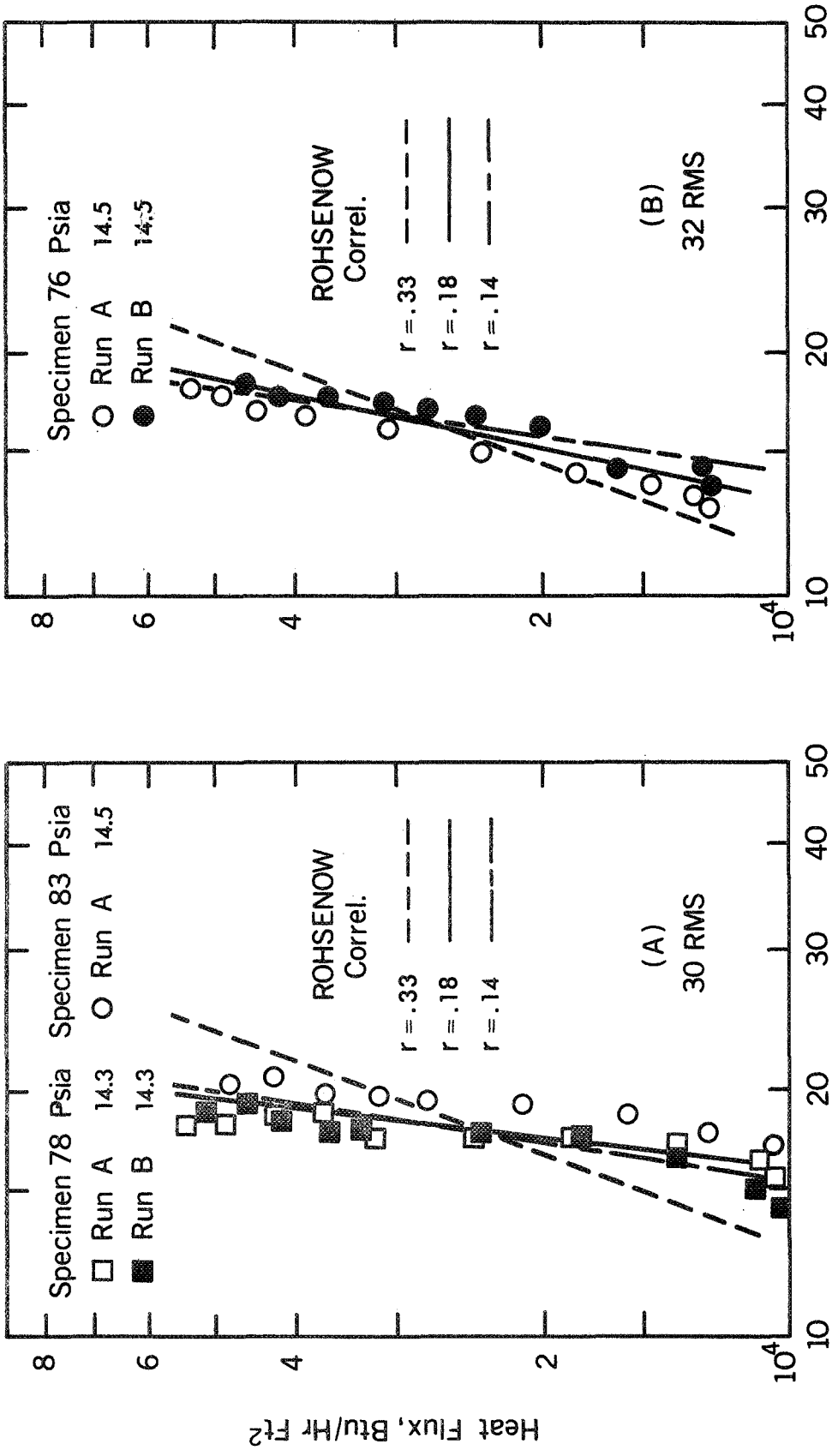

FIG. 16 HEAT FLUX VERSUS SUPERHEAT: ETCHED SURFACES [30 AND 32 RMS]

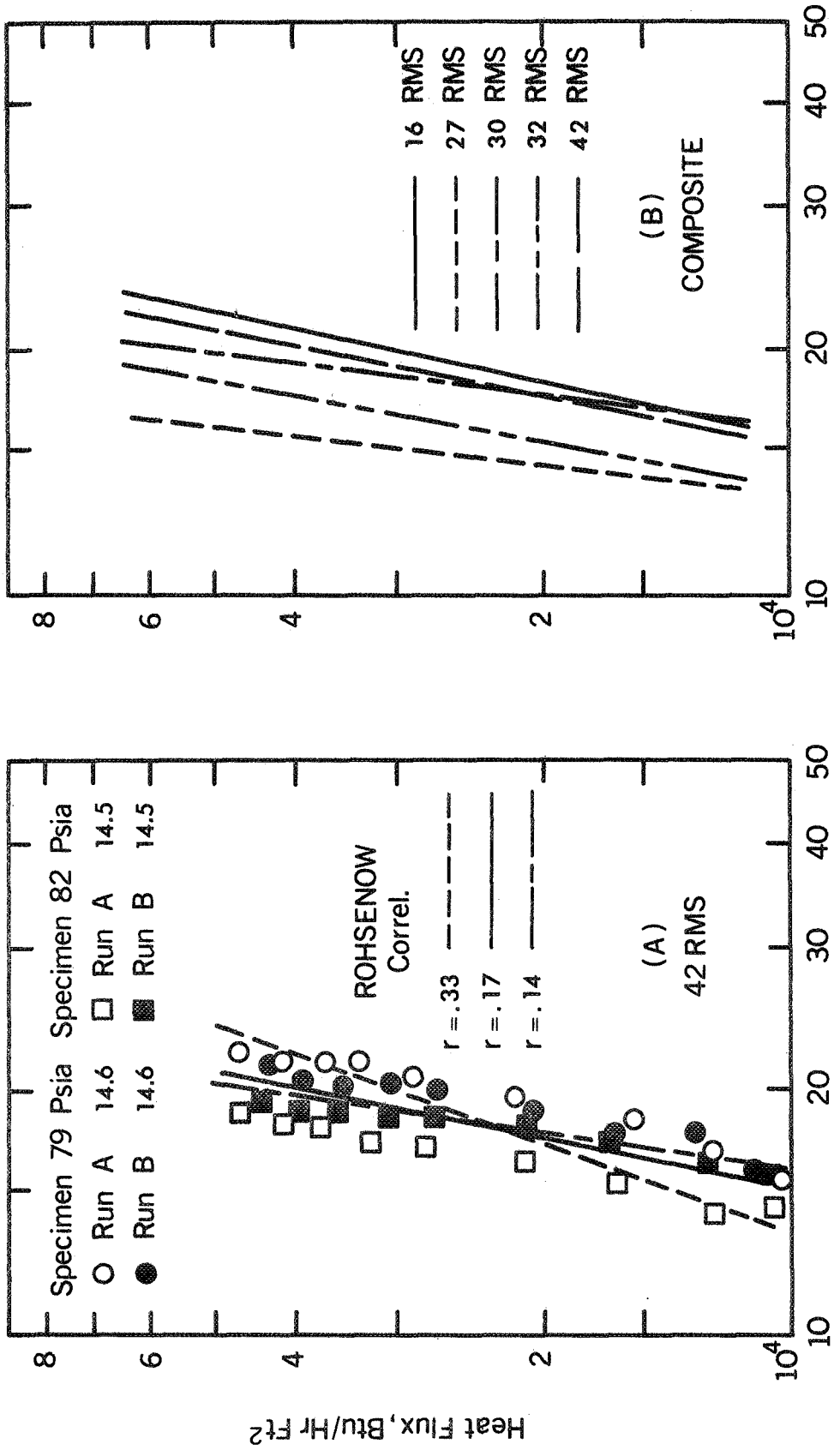

FIG. 17 HEAT FLUX VERSUS SUPERHEAT: ETCHED SURFACES [42 RMS AND COMPOSITE]

surface preparation technique. This statement is made on the basis of the disagreement between the slopes of the Rohsenow correlation equation using r = 0.33 and the least-squares fits of the data. The exponent r may also be a function of liquid-surface combination. These points are not discussed in the literature.

Some explanation of the determination of the exponent r in this study is in order since the value of the exponent is the reciprocal of the least-squares curve fit slope. Data were collected for several etched specimens. Some specimens were prepared in pairs, being subjected to the same immersion time; hence, data for each pair of surfaces are indicated on the same graph. The paired surfaces are referred to as companion specimens. There exists two possibilities for fitting the data of the companion specimens. Each specimen can be fitted separately, or the data for the pairs can be fitted using a least squares curve fit. Both techniques were used. However, only the least-squares curve fits for the pairs are shown in Figs. 15-17 by the dark solid lines. Naturally, where only one specimen is tested there is no pairing according to etching time. There then exist many ways to treat the Rohsenow correlation and the data. The three ways used in this study can be summarized as follows:

1. Values of C_{sf} were calculated from the data for each specimen and pair of specimens using r = 0.33 (Rohsenow's recommendation);
2. C_{sf} and the value of the exponent r were calculated for each specimen and each pair of specimens;
3. C_{sf} values were obtained for each specimen and pair of speci-

mens using an exponent r calculated by averaging the slopes of the least-squares fits for each specimen or each pair of specimens.

It should be noted that these C_{sf} values are averages for the data.

Tables 5 and 6 give the results of calculations made with the Rohsenow equation and the data shown in Figs. 15-17. The order of presentation of Figs. 15-17 is according to immersion time in the hydrochloric acid bath. The data scatter is not over $\pm$ 15% which is acceptable. This is extremely good when companion specimen data are compared since the data are for separate surfaces. An external error analysis of the experimental set-up as given in Appendix B yields an estimate of $\pm$ 13.2%. The tables give the values of C_{sf} and r for each specimen and for the paired specimens. The figures show the Rohsenow correlation with r values taken from Table 6. The dark solid line represents both the least-squares curve fit and the adjusted Rohsenow correlation with an appropriate value of r_2 taken from Table 6. Figure 17-B is a composite of the least squares fits for all of the paired specimens.

An inspection of the figures with respect to r values shows that, for the most part, the Rohsenow equation with r = 0.33 is not in good agreement with the least-squares curve fits. The Rohsenow correlation with adjusted values of r_2 and r_3 from Table 6 does show better agreement with the least squares fits as should be the case. The average value of r_3 equal to 0.14 from Table 6 appears to be satisfactory for all the data. This value is recommended for chemically etched surfaces prepared in the present manner rather than the value of 0.33 given by Rohsenow.

TABLE 5

COEFFICIENT C_{sf} AND EXPONENT r OF ROHSENOW EQUATION

FOR INDIVIDUAL ETCHED DATA

Specimen	rms	C_{sf_1}	r_1	C_{sf_2}	r_2	C_{sf_3}	r_3
80	16	0.0147	0.33	0.0122	0.19	0.0113	0.13
77	25	0.0108	0.33	0.0085	0.14	0.0084	0.13
78	30	0.0134	0.33	0.0099	0.10	0.0103	0.13
76	32	0.0121	0.33	0.0096	0.15	0.0090	0.13
79	42	0.0151	0.33	0.0123	0.19	0.0114	0.13
84	28	0.0128	0.33	0.0093	0.09	0.0098	0.13
83	30	0.0149	0.33	0.0110	0.12	0.0112	0.13
82	42	0.0136	0.33	0.0107	0.16	0.0103	0.13

TABLE 6

COEFFICIENT C_{sf} AND EXPONENT r OF ROHSENOW EQUATION

FOR ETCHED DATA GROUPED ACCORDING TO IMMERSION TIME

Specimen	rms	C_{sf_1}	r_1	C_{sf_2}	r_2	C_{sf_3}	r_3
77 & 84	27	0.0118	0.33	0.0089	0.12	0.0092	0.14
78 & 83	30	0.0139	0.33	0.0102	0.10	0.0107	0.14
79 & 82	42	0.0144	0.33	0.0115	0.17	0.0110	0.14
80	16	0.0147	0.33	0.0122	0.19	0.0114	0.14
16	32	0.0125	0.33	0.0103	0.18	0.0098	0.14

NOTE:
1. The exponent r_1 equals 0.33 (presented in the literature).
2. The exponent r_2 is calculated from the reciprocal of the slope of the individual least square curve fit for the rms in question.
3. The exponent r_3 is calculated from the reciprocal of the average of the slopes of the least square curve fits of the data for a particular preparation technique.

If all the data in Figs. 15-17 are considered, it can be seen that there is an increase and subsequent decrease in heat transfer with increasing immersion time and rms. This trend is shown in Fig. 17-B which presents a composite of the data in terms of least-squares curve fits of the various groups. It can be seen that rms is not directly correlated, which agrees with the work of Berenson [20]. The data show a trend similar to that obtained from mechanically polished surfaces [55] where heat transfer is not a function of macroscopic rms surface roughness. The data also indicate that the etching process improves nucleation from microscopic sites and then destroys the usefulness of the sites. The process may be cyclic. Consider two types of cavities subjected to etching--conical crevices and re-entrant cavities. The crevices would be deepened and widened with etching time. The re-entrant cavities would be changed to large pits. Both conditions would indicate an increase in roughness, and yet nucleation would be reduced. As the etching process continues, small crevices or cavities might be produced at the bottom of the old erosions which in turn should increase nucleation. The process could possibly continue through several cycles until the specimen is corroded beyond a state of usefulness.

Some final consideration should be given to the manipulation of the Rohsenow correlation. The value of 0.14 for the exponent may be altered somewhat for stainless steel specimens etched with hydrochloric acid when more data are available. This change in r would change the values of C_{sf} for each etching time. It is felt that 0.14 is a more representative value of r than 0.33 for the data collected. The values

of C_{sf} and corresponding r values in Tables 5 and 6 for the various specimens, either singularly or paired, represent coefficients and exponents applicable to situations where surfaces are similar to those in Table 4. The values of C_{sf} and r in Tables 5 and 6 apply only to stainless steel and water for the surface preparation technique and etching times indicated. It is clear that there exists a value of r for each preparation technique and possibly for each surface-liquid combination. The foregoing also points out the possibility that a similar analysis might be applied to pool boiling data from the literature for other surface-liquid combinations and surface preparation techniques. This is the case, as will be seen in Chapter V.

B. Elevated Pressure Data

Data collected for pool boiling of water from chemically etched surfaces at four pressures are presented to illustrate the changes in wall superheat as a function of pressure.

Deterioration of the epoxy used to bond the test specimen to the glass compound block limited useful data runs per specimen to approximately four. A total of 24 test runs on seven specimens are presented.

The data are presented as heat flux versus wall superheat. A least-squares curve fit is shown for each run as a dotted line; the Rohsenow correlation with r = 0.33 is shown as a solid line. The same scale is used in each graph for ease of comparison.

One objective of the study is analysis of the displacement of the nucleate boiling heat-flux-versus-superheat curve with pressure

changes. The displacement is clearly shown in Figs. 18 and 19 for stainless steel surfaces etched in hydrochloric acid for six hours. However, the information in Fig. 20 for a mill surface control specimen should be noted first. The curves are shifted toward a lower wall superheat with increasing pressure for a constant heat flux. This result is anticipated and is in agreement with current theory. The results for the chemically etched surfaces in Figs. 18 and 19 exhibit a backshift at higher pressures which is in complete contradiction with the theory. The shift occurs only for the 100 psia run in Fig. 18, whereas both the 50 and 100 psia runs are shifted to higher superheats in Fig. 19.

A period of time was allowed to elapse between consecutive runs on a single specimen. This usually amounted to at least one day. The 100 psia run in Fig. 18 was conducted on the sixth day while the 50 and 100 psia tests in Fig. 19 were on the fifth and fifteenth days of the sequence encountered during the present investigation. The dramatic shifts of the boiling curve in Fig. 19 are attributed in part to surface aging. This is true also of the shift shown in Fig. 18 and in Fig. 21 (for a specimen etched two hours).

A total of 23 additional tests on nine specimens etched from two to seven hours, were conducted. Although graphs of these runs are not shown, results are similar to those presented. No distinct correlation of the shift with the etching time has been discerned.

There is an indication that the pressure history influences the suspected aging effect. This is shown by the test sequence in Fig. 22.

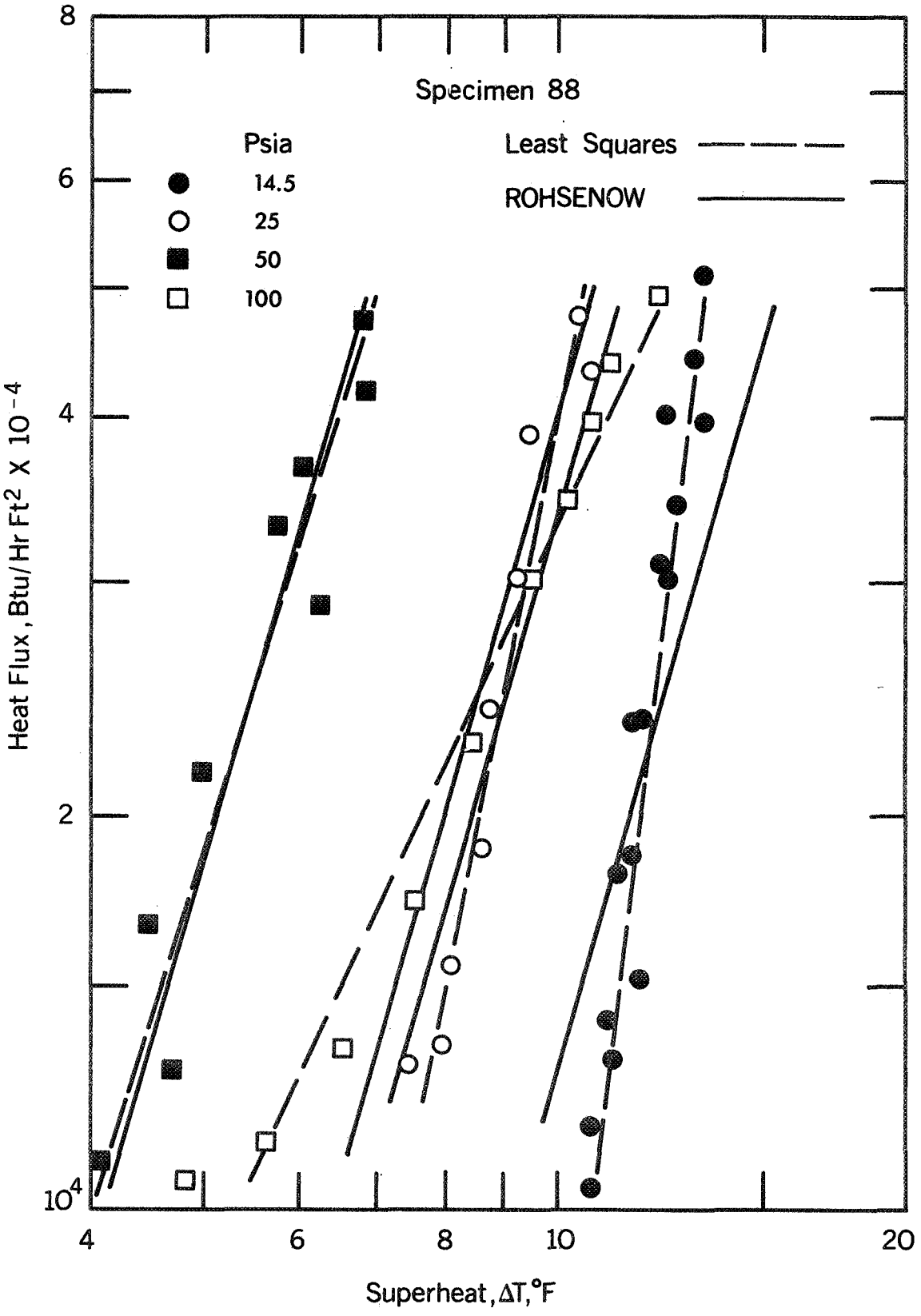

FIG. 18 HEAT FLUX VERSUS SUPERHEAT FOR A SPECIMEN ETCHED IN HCL FOR SIX HOURS [SPECIMEN 88]

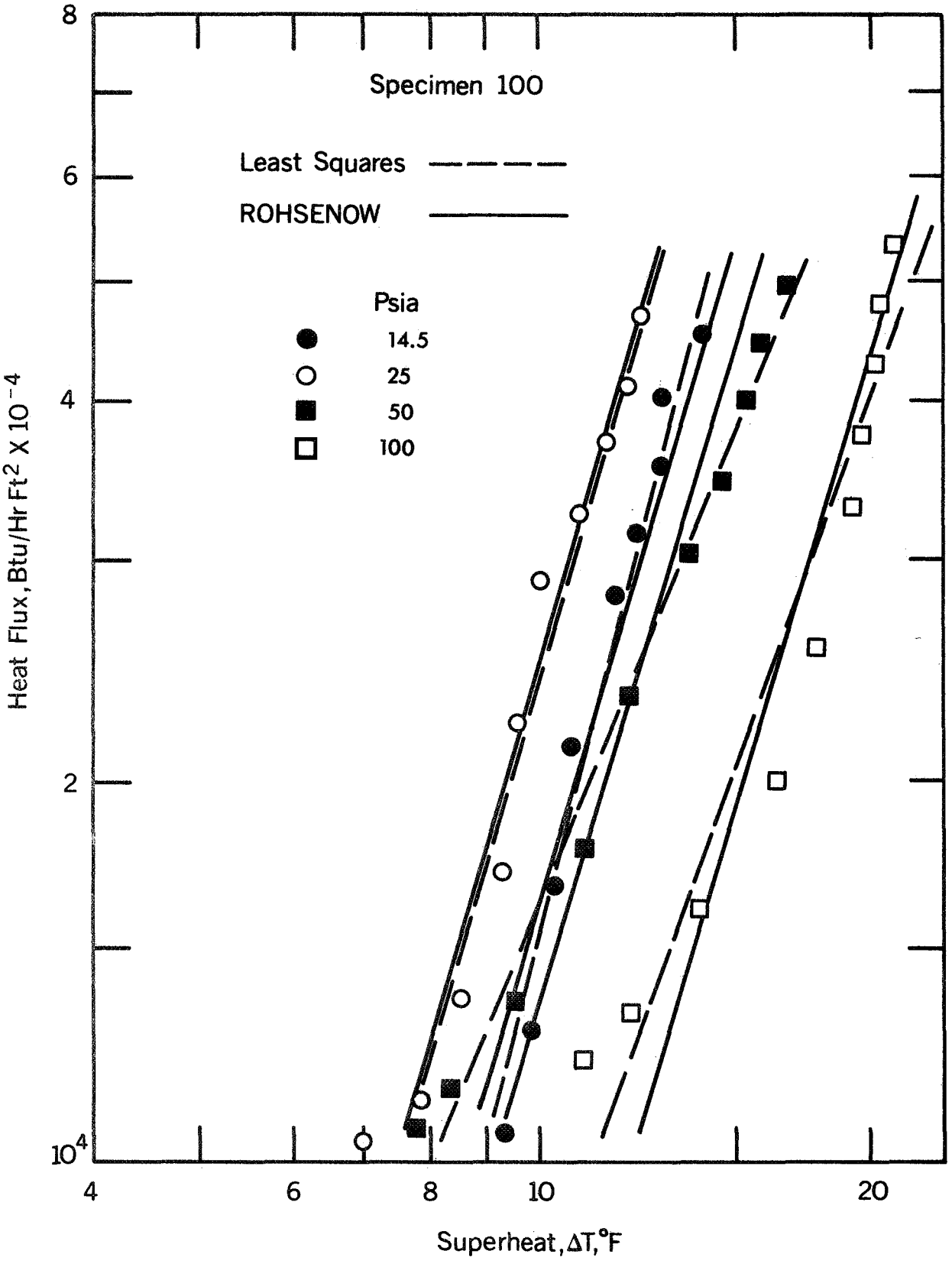

FIG. 19 HEAT FLUX VERSUS SUPERHEAT FOR A SPECIMEN ETCHED IN HCL FOR SIX HOURS [SPECIMEN 100]

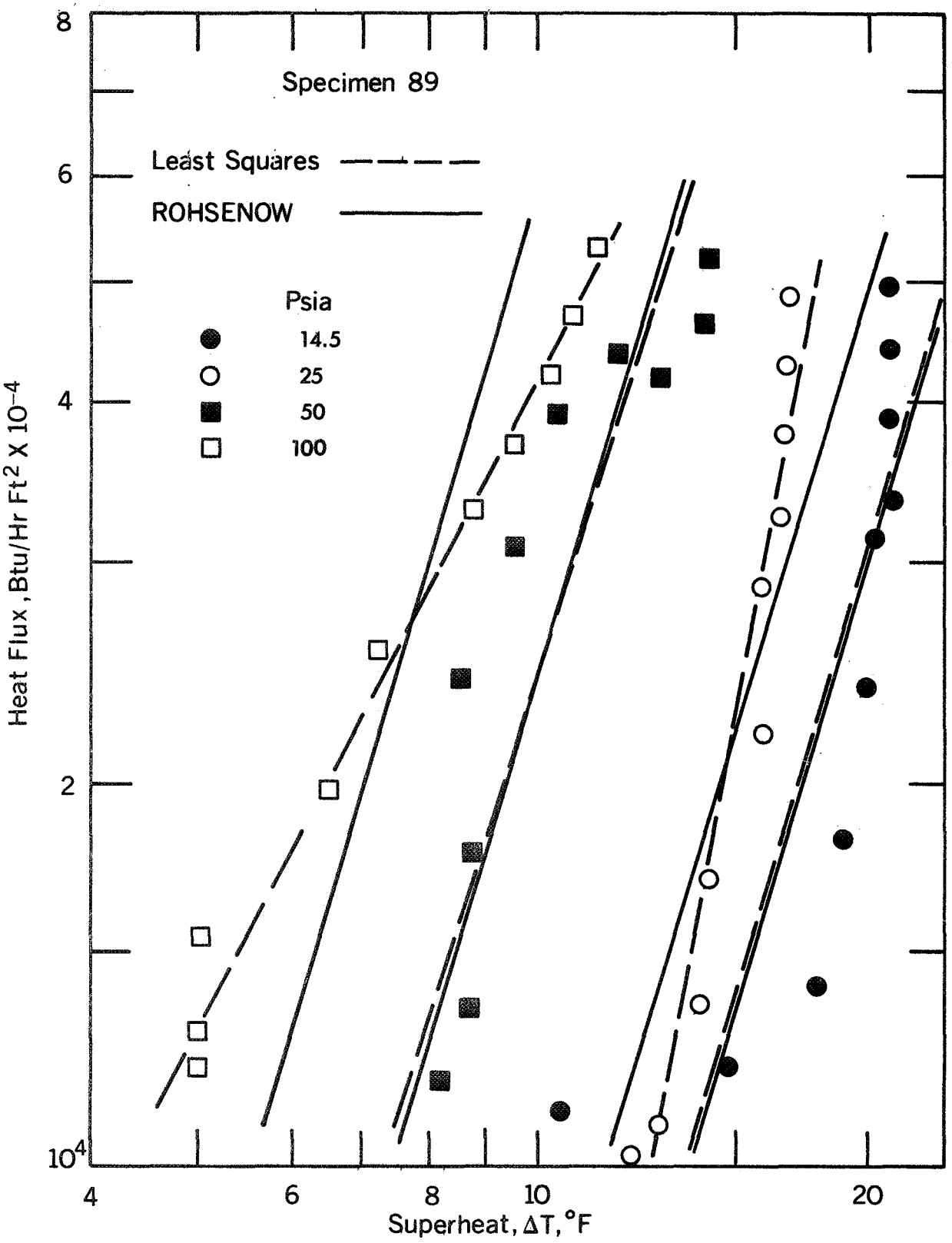

FIG. 20 HEAT FLUX VERSUS SUPERHEAT FOR A MILL SURFACE CONTROL SPECIMEN [SPECIMEN 89]

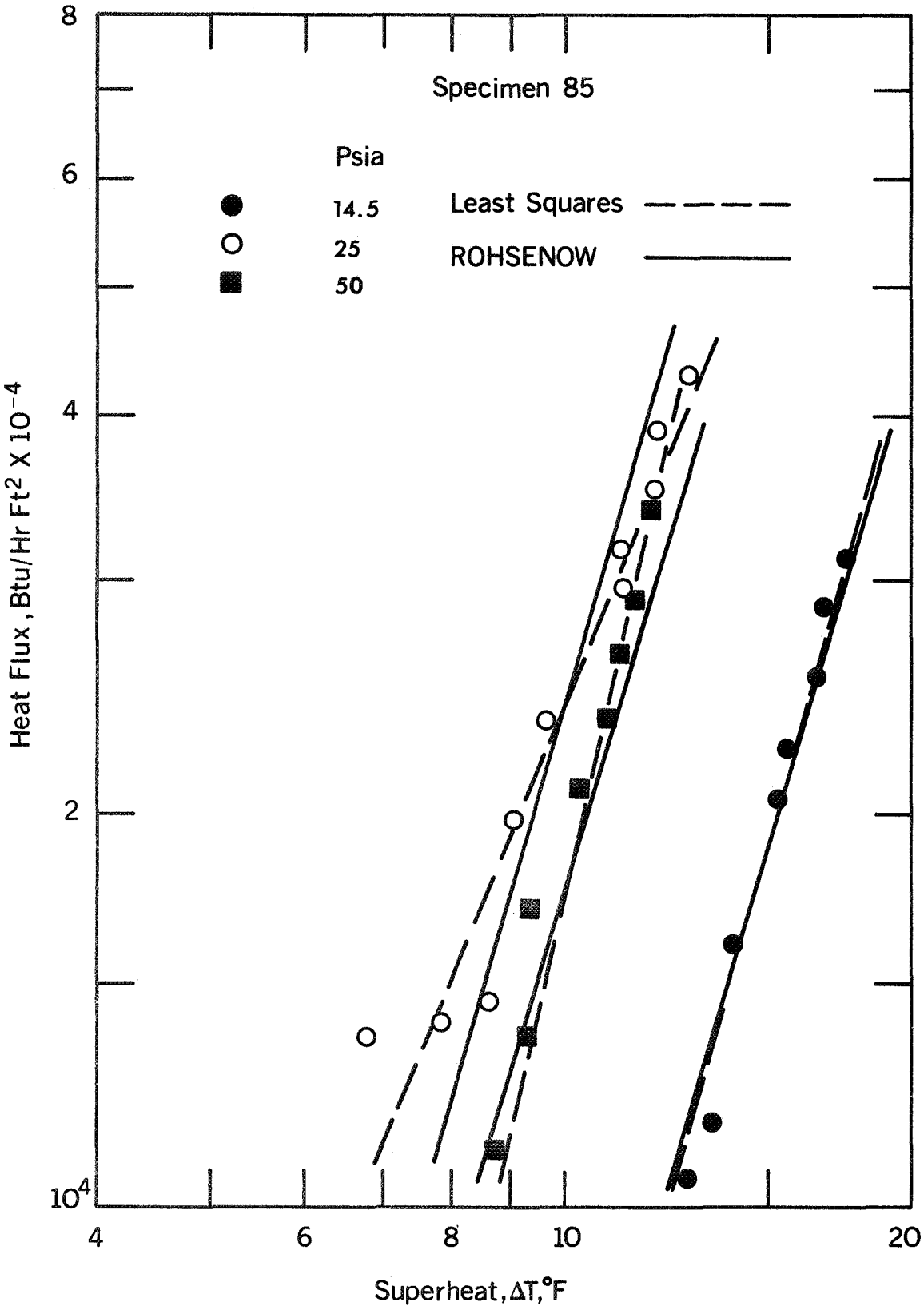

FIG. 21 HEAT FLUX VERSUS SUPERHEAT FOR A SPECIMEN ETCHED IN HCL FOR TWO HOURS [SPECIMEN 85]

The previous data (Figs. 18-21) were obtained in ascending order of pressure, with the test at atmospheric pressure conducted first in each sequence. However, the data in Fig. 22 were obtained with descending order of pressure in which the 100 psia run was conducted first. In this case, the shift was not obtained. The additional tests under similar conditions--not shown graphically--exhibit the same character with no backshift. The results indicate a severe aging effect for the specimens tested in the low-to-high pressure sequence. Also, it is possible that the coupled effects of pressure and aging somehow inhibit the vapor formation process.

A second facet of the data is a definite decrease in slope of the heat-flux-versus-superheat curve with increasing pressure. This is illustrated in Figs. 23 and 24 for a seven-hour and a two-hour etched specimen and also in Figs. 18-22. It may be noticed that at the lower pressures the least-squares estimate has a slope greater than the Rohsenow correlation. The Rohsenow equation is based on an exponent $r = 0.33$ and thus will have a constant slope throughout. The least-squares slopes are seen to decrease with increasing pressure until they are generally less than the Rohsenow slope at the higher pressures. Least-square and Rohsenow lines are not available for the atmospheric data of Fig. 23.

The decrease in slope with increasing pressure has not been analyzed in the literature. An effect which has not shown up strongly on other surfaces has probably been amplified by the sensitivity to pressures changes of the chemically etched surface. This suggests that

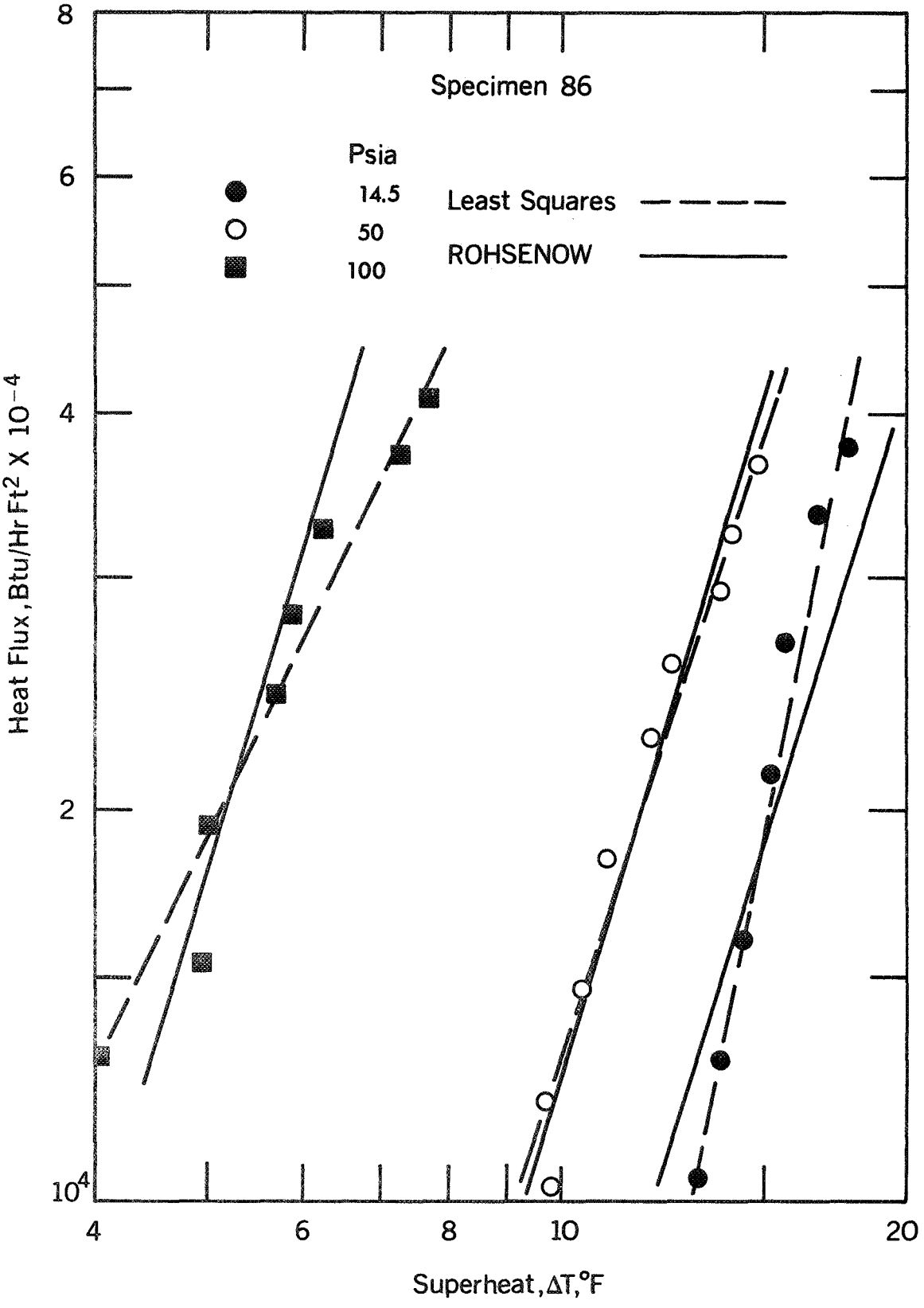

FIG. 22 HEAT FLUX VERSUS SUPERHEAT FOR A SPECIMEN ETCHED IN HCl FOR SIX HOURS [SPECIMEN 86]

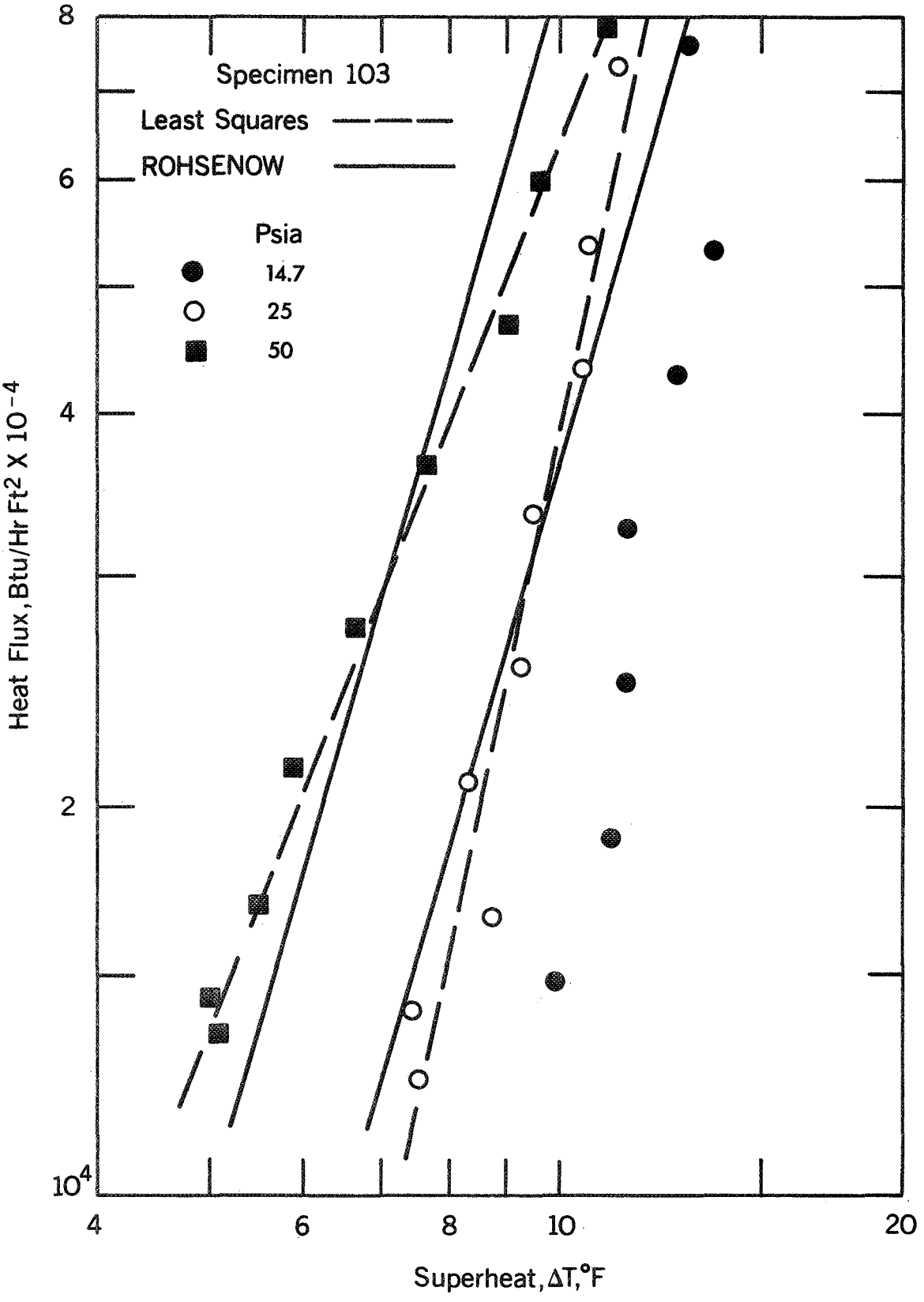

FIG. 23 HEAT FLUX VERSUS SUPERHEAT FOR A SPECIMEN ETCHED IN HCl FOR SEVEN HOURS [SPECIMEN 103]

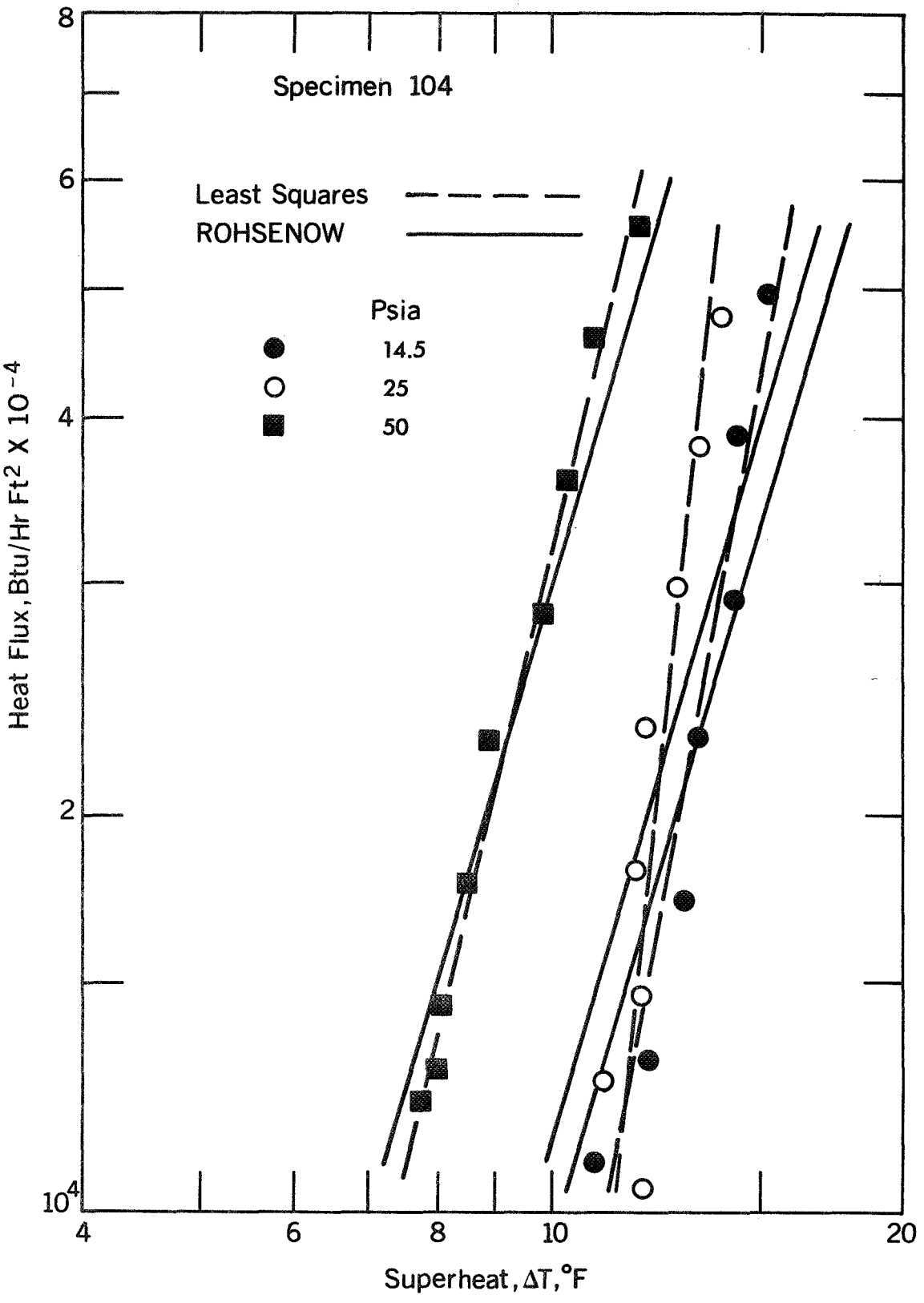

FIG. 24 HEAT FLUX VERSUS SUPERHEAT FOR A SPECIMEN ETCHED IN HCl FOR TWO HOURS [SPECIMEN 104]

for this type surface, the exponent r in the Rohsenow correlation may be a function of the system pressure. This point should be investigated further.

V. ANALYSIS OF POOL BOILING CORRELATIONS

Several design correlations have been advanced in recent years [9-12] but no equation correlating the general boiling case is available at present. The Rohsenow [3] correlation has been shown to be adjustable for a variety of boiling situations [89], but it does not consider every variable. The present chapter contains both an analysis and extension of the data and correlation procedures presented in the previous chapter. Previous analytical studies are analyzed and compared with the data. The comparisons in general illustrate the shortcomings of the correlation equations in the literature.

A. Evaluation of Constants for Rohsenow Correlation

The Rohsenow equation [3]

$$\frac{C_\ell\ (T_w - T_s)}{h_{\ell v}} = C_{sf}\left(\frac{q/A}{\mu_\ell h_{\ell v}}\sqrt{\frac{g_c\sigma}{g(\rho_\ell - \rho_v)}}\right)^r\left(\frac{C_\ell\mu_\ell}{k_\ell}\right)^s \qquad \text{(II-17)}$$

is the most noted method of reducing and correlating experimental data in the regime of nucleate pool boiling. The equation accounts for the pool boiling phenomenon in terms of fluid properties, the coefficient C_{sf} and the exponents r and s. The coefficient is supposed to account for surface-liquid combination, the exponent s accounts for surface cleanliness and r represents the reciprocal of the least-squares slope for the heat flux-superheat data in question. The equation is unique

in that only one set of experimental values of q/A and ΔT is necessary to determine the coefficient C_{sf}. Once C_{sf} is obtained the behavior of a given surface-liquid combination can be determined for other values of ΔT and any other pressure and/or gravitational field. The Prandtl number exponent, s, varies from 0.8 to 2.0. Rohsenow initially recommended a value of 1.7 for clean surfaces for all surface-liquid combinations. However, Rohsenow has recently recommended that this value be changed to 1.0 [88] for water.

Rohsenow [3] determined the exponent of the heat flux term, r, to be 0.33 by analysis of experimental data in the literature. The data in the previous chapter supports the contention that the heat flux exponent may vary for different types of surface-liquid combinations and surface preparation techniques. Prima facie the value of 0.33 has been accepted in the literature in the past.

The premise that r in the Rohsenow equation is a function of surface preparation and surface-liquid combination was investigated by cross-correlating pool boiling data from the literature. The data collected [3,15,16,18-21,29,32,52,90-93] and summarized in Appendix C were grouped according to the surface-liquid combination and preparation technique. Surface-liquid combinations included

1. Water - stainless steel
2. Water - copper
3. n-pentane - copper
4. n-pentane - nickel
5. n-pentane - inconel

6. n-pentane - zinc

7. Carbon tretrachloride - copper

and the different preparation techniques investigated were

1. Polishing and grinding

2. Chemical etching

3. Artificial scoring and pitting

4. Lapping

5. Coating

Heat flux and superheat data for all runs on each surface were fitted with a least-squares curve fitting technique. Errors in both ordinate and abscissa were assumed. In addition, the data for all of the surfaces prepared with a particular preparation technique were fitted for each surface-liquid combination. The fitted curves [94]--in the interest of brevity--are not shown.

The Rohsenow equation, Eq. (II-17) was used with the least-squares curve fits of the data for each surface and grouping of surfaces to obtain

1. Values of C_{sf_1} for each surface: A value of $r_1 = 0.33$ was used and both values are shown in Table 7.

2. Values of C_{sf_2} and r_2 for each surface: The value of r_2 was the reciprocal of the slope of the least-squares fit for each surface, and both values are shown in Table 7.

3. Values of C_{sf_3} and r_3 for each surface: The value of r_3 was the reciprocal of the average of the slopes of the least-squares curve fits for the data of a particular preparation technique for a given surface-liquid combination. Both values are shown in Table 7.

4. Values of $\overline{C_{sf_3}}$ (the bar indicates the average value) and r_3 for each grouping of data according to preparation technique for a certain surface-liquid combination: The value of r_3 was calculated as before, and $\overline{C_{sf_3}}$ is based

TABLE 7

EVALUATION OF CONSTANTS FOR ROHSENOW EQUATION

Run Numbers	Surface Preparation	C_{sf_1}	r_1	C_{sf_2}	r_2	C_{sf_3}	r_3
A.	n-Pentane on Copper Polished with Emery Paper [16]						
10-13	4/0 Emery	0.0141	0.33	0.0129	0.10	0.0129	0.10
14,15	4/0 Emery	0.0164	0.33	0.0156	0.11	0.0156	0.10
B.	n-Pentane on Nickel Polished with Emery Paper [16]						
1	4/0 Emery	0.0151	0.33	0.0146	0.18	0.0145	0.13
2	2/0 Emery	0.0133	0.33	0.0129	0.10	0.0129	0.13
3	0 Emery	0.0127	0.33	0.0112	0.12	0.0112	0.13
4	1 Emery	0.0114	0.33	0.0103	0.12	0.0104	0.13
5	2 Emery	0.0108	0.33	0.0097	0.18	0.0094	0.13
C.	Water on Copper Polished with Emery Paper [29,32]						
I-1,I-2,I-3	4/0 Emery	0.0142	0.33	0.0132	0.24	0.0119	0.10
II-1	3/0 Emery	0.0135	0.33	0.0109	0.13	0.0106	0.10
III-1,III-2	2/0 Emery	0.0126	0.33	0.0102	0.15	0.0097	0.10
IV-1,IV-2	0 Emery	0.0115	0.33	0.0087	0.09	0.0088	0.10
V-1	1 Emery	0.0107	0.33	0.0077	0.11	0.0077	0.10
VI-1,VI-2	2 Emery	0.0092	0.33	0.0067	0.06	0.0070	0.10
VII-1	No. 140 Mesh Carborundum	0.0090	0.33	0.0062	0.06	0.0065	0.10
1	4/0 Emery	0.0152	0.33	0.0150	0.19	0.0150	0.10
D.	Carbon Tetrachloride on Copper Polished with Emery Paper [29]						
I	4/0 Emery	0.0074	0.33	0.0092	0.20	0.0070	0.09
IV	0 Emery	0.0075	0.33	0.0068	0.13	0.0066	0.09
VI	2 Emery	0.0063	0.33	0.0053	0.05	0.0054	0.09
E.	n-Pentane on Copper, Lapped with Grit E [20]						
16,17	#120 E Grit	0.0037	0.33	0.0040	0.20	0.0042	0.21
7,8,9	#120 E Grit	0.0057	0.33	0.0062	0.21	0.0062	0.21
10	#120 E Grit	0.0050	0.33	0.0053	0.20	0.0053	0.21

Run Numbers	Surface Preparation	C_{sf_1}	r_1	C_{sf_2}	r_2	C_{sf_3}	r_3
	F. n-Pentane on Nickel, Lapped with Grit D [20]						
39	#160 D Grit	0.0043	0.33	0.0050	0.20	0.0050	0.20
	G. n-Pentane on Inconel, Lapped with Grit D [20]						
34	#160 D Grit	0.0072	0.33	0.0075	0.47	0.0075	0.47
	H. Carbon Tetrachloride on Copper, Lapped with Grit E [20]						
19,20	#120 E Grit	0.0331	0.33	0.0034	0.23	0.0034	0.23
	I. n-Pentane on Nickel with Mirror Finish [20]						
38		0.0154	0.33	0.0135	0.47	0.0135	0.47
	J. n-Pentane on Copper with Mirror Finish [20]						
2,3		0.0171	0.33	0.0146	0.48	0.0146	0.48
	K. n-Pentane on Inconel with Mirror Finish [20]						
33,36		0.0180	0.33	0.0176	0.35	0.0176	0.35
	L. n-Pentane on Copper Rubbed with Emery [20]						
31	320 Emery	0.0093	0.33	0.0097	0.29	0.0093	0.33
32	60 Emery	0.0058	0.33	0.0054	0.39	0.0058	0.33
	M. Water on Copper with Mirror Finish [21]						
A		0.0091	0.33	0.0142	0.60	0.0142	0.60
	N. Water on Copper, Mirror Finish Scored by Steel [21]						
B	Scratches 1" Apart	0.0073	0.33	0.0123	0.65	0.0136	0.71

Run Numbers	Surface Preparation	C_{sf_1}	r_1	C_{sf_2}	r_2	C_{sf_3}	r_3
N. Water on Copper, Mirror Finish Scored by Steel [21] (cont'd)							
C	Scratches 1/2" Apart	0.0071	0.33	0.0115	0.66	0.0123	0.71
D	Scratches 1/4" Apart	0.0062	0.33	0.0133	0.89	0.0104	0.71
E	Scratches 1/8" Apart	0.0072	0.33	0.0113	0.68	0.0117	0.71
O. Water on Stainless Steel, Ground and Polished [52]							
108,110,111	Ground	0.0065	0.33	0.0063	0.30	0.0069	0.37
119,120	Ground	0.0081	0.33	0.0080	0.33	0.0085	0.37
101-104	Ground	0.0090	0.33	0.0101	0.42	0.0095	0.37
112,113,114	Polished	0.0100	0.33	0.0133	0.52	0.0107	0.37
P. Water on Stainless Steel, Surface Milled [93]							
1	Smooth	0.0215	0.33	0.0198	0.27	0.0198	0.27
Q. Water on Stainless Steel, Surface Milled [93]							
3-P	Pitted	0.0173	0.33	0.0200	0.41	0.0200	0.41
R. Water on Stainless Steel with Teflon on the Surface [93]							
7-ST	Smooth	0.0066	0.33	0.0097	0.48	0.0087	0.44
3-PT	Pitted	0.0053	0.33	0.0081	0.58	0.0069	0.44
2-PT	Pitted	0.0054	0.33	0.0059	0.36	0.0072	0.44
S. n-Pentane on Zinc-Crystals With Polished Surface [15]							
1	Smooth	0.0088	0.33	0.0086	0.58	0.0086	0.58
T. Water on Paraffin-Treated Copper, Polished with Emery Paper [19]							
	3/0 Emery w Cavities	0.0138	0.33	0.0139	0.26	0.0140	0.20

Run Numbers	Surface Preparation	C_{sf_1}	r_1	C_{sf_2}	r_2	C_{sf_3}	r_3
	T. Water on Paraffin-Treated Copper, Polished with Emery Paper [19] (cont'd)						
	3/0 Emery w/o Cavities	0.0157	0.33	0.0153	0.16	0.0153	0.20
	U. Water on Stainless Steel, Polished with Emery Paper [91]						
1-A,B,C	600 Emery	0.0140	0.33	0.0140	0.33	0.0129	0.26
2-A,B,C	600 Emery	0.0155	0.33	0.0153	0.32	0.0141	0.26
3-A	600 Emery	0.0149	0.33	0.0139	0.28	0.0134	0.26
4-A,B,C	320 Emery	0.0120	0.33	0.0107	0.24	0.0110	0.26
5-A,B,C	320 Emery	0.0136	0.33	0.0125	0.26	0.0124	0.26
6-A,B,C	320 Emery	0.0127	0.33	0.0113	0.23	0.0117	0.26
7-A,B,C	80 Emery	0.0128	0.33	0.0114	0.23	0.0117	0.26
8-B,C	80 Emery	0.0106	0.33	0.0098	0.26	0.0097	0.26
9-A,B,C	36 Emery	0.0120	0.33	0.0105	0.22	0.0109	0.26
10-A,B,C	36 Emery	0.0136	0.33	0.0120	0.23	0.0124	0.26
	V. Water on Stainless Steel, Etched with 37% Hydrochloric Acid [90]						
76-A,B	Etched 6 Hr	0.0121	0.33	0.0096	0.15	0.0090	0.13
77-A,B	Etched 4 Hr	0.0108	0.33	0.0085	0.14	0.0084	0.13
78-A,B	Etched 5 Hr	0.0134	0.33	0.0099	0.10	0.0103	0.13
79-A,B	Etched 7 Hr	0.0151	0.33	0.0123	0.19	0.0114	0.13
80-A,B	Etched 2 Hr	0.0147	0.33	0.0122	0.19	0.0113	0.13
82-A,B	Etched 7 Hr	0.0136	0.33	0.0107	0.16	0.0103	0.13
83-A	Etched 5 Hr	0.0149	0.33	0.0110	0.12	0.0112	0.13
84-A,B	Etched 4 Hr	0.0128	0.33	0.0093	0.09	0.0098	0.13

NOTE:
1. The exponent r_1 equals 0.33 (presented in the literature).
2. The exponent r_2 is calculated from the reciprocal of the slope of the individual least square curve fit for the surface in question.
3. The exponent r_3 is calculated from the reciprocal of the average of the slopes of the least square curve fits of the data for a particular preparation and liquid surface combination.

on the assumption that the variation in a preparation technique is negligible. The results of these calculations are given in Table 8.

5. Values of $\overline{C_{sf_1}}$ and r_1 for each grouping of data according to the preparation technique for a certain surface-liquid combination: The value of $r_1 = 0.33$ was used as before, and $\overline{C_{sf_1}}$ is based on the assumption that variation in a preparation technique is negligible. The results of these calculations are given in Table 8.

Appropriate values of the exponent s = 1.0 or 1.7 were used in the calculations with Eq. (II-17).

Evidence to support the premise that r values do vary can be seen from Tables 7 through 9 and graphically in Figs. 25 through 30. Table 9 shows the deviation of r_3 values for the grouped specimens and an r_1 value of 0.33 from the r_2 values calculated for each specimen. The table indicates that 68.3 percent of the r_3 values calculated for the grouped data are within approximately 30 percent of the r_2 values for the individual specimens. The r_1 value of 0.33 is within approximately 30 percent of the r_2 values of the individual specimens for only 15.8 percent of the cases examined. Table 10 shows the deviation of $\overline{C_{sf_1}}$ and $\overline{C_{sf_3}}$ values from C_{sf_2} values for each specimen. As one can see after considering Tables 7 through 10, $\overline{C_{sf_3}}$ or C_{sf_3} and r_3 values can be used with the Rohsenow equation to get a better representation of the data than is possible with $\overline{C_{sf_1}}$ or C_{sf_1} and r_1 values.

It is suggested that the tabulated values of r_3 and $\overline{C_{sf_3}}$ or C_{sf_3} be used with the Rohsenow correlation for corresponding surface-liquid combinations and preparation techniques. $\overline{C_{sf_3}}$ values are tabulated for those who may argue that accounting for slight variations in surface

TABLE 8

SUMMARY OF COEFFICIENTS AND EXPONENTS FOR THE ROHSENOW EQUATION

Reference	Liquid-Surface Combinations	$\overline{C_{sf_1}}$	r_1	$\overline{C_{sf_3}}$	r_3	q/A Range Btu/hr ft^2
16	n-Pentane on Emery Polished Copper	0.0154	0.33	0.0145	0.10	3,900 - 28,275
16	n-Pentane on Emery Polished Nickel	0.0127	0.33	0.0117	0.13	2,250 - 36,000
29, 32	Water on Emery Polished Copper	0.0128	0.33	0.0109	0.10	8,800 - 260,000
29	Carbon Tetrachloride on Emery Polished Copper	0.0070	0.33	0.0063	0.09	4,140 - 66,250
19	Water on Emery Polished, Paraffin Treated Copper	0.0147	0.33	0.0146	0.20	14,000 - 300,000
20	n-Pentane on Lapped Copper	0.0049	0.33	0.0054	0.21	6,600 - 90,000
20	n-Pentane on Emery Rubbed Copper	0.0074	0.33	0.0074	0.33	13,500 - 100,000
21	Water on Scored Copper	0.0068	0.33	0.0117	0.71	1,800 - 52,000
52	Water on Ground and Polished Stainless Steel	0.0080	0.33	0.0085	0.37	8,600 - 53,000
93	Water on Teflon Pitted Stainless Steel	0.0058	0.33	0.0076	0.44	600 - 84,000
90	Water on Chemically Etched Stainless Steel	0.0133	0.33	0.0102	0.13	9,202 - 54,819
91	Water on Mechanically Polished Stainless Steel	0.0132	0.33	0.0121	0.26	8,957 - 57,422

TABLE 9

TABULATION OF PERCENT DEVIATION

OF r_3 AND r_1 FROM r_2 VALUES

Percent Deviation of r_3 and r_1 Values From r_2 Values (r_3 Values for Grouped Specimens Only)	Percent of r_3 Values Within Deviation Percentage	Percent of r_1 Values Within Deviation Percentage
10%	36.8	5.3
20%	57.8	15.8
30%	68.3	15.8
40%	81.5	36.8
50%	92.0	42.0
> 50%	8.0	58.0

TABLE 10

TABULATION OF PERCENT DEVIATION

OF $\overline{C_{sf_3}}$ AND $\overline{C_{sf_1}}$ From C_{sf_2} Values

Percent Deviation of $\overline{C_{sf_3}}$ and $\overline{C_{sf_1}}$ Values From C_{sf_2} Values	Percent of $\overline{C_{sf_3}}$ Values Within Deviation Percentage	Percent of $\overline{C_{sf_1}}$ Values Within Deviation Percentage
10%	42.6	25.9
20%	66.7	42.5
30%	83.3	66.6
40%	92.6	77.7
50%	96.3	88.2
> 50%	3.7	11.2

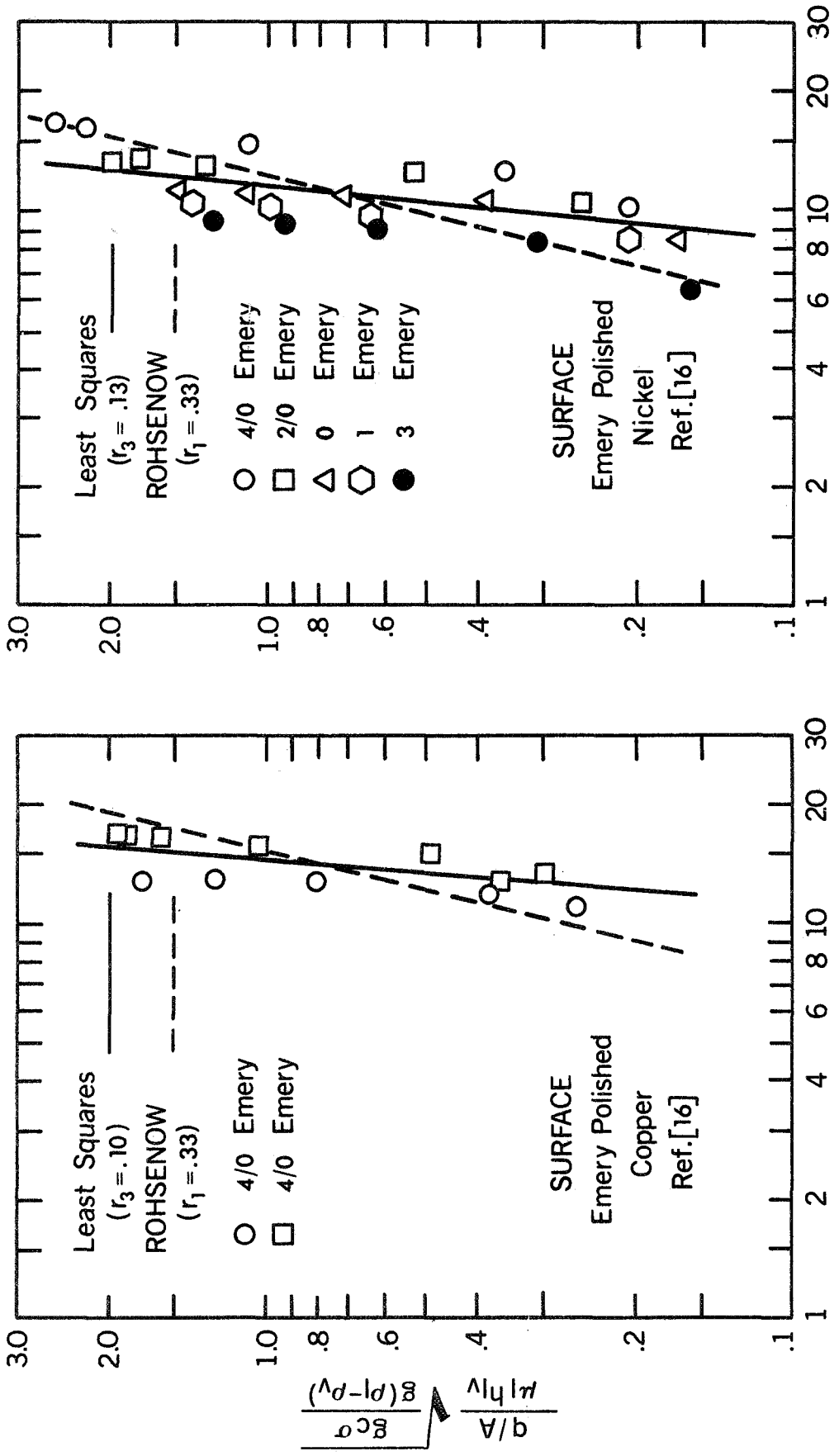

FIG. 25 CORRELATION OF POOL BOILING DATA FOR N-PENTANE

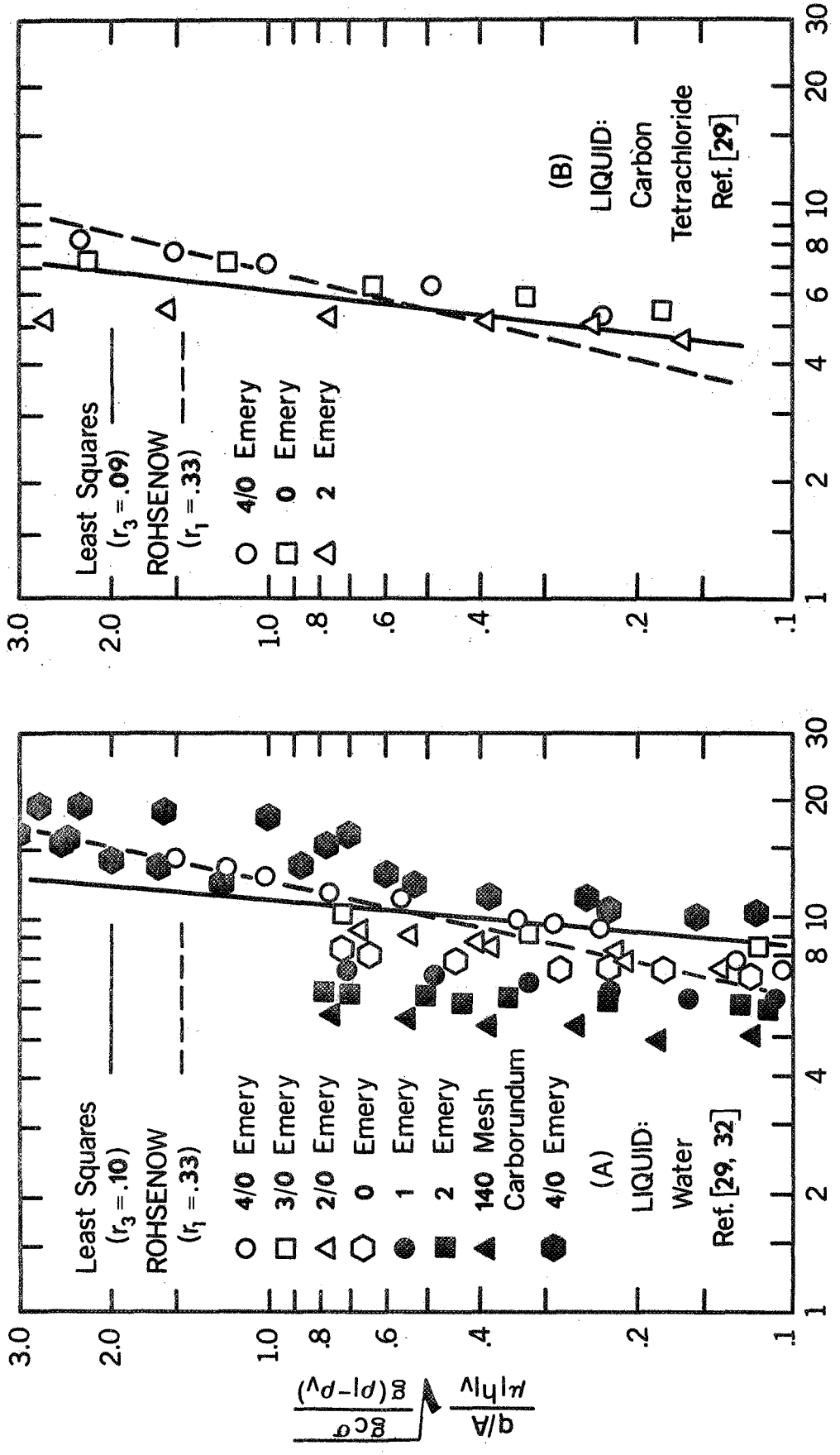

FIG. 26 CORRELATION OF POOL BOILING DATA FOR EMERY POLISHED COPPER

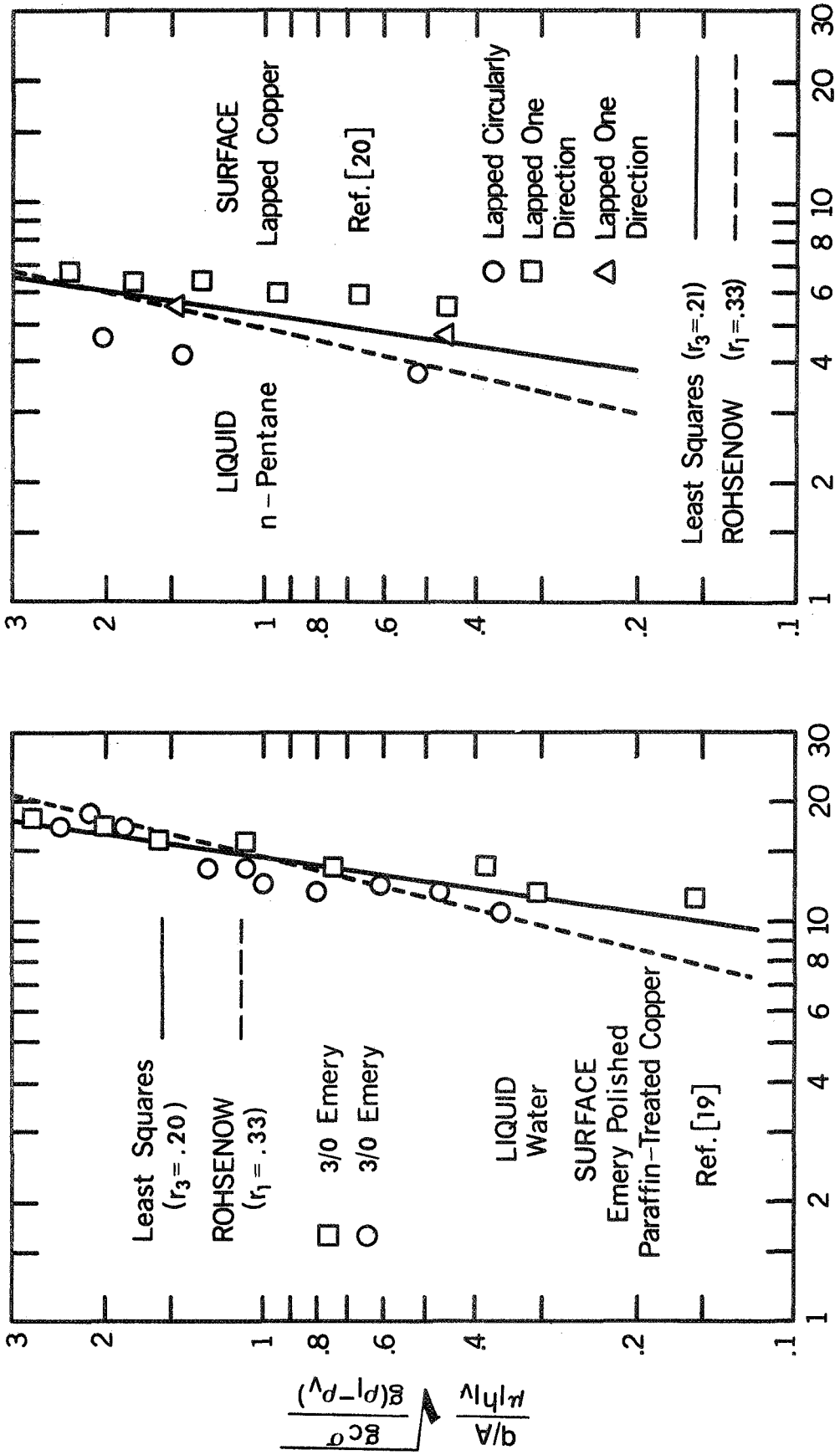

FIG. 27 CORRELATION OF POOL BOILING DATA FOR COPPER SURFACES

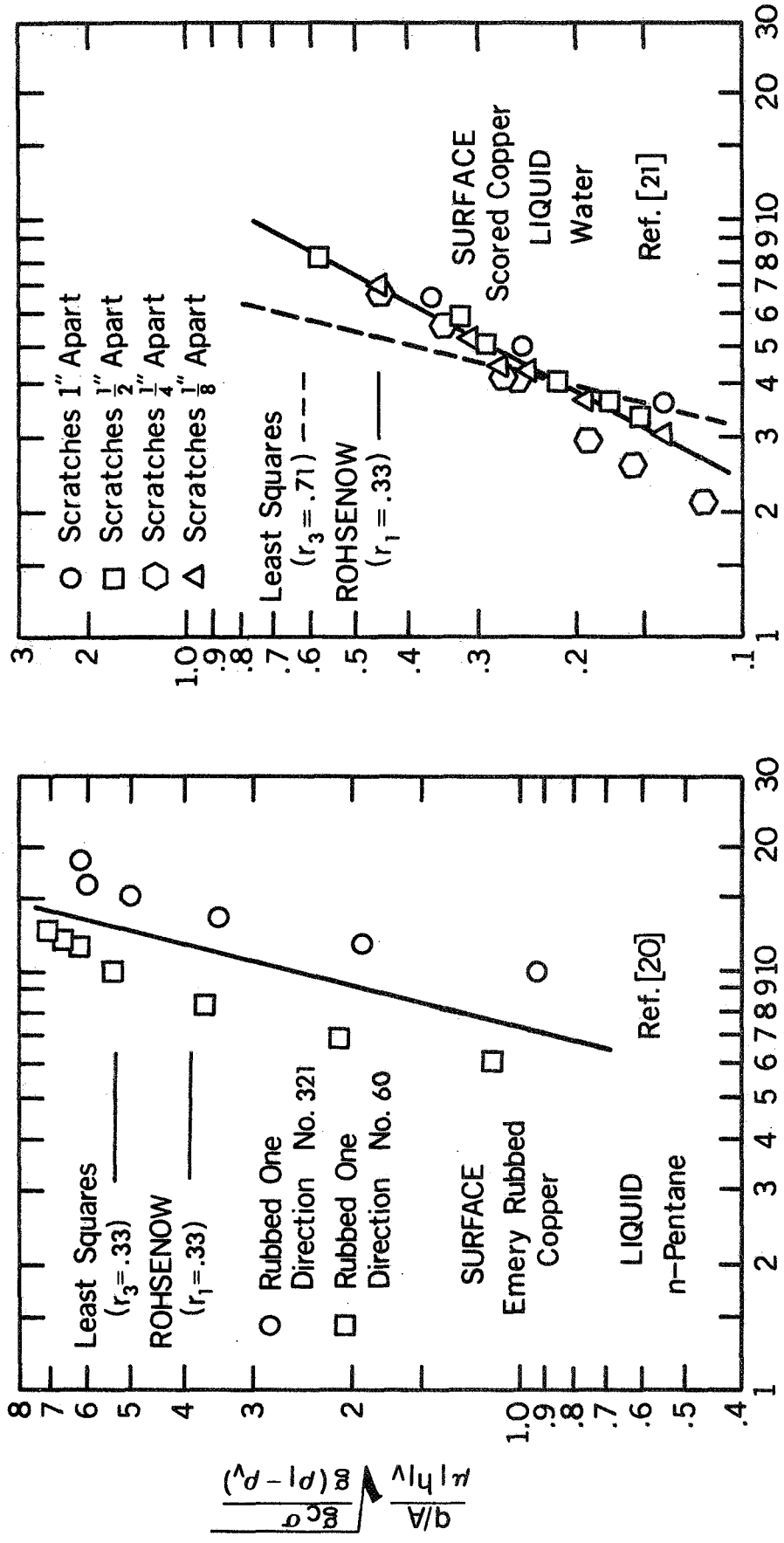

FIG. 28 CORRELATION OF POOL BOILING DATA FOR COPPER SURFACES

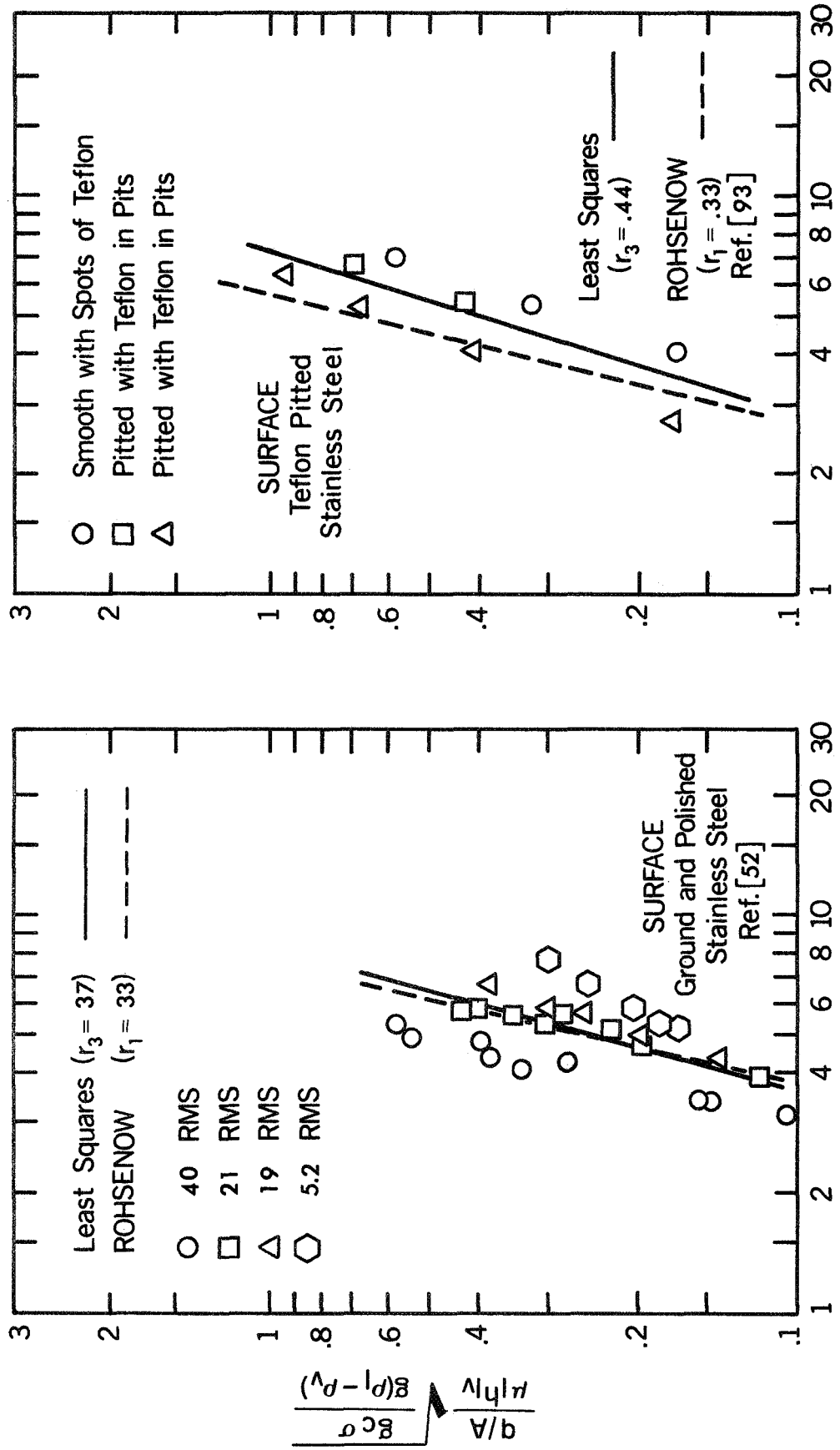

FIG. 29 CORRELATION OF POOL BOILING DATA FOR WATER ON STAINLESS STEEL

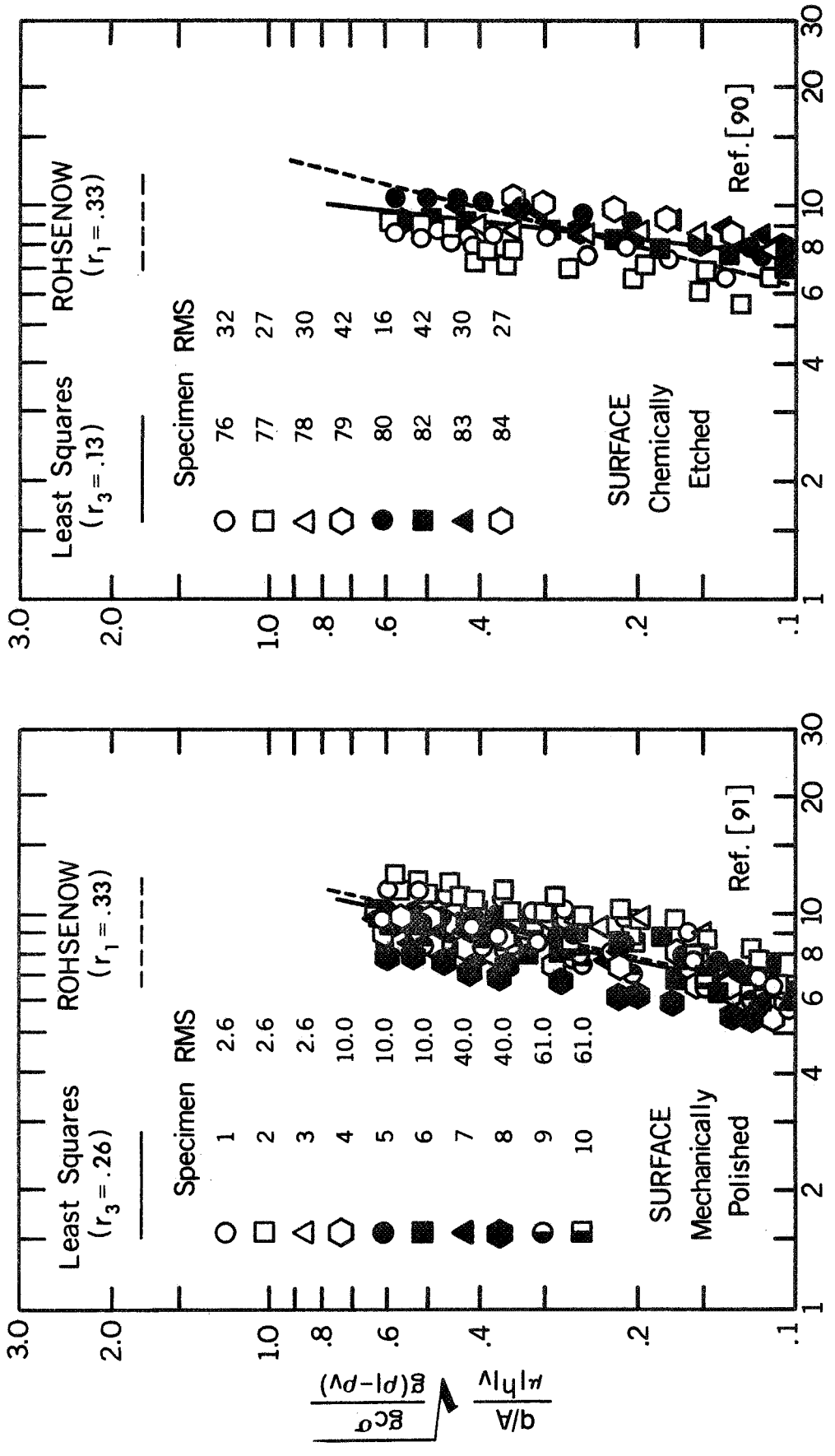

FIG. 30 CORRELATION OF POOL BOILING DATA FOR WATER BOILING FROM POLISHED AND ETCHED STAINLESS STEEL

preparation for a particular technique gives a minimal variation in the superheat for a given heat flux. The data are correlated in terms of $\overline{C_{sf_3}}$ and r_3 in Figs. 25 through 30. $\overline{C_{sf_1}}$ and C_{sf_1} values are tabulated for those who wish to rely on r_1.

As mentioned, the data of Appendix C are presented graphically in Figs. 25 through 30. Individual datum points for each surface combination are specified. The least-squares fits of the data are shown as solid lines. The reciprocals of the slopes of the solid lines are the r_2 values in Table 7. The dotted lines represent the Rohsenow correlation with $r_1 = 0.33$.

In general, the least-squares slopes of the data do not agree with the Rohsenow correlation with $r_1 = 0.33$. However, the solid lines and the Rohsenow correlation line coincide if the reciprocal slopes of the least-squares fits are used. The data of Gaertner and Westwater [18] were not correlated because of the absence of property data on their aqueous nickel salt solution. The authors' graph of heat flux versus superheat was used to obtain a slope of 6.5 ($r_2 = 0.15$) which does not agree with an r_1 of 0.33.

Figures 25 through 30 show correlations with the Rohsenow equation of the grouped data. The figures show in solid lines the correlation using the $\overline{C_{sf_3}}$ and r_3 values for the grouped data. Both the average r_3 value and $\overline{C_{sf_3}}$ value for each group are given in Table 8. The dotted lines indicate the inadequacy of using $r_1 = 0.33$.

The cross-correlation of pool boiling data from the literature shows that r values for the Rohsenow equation must be given for surface preparation and surface-liquid combination. The study also adds several

possible values for r and C_{sf} for the Rohsenow equation for the surface conditions tabulated. Table 9 illustrates that 68.3 percent of the grouped data can best be correlated within ±30 percent with respect to r_2 values if r_3 values are used. This figure compares with 15.8 percent for values of r_1. The value of r_2 is the reciprocal of the slope of the least-squares fit of the heat-flux-versus-superheat data for a particular surface. Table 10 indicates the improvement in C_{sf} values when the tabulated r_3 values are used.

The reader is left with a choice of r values and C_{sf} values to use. Values of C_{sf_3} and r_3, as given in Table 7, can be used if one considers the r_3 values for the groups to be representative of the preparation technique. This would appear to be a reasonable assumption based on the results presented in Tables 9 and 10. Average values of C_{sf_3} for the groups obtained from Table 8 are applicable for the cases where the surface preparation techniques are known in general terms or where one considers that variations in surface preparation techniques give only a minimal change in heat flux or superheat data. The $\overline{C_{sf_1}}$ and C_{sf_1} values based on $r_1 = 0.33$ are presented since values of C_{sf} are usually in terms of $r_1 = 0.33$ in the literature although the results of this study show the desirability of using C_{sf_3} and r_3 values.

All data presented were collected under atmospheric pressure and standard gravity conditions. Some evidence exists at present to indicate that r values may be a function of system pressure. This point should be investigated to insure that Tables 7 through 10 are applicable to the cases where system pressure is not atmospheric.

B. Model Studies on Wall Superheat

The elevated pressure data which have been presented illustrate several important features which have not received attention in the literature on pool boiling. The present theory will not account for the slope change of the nucleate boiling curve or for the occasional backshift with increasing pressure. Several recent correlations have been studied in an attempt to clarify the phenomena involved. These correlations include the work of Lienhard and Schrock [4], Borishansky et al. [5], and Rohsenow [3]. The main items of interest in the study of correlations are:

1. Prediction of the displacement of the nucleate boiling heat-flux-versus-wall-superheat curve with pressure.
2. Correlation of the slope change of the heat flux curve with pressure and effective roughness.
3. Investigation of sensitivity of a prepared surface to pressure changes.

The correlations are discussed and compared with the data of this study as follows:

1. Lienhard-Schrock Correlation

The design correlation recently forwarded by Lienhard and Schrock [4] was investigated for its applicability in predicting the displacement of the nucleate boiling curve with pressure. The relation

$$\left.\frac{\partial \ln \Delta T}{\partial \ln p}\right|_q = -\text{constant} \qquad \text{(V-1)}$$

developed by Bonilla et al. [95,96] to correlate wall superheat with

change in pressure formed the basis of their analysis. The objective of their study was to determine the form of the derivative in Eq. (V-1) and to indicate how it might be used in practice. The equation advanced by Bonilla et al. is

$$\left.\frac{\partial \ell n\ \Delta T_r}{\partial p_r}\right|_q = f_1(p_r) \tag{V-2}$$

where Eq. (V-1) is a special case of Eq. (V-2).

van der Waal's equation was used by the authors to determine the superheated liquid properties. They advanced the hypothesis:

$$\left.\frac{\partial \ell n\ \Delta T_r}{\partial p_r}\right|_q = \frac{d\ \ell n\ \Delta T_{rM}}{dp_r} \tag{V-3}$$

or "the superheat, ΔT, for any configuration and heat flux is directly proportional to the van der Waal maximum superheat, ΔT_M." Values of the derivative in Eq. (V-3) were determined by graphical differentiation. These values--obtained by Lienhard and Schrock--are given in Table 11. The correlation based on van der Waal's equation is compared with experimental data [40,97] in Fig. 31. The hypothesis based on van der Waal's equation, indicated by the dashed line, is seen to be successful in correlating the data.

The correlation is put into a more useful form for the present study by integrating Eq. (V-2)

$$\exp\left[-\int_0^{p_r} \left.\frac{\partial \ell n\ \Delta T_r}{\partial p_r}\right|_q dp_r\right] = \exp\left[-\int_0^{p_r} f_1(p_r)\,dp_r\right] \tag{V-4}$$

TABLE 11

PROPERTIES OF A SATURATED VAN DER WAAL'S FLUID

CALCULATED BY LIENHARD AND SCHROCK[10]

P_{rs}	$-\frac{d\ell n \Delta T_{rM}}{dp_r}$
0	∞
0.00002	1600.0
0.0001	370.0
0.0005	118.0
0.001	71.0
0.005	21.2
0.01	12.8
0.05	5.48
0.1	3.93
0.20 → 0.38	3.17
0.4	3.25
0.45	3.41
0.5	3.53
0.55	3.98
0.6	4.35
0.65	5.524
1.0	∞

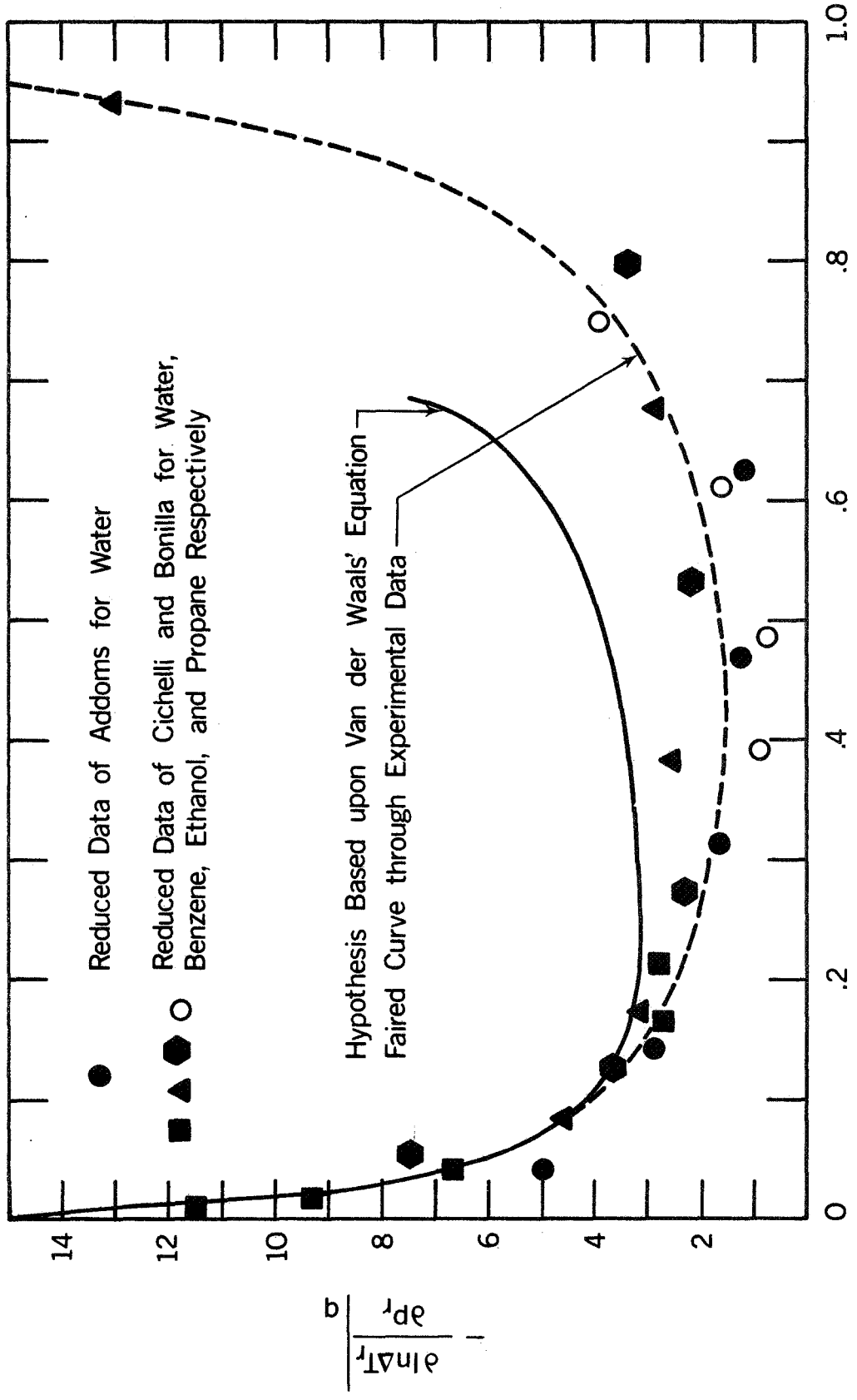

FIG. 31 CORRELATION OF $(\partial \ln \Delta T_r / \partial p_r)_q$ IN THE HIGH PRESSURE RANGE

to obtain

$$\frac{(\Delta T)_{p_r=0}}{\Delta T} = f_2(p_r) \qquad \text{(V-5)}$$

where the function $f_2(p_r)$ is obtained from Fig. 31. However, for the low p_r range, the function must be obtained from the calculated data in Table 11. This is accomplished by graphically or numerically integrating the tabular data. The functions obtained for various reduced pressures, in the form of Eq (V-5), are used to form the ratio of the reference superheat to the superheat of interest. The latter is given by

$$\frac{\Delta T_{ref}}{\Delta T_{int}} = \left[\frac{(\Delta T)_{p_r=0}}{\Delta T_{int}}\right]\left[\frac{\Delta T_{ref}}{(\Delta T)_{p_r=0}}\right] \qquad \text{(V-6)}$$

Figure 32 yields the information necessary to determine the bracketed terms in Eq. (V-6). For the low p_r range, the information for Eq. (V-6) is obtained by integration.

Thus, if the shape of the heat-flux-versus-superheat curve is known for some reference pressure, it can be displaced at constant heat flux for any other pressure of interest by using Eq. (V-6). For simplified calculations, Lienhard and Schrock present the approximate relation:

$$\frac{\Delta T_{ref}}{\Delta T_{int}} = \frac{1.6 + 6.5\ p_{r_{int}}}{1.6 + 6.5\ p_{r_{ref}}} \qquad \text{(V-8)}$$

for the range $0.01 < p_r < 0.65$. However, the simplified equation is not used for this investigation since the reference pressure is 14.7 psia ($p_r = 0.0046$) which is not within the range of approximate validity for the simplified equation.

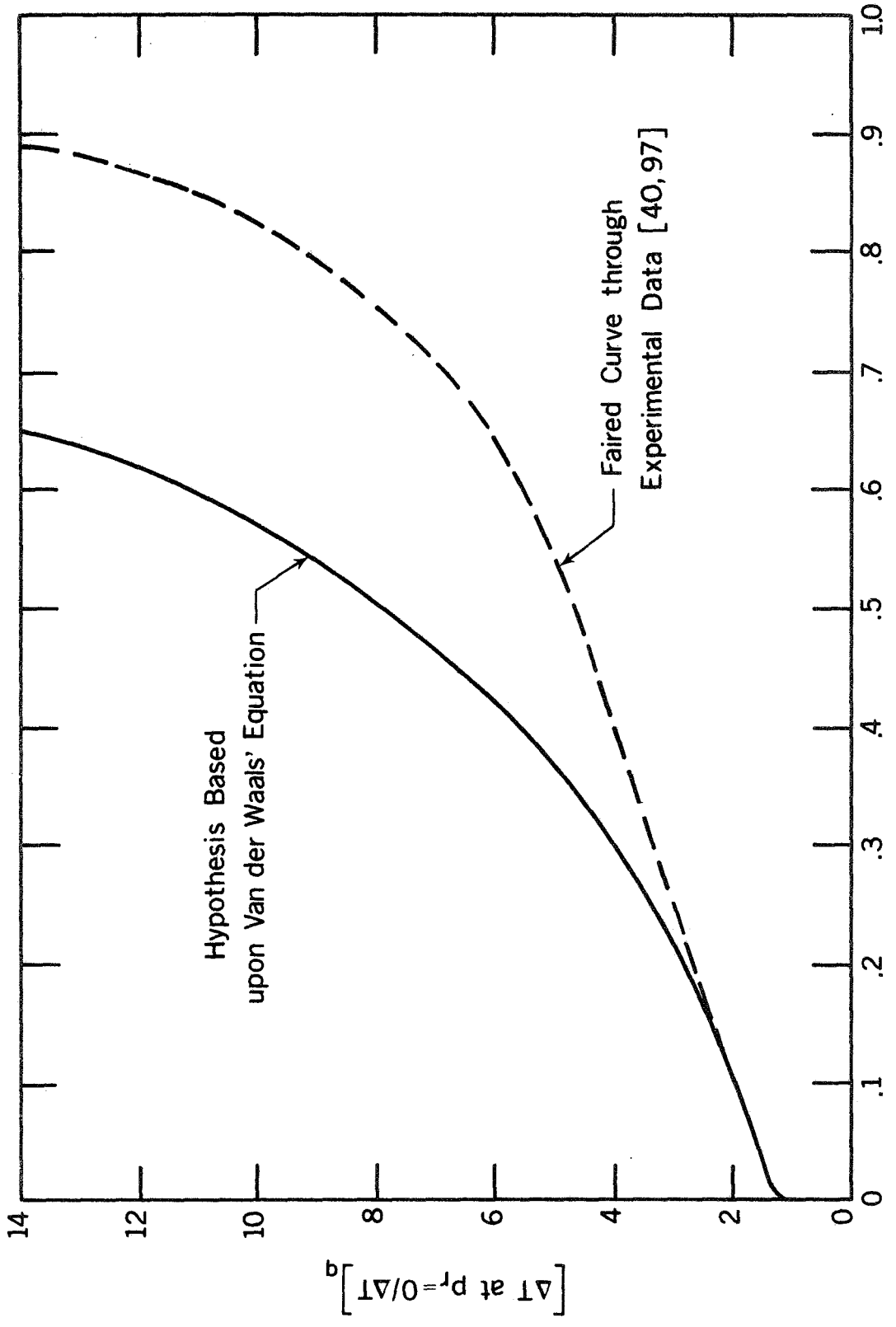

FIG. 32 PRESSURE DEPENDENCE OF WALL SUPERHEAT IN NUCLEATE BOILING [4]

The procedure for comparing the correlation of Lienhard and Schrock to the present data (14.7 to 100 psia) consists of

a. Fitting a curve to the calculated van der Waal's data in Table 11 over the range of interest.

b. Integrating the expression found in step a numerically to obtain the function $f_2(p_r)$, Eq. (V-5).

c. Forming the ratio of Eq. (V-6).

The results are shown in Table 12 and are compared graphically with data from specimen 86 in Fig. 33.

TABLE 12

CORRELATION OF WALL SUPERHEAT RESPONSE TO PRESSURE CHANGE IN NUCLEATE BOILING [4]

Pressure psia	Reduced Pressure	$\Delta T_{p_r=0}/\Delta T_{int}$	$\Delta T_{p_r=0}/\Delta T_{ref}$	$\Delta T_{int}/\Delta T_{ref}$
14.7	0.0046	0.6859	0.6859	1.000
25.0	0.0078	0.7813	0.6859	0.878
50.0	0.0156	0.9607	0.6859	0.714
100.0	0.0312	1.2660	0.6859	0.542
200.0	0.0624	1.6403	0.6859	0.418
300.0	0.09369	1.8714	0.6859	0.367

The data of Table 12 may be used to obtain $\Delta T_{int}/\Delta T_{ref}$ for a pressure reference corresponding to atmospheric pressure. Thus, for

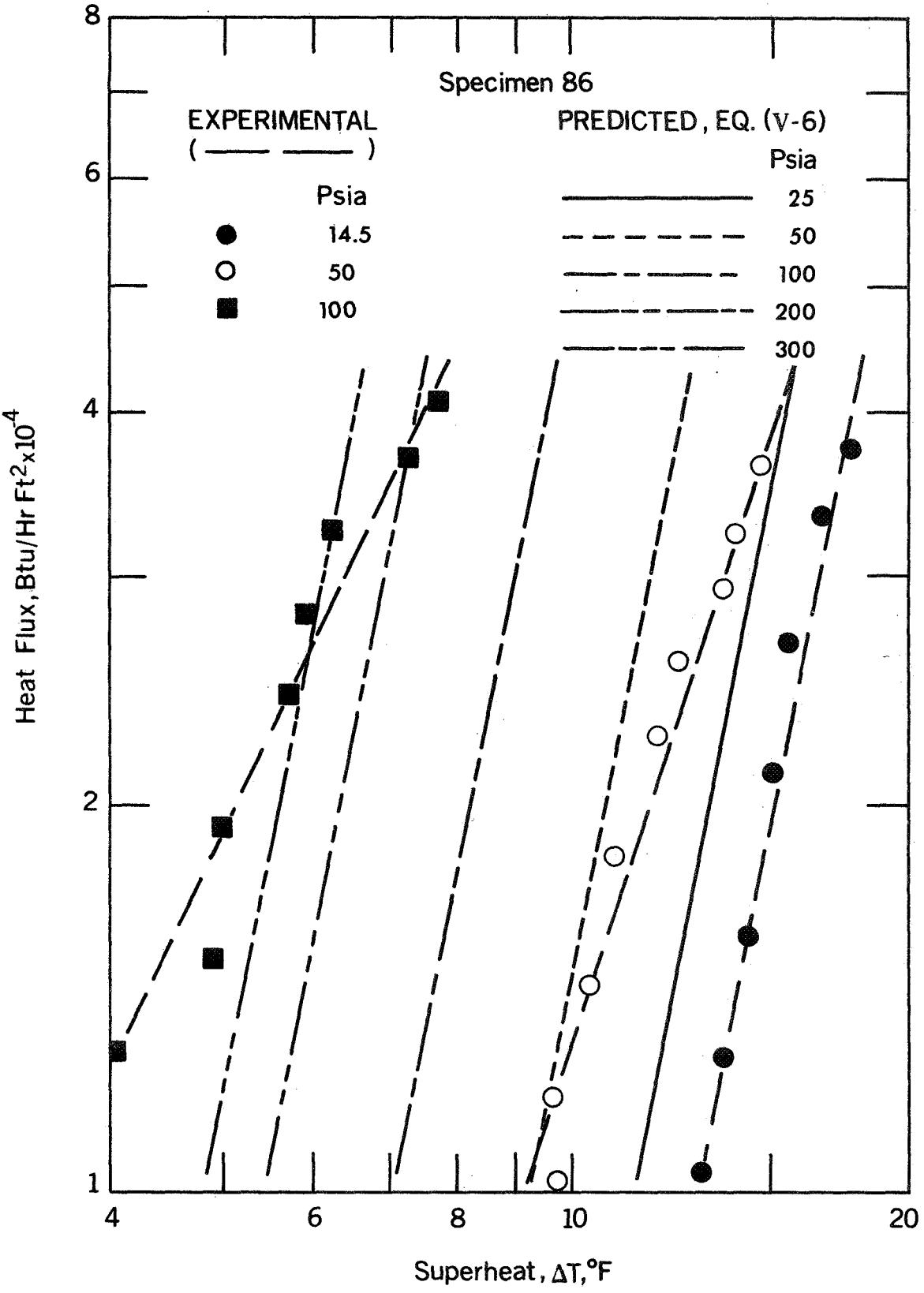

FIG. 33 DEPENDENCE OF WALL SUPERHEAT ON PRESSURE FOR A CHEMICALLY ETCHED SURFACE IN NUCLEATE BOILING

higher pressures, the percentage of the reduction in superheat (for a constant heat flux) can be read directly from Table 12. The tabulated data are compared with typical test results from a six-hour etched specimen in Fig. 33. The heat flux curve for atmospheric pressure is used as the reference line; hence, the experimental and the predicted curves for atmospheric pressure will necessarily be identical. Also, an inherent feature of the Lienhard and Schrock correlation is: all predicted curves will have the same slope as the reference curve. Thus, the predicted curves will be displaced horizontally to the left with a constant slope as system pressure is increased. The data used for comparison are those for which the backshift was not obtained at higher pressures. There is no advantage to comparing the correlation with the shifted data since the correlation will not predict such phenomena. Also, the correlation does not contain a surface parameter and, hence, will not account for major differences in surface type and preparation. The predicted and experimental curves for 50 psia agree at a low heat flux value but disagree at higher values because of the slope change for the measured data. The flexibility of the correlation is, therefore, limited by the fact that slope changes cannot be accounted for.

Also, a serious deficiency arises from the fact that surface effects are not accounted for in the correlation presented by Lienhard and Schrock. The amount of shift of the heat flux curve with pressure is influenced to some extent by the type and degree of surface roughness. The type of surface treatment controls the sensitivity and, thus, the response of the surface to pressure and to other effects such as aging.

2. Borishansky Correlation

Surface parameters are included in the correlations by Rohsenow [3] and Borishansky et al. [5]. Thermodynamic similarity is used in [5] to generalize heat transfer data. The correlation presented is

$$\frac{(q/A)^{0.3}/\Delta T}{[(q/A)^{0.3}/\Delta T]_{p_r=0.029}} = f_3(p_r) \qquad \text{(V-8)}$$

The choice of 0.029 for a reduced reference pressure appears to be convenient but arbitrary. Also, a restriction on the proposed equation is that

$$q/A \simeq \Delta T^{3.33} \qquad \text{(V-9)}$$

which indicates that the slope of the heat-flux-versus-superheat curve is 3.33. This is a good approximation for many surface finishes [20,52] and is similar to the slope prescribed by the correlation of Rohsenow [3]. Equation (V-9) is not a good approximation for chemically etched surfaces. A better approximation can be obtained as follows.

It is shown in the previous section that the Rohsenow equation is adjustable for a wide range of surface conditions [89]. Table 13 lists the values of the parameters in Rohsenow's equation for water boiling from milled, polished, and chemically etched stainless steel [81,12,89]. This suggests for the exponent in Eq. (V-9):

Surface	Exponent
Milled	3.00
Mechanically Polished	3.85
Chemically Etched	7.70

TABLE 13

COEFFICIENT C_{sf} AND EXPONENT r OF ROHSENOW CORRELATION FOR VARIOUS SURFACE FINISHES

Surface	Liquid	Surface Finish	C_{sf}	r	Reference
304 Stainless	Water	Milled	0.0081	0.33	81, 6
304 Stainless	Water	Mechanically Polished	0.0121	0.26	89
304 Stainless	Water	HCL Etched	0.0102	0.13	89

Thus, it is suspected that the slope of 3.33 used by Borishansky et al. [5] can be adjusted for varying surface conditions. Then, thermodynamic similarity can be used to represent the pool boiling data as a function of reduced pressure, Eq. (V-8). For chemically etched surfaces, it has been found [55] that

$$q/A = \Delta T^{7.70} \qquad \text{(V-10)}$$

thus, the exponent r = 0.13. If reduced atmospheric pressure is chosen as the reference pressure, that is, $p_r = 0.0046$, then the adjusted Borishansky correlation becomes

$$\frac{(q/A)^{0.13}/\Delta T}{[(q/A)^{0.13}/\Delta T]_{p_r=0.0046}} = f_4(p_r) \qquad \text{(V-11)}$$

The adjusted correlation, Eq. (V-11), is used to correlate the chemically etched data in Figs. 18 through 24, as shown in Fig. 34.

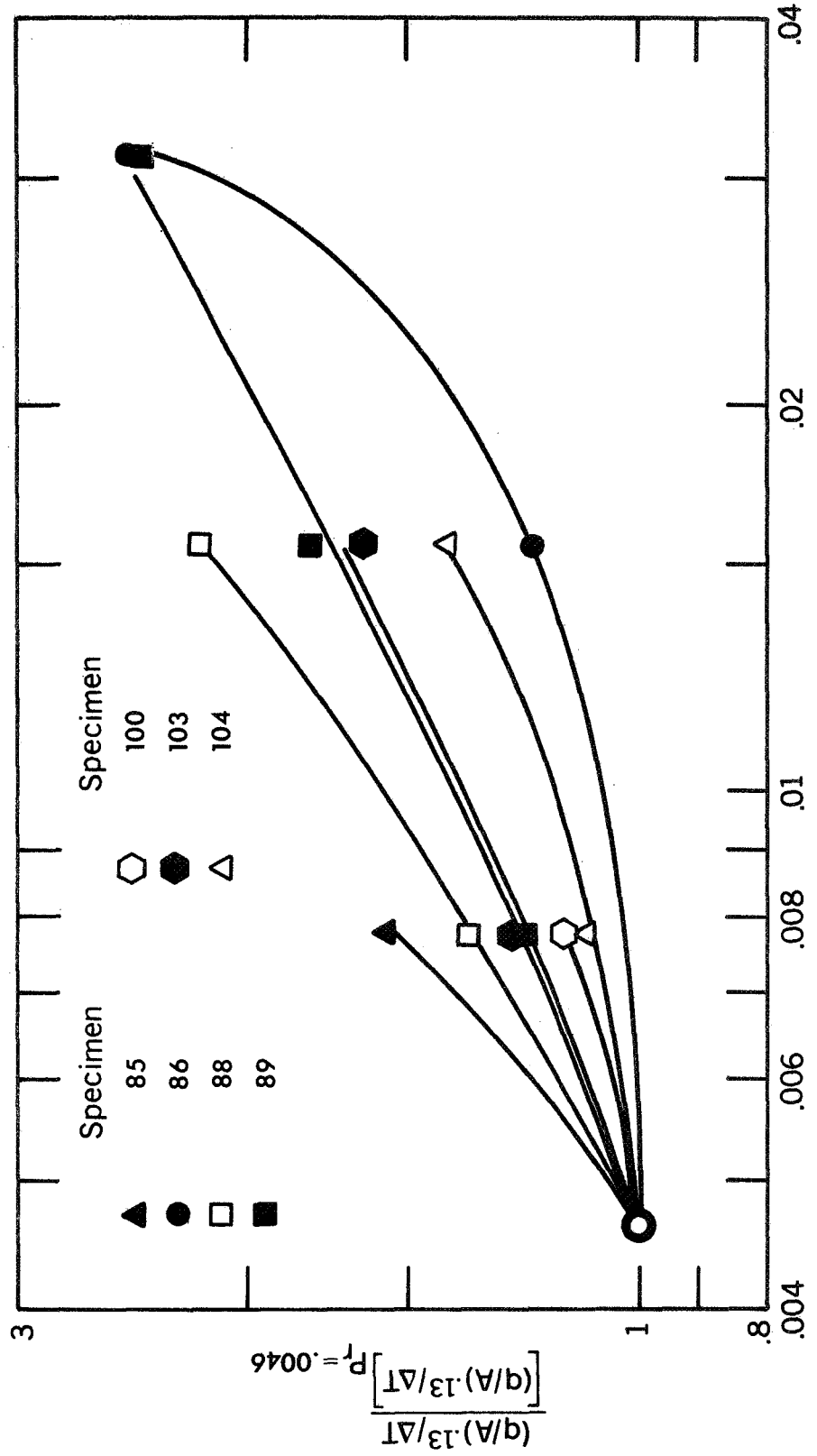

FIG. 34 ADJUSTED CORRELATION OF BORISHANSKY, ET. AL. [5] FOR NUCLEATE BOILING FROM CHEMICALLY ETCHED SURFACES

These data cannot be compared with the data used by Borishansky et al. [5] because of the differences in the forms of the correlation equations and because their original data were not given. However, the overall form of Fig. 34 compares favorably with that of Borishansky. The data scatter is approximately equal in both cases. It is interesting to note that four points are not plotted in Fig. 34. These points correspond to the data runs in which a backshift in superheat is obtained with increasing pressure. Thus, the Borishansky correlation completely fails to predict the occurrence of this phenomenon. However, this is as would be expected.

It appears feasible to use an adjusted form of the Borishansky correlation to account for changes in the slope of the heat-flux-versus-superheat curve with changes in pressure. This is possible because of the applicability of Eq. (V-10) and is demonstrated in Fig. 34. The requirement that unique values of the heat flux exponent r be established for each surface and preparation technique, however, decreases the utility of the correlation.

3. Rohsenow Correlation

It appears from the preceding discussion and the comparison with the work of Lienhard and Schrock that the development of any general correlation for pool boiling is prohibited, at present, by insufficient knowledge of the surface. The Rohsenow correlation, which has been known for quite sometime, should be as applicable, and possibly more accurate, in predicting the heat flux change with pressure than

either of the two previous correlations. This will be checked now as a matter of reference.

When the value of the exponent s is taken as 1.0 [88], the Rohsenow equation, Eq. (II-17), can be solved for the wall superheat as

$$\Delta T = C_{sf} \frac{\mu_\ell h_{\ell v}}{k_\ell} \left(\frac{q/A}{\mu_\ell h_{\ell v}} \sqrt{\frac{g_c \sigma}{g(\rho_\ell - \rho_v)}} \right)^r \qquad \text{(V-12)}$$

As written, the relation between wall superheat and heat flux contains only fluid and vapor properties, the coefficient C_{sf}, and the exponent r. The values of r and C_{sf} may be taken from Table 13 for the etched surface. The wall superheat change with pressure can then be predicted using the appropriate property values and various values of the heat flux. The results of the prediction are shown in Fig. 35.

As noted from the figure, the comparison is not as good as that obtained by Lienhard and Schrock. Actually, neither prediction is adequate for the purpose at hand. It should be pointed out that the analysis of Lienhard and Schrock is artificial; that is, the atmospheric data are used as a starting point and are matched perfectly. On the other hand, the Rohsenow analysis requires only the values of the coefficient C_{sf} and the exponent r as a starting point. This would indicate the greater flexibility of the Rohsenow equation.

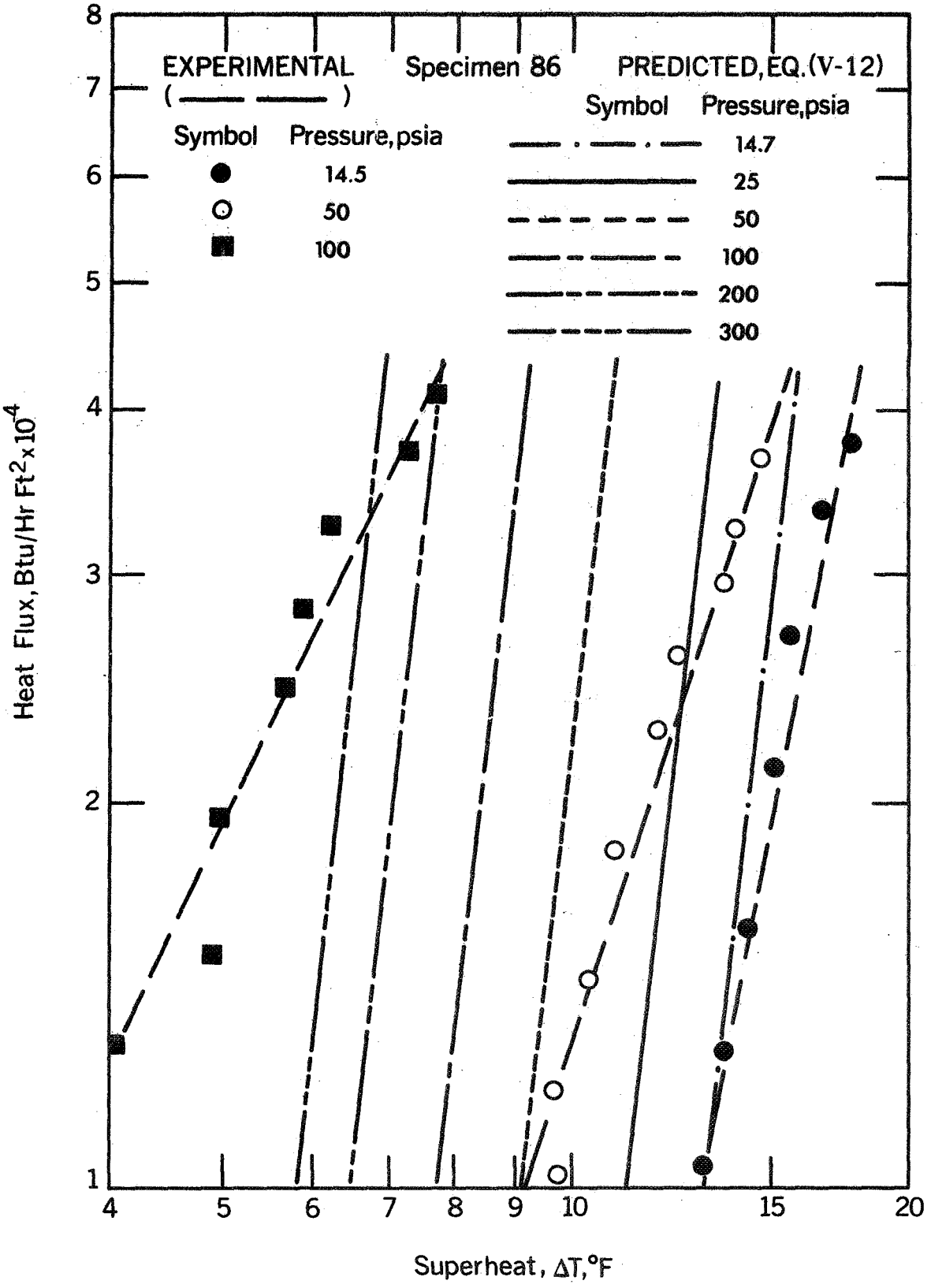

FIG. 35 ROHSENOW PREDICTION OF PRESSURE INFLUENCE ON WALL SUPERHEAT

VI. ANALYSIS OF SATURATED DISCHARGE

Several theories have recently been forwarded concerning the general analysis of the blowdown problem [84,85,98]. Moody's predictive model [85] has been employed by other authors [99] in comparing results of blowdown tests. Moody [100] has also presented an analysis of liquid/vapor action in a saturated system during blowdown. However, most of the models currently available are not entirely satisfactory for predicting system response during a pressure decay. Most analyses consider liquid blowdown and completely ignore, or pay only cursory attention to, the problem of vapor discharge.

The present model is an attempt to simulate the behavior of a saturated system during a vapor discharge from some elevated pressure to atmospheric conditions. A model of the depressurization facility is shown in Fig. 36. Initially, the system contains saturated water and steam at some elevated pressure. The initial conditions are assumed to be known. The system is suddenly exposed to a reduced pressure (atmospheric), and a solution is sought for: the mass of liquid and vapor as a function of time; mass flow rate of the liquid/vapor escaping the system; the temperature of each phase (liquid/vapor) as a function of discharge time; and the specific volume of vapor as a function of time. Also the liquid remaining in the vessel after a discharge is determined.

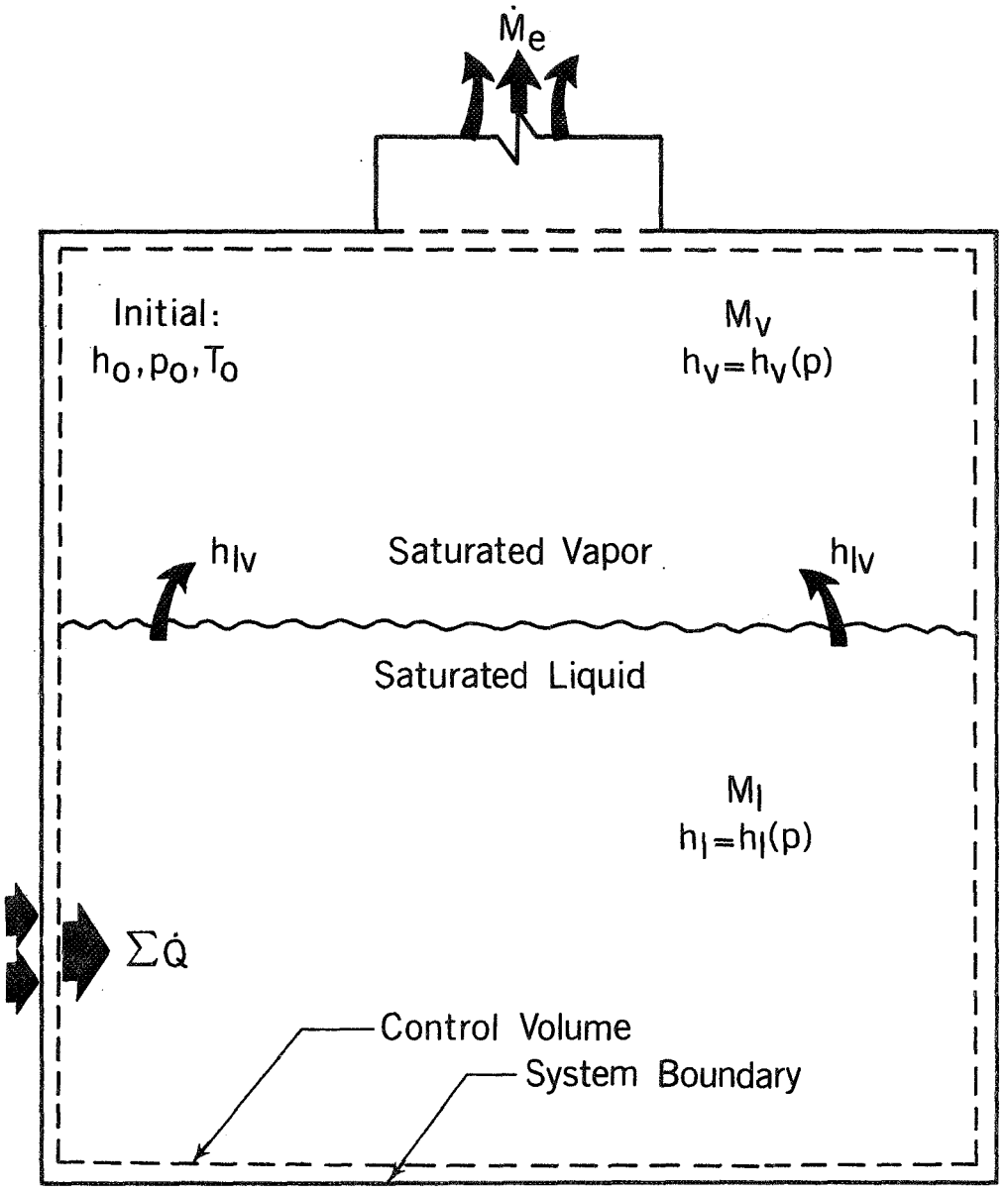

FIG. 36 POOL BOILING DEPRESSURIZATION MODEL

A. System Equations

It should be pointed out at the beginning that no attempt was made in the analysis to account for the large scale containment systems currently in existence. The model is developed strictly for the present depressurization facility as shown in Fig. 12. Results obtained from the current system will, however, be compared with large-scale blowdown tests to point out the applicability of modeling for the large-scale systems.

The procedure followed in the analysis is similar to that of Brown [101,102] and Coughren [70]. That is, the use of a continuum of steady states to simulate the transient has been avoided. Instead, a transient thermodynamic analysis will be developed which accounts for the various mass and energy storage phenomena within the system. The method is:

1. Analyze the system as a whole yielding mass, volume, and energy relationships;
2. Analyze the various subsystems (liquid/vapor) to obtain appropriate mass, volume, and energy relationships;
3. Analyze the connecting mechanisms (interphase) to obtain the appropriate balance equations;
4. Apply various boundary conditions as determined by the physics of the processes involved.

Simultaneous solution of the equations obtained will generate the required solution.

Mass and energy flow into the system will be considered to be positive. System expansion energy is also considered to be a positive quantity. The model of Fig. 36 is used along with the assumption of a controlled, saturated discharge in which vapor only is vented from the system. The velocity of the liquid/vapor interface is considered negligible according to the controlled discharge assumption, and there is no condensation within the system during a transient. It is also assumed that flashing occurs only at the interface and that there is no flow resistance within the boiler, condenser, or blowdown pipe.

System as a Whole

During a transient, the appropriate mass balance is determined as follows: The mass rate of change of the liquid plus the mass rate of change of vapor within the vessel must equal the mass rate of exit from the vessel, or

$$\dot{M}_\ell + \dot{M}_V = \dot{M}_e \tag{VI-1}$$

The total volume of the vessel is constant; thus,

$$\dot{v} = \dot{\overline{M_\ell v_\ell}} + \dot{\overline{M_V v_V}} = 0 \tag{VI-2}$$

or

$$M_\ell \dot{v}_\ell + \dot{M}_\ell v_\ell + M_V \dot{v}_V + \dot{M}_V v_V = 0 \tag{VI-3}$$

which may be written in the form

$$v_\ell \dot{M}_\ell + v_V \dot{M}_V + M_g \dot{P} = 0 \tag{VI-4}$$

where

$$M_g = M_\ell v'_\ell + M_v v'_v$$

The energy equation is given as

$$\dot{\Sigma Q} + \dot{\Sigma KW} + \dot{\Sigma hm} = \dot{\Sigma \overline{Mu}} + \dot{PV} \qquad \text{(VI-5)}$$

When the assumptions of constant total volume and no kinetic work are considered, Eq. (VI-5) becomes

$$\dot{\Sigma Q} + \dot{\Sigma hm} = \dot{\Sigma \overline{Mu}} \qquad \text{(VI-6)}$$

where it is assumed that the convected energy across the boundary is that of steam alone. Thus,

$$\dot{\Sigma Q} + h_v \dot{M}_e = \dot{\overline{M_\ell u_\ell}} + \dot{\overline{M_v u_v}} \qquad \text{(VI-7)}$$

The rate of heat transfer $\dot{Q}$ is determined by the physics of the particular process and consists of three terms: $\dot{Q}_1$ from the preheaters to the liquid, $\dot{Q}_2$ from the heated specimen to the liquid, and $\dot{Q}_3$ transferred from the hotter walls to the liquid bulk. The first two terms can be measured through appropriate instrumentation and should not vary appreciably from the steady state value. For $\dot{Q}_3$, we can take

$$\dot{Q}_3 = M_w C_p \frac{dT}{dt} \qquad \text{(VI-8)}$$

by measuring the transient temperature variation of the portion of the walls covered by the liquid. The use of Eq. (VI-8) entails the assumption that the liquid/vapor interface is not disturbed appreciably during a transient. This may be approximated by a slow discharge; i.e., blowdown through a small diameter orifice. However, for a rapid transient, the interface

heaves violently upward and downward, thus requiring other means of analysis.

We may write Eq. (VI-7) as

$$\dot{\Sigma Q} + h_v \dot{M}_e = M_\ell \dot{u}_\ell + \dot{M}_\ell u_\ell + M_v \dot{u}_v + \dot{M}_v u_v \qquad \text{(VI-9)}$$

or

$$\dot{\Sigma Q} + h_v \dot{M}_e = u_\ell \dot{M}_\ell + u_v \dot{M}_v + \dot{M}_u P \qquad \text{(VI-10)}$$

where

$$M_u = M_\ell u'_\ell + M_v u'_v$$

Liquid Subsystem

If kinetic work is considered negligible, the energy equation becomes

$$\dot{\Sigma Q}_\ell + \Sigma h_\ell \dot{M}_\ell = \overline{\dot{M}_\ell u_\ell} + P_\ell \overline{\dot{M}_\ell v_\ell} \qquad \text{(VI-11)}$$

Each term of Eq. (VI-11) will be considered separately. The heat transfer to the liquid consists of the same three terms previously mentioned for the entire system. The convected energy is a result of the flashing of liquid to vapor. The stored energy of the liquid is decreased by two mechanisms: decrease of thermal energy of the stored matter $M_\ell \dot{u}_\ell$, and loss of matter $\dot{M}_\ell u_\ell$. Also, all the heat added to the system goes into the liquid phase. When one considers the two terms connected with the liquid expansion energy, Eq. (VI-11) becomes

$$\dot{\Sigma Q} + h_{\ell}\dot{M}_{\ell} = M_{\ell}\dot{u}_{\ell} + \dot{M}_{\ell}u_{\ell} + P_{\ell}M_{\ell}\dot{v}_{\ell} + P_{\ell}\dot{M}_{\ell}v_{\ell} \qquad \text{(VI-12)}$$

or, if one expands the enthalpy and collects the terms,

$$\dot{\Sigma Q} = M_{\ell}\ (\dot{u}_{\ell} + P_{\ell}\dot{v}_{\ell}) \qquad \text{(VI-13)}$$

or

$$\dot{\Sigma Q} = M_{\ell}\ (\dot{h}_{\ell} - \dot{P}_{\ell}v_{\ell}) \qquad \text{(VI-14)}$$

Equations (VI-13) and (VI-14) are alternative forms which may be used in the analysis. They may be manipulated to yield

$$\dot{\Sigma Q} = M_{\ell}\dot{P}_{\ell}\ (u_{\ell}' + P_{\ell}v_{\ell}') \qquad \text{(VI-15)}$$

and

$$\dot{\Sigma Q} = M_{\ell}\dot{P}_{\ell}\quad (h_{\ell}' - v_{\ell}) \qquad \text{(VI-16)}$$

Vapor Subsystem

There is no kinetic work imparted to the vapor. Also, the assumption of no heat transfer to the vapor is made. This is reasonable because of the low thermal conductivity of the vapor as compared with that of the liquid. The energy balance for the vapor phase becomes

$$\Sigma h_{V}\dot{M}_{V} = \Sigma\overline{\dot{M}_{V}u_{V}} + \overline{\dot{P}_{V}M_{V}v_{V}} \qquad \text{(VI-17)}$$

The convected energy consists of energy convected into the steam subsystem because of flashing of liquid and transport of vapor out of the steam portion through the top blowdown valve. It is assumed that only vapor is

blown from the vessel. Again, this will apply only for a controlled or slow depressurization since droplets of liquid will be entrained in the vapor during a rapid transient. When Eq. (VI-17) is expanded, there is obtained

$$h_v\dot{M}_v + h_v\dot{M}_e = M_v\dot{u}_v + \dot{M}_v u_v + P_v(M_v\dot{v}_v + \dot{M}_v v_v) \qquad \text{(VI-18)}$$

or

$$h_v\dot{M}_e = M_v(\dot{u}_v + P_v\dot{v}_v) \qquad \text{(VI-19)}$$

This can also be written as

$$h_v\dot{M}_e = M_v(\dot{h}_v - \dot{P}_v v_v) \qquad \text{(VI-20)}$$

where Eqs. (VI-19) and (VI-20) are alternative forms which may be utilized in the analysis. These may be manipulated, analogously to those for the liquid subsystem, to obtain

$$h_v\dot{M}_e = M_v\dot{P}_v(u_v' + P_v v_v') \qquad \text{(VI-21)}$$

and

$$h_v\dot{M}_e = M_v\dot{P}_v(h_v' - v_v) \qquad \text{(VI-22)}$$

Interphase Relationships

The next step consists of identification and analysis of the various mechanisms occurring at the liquid/vapor interface. The interface is considered as having no mass or volume. However, both mass and energy

may cross the interface. The following assumptions apply for the interface region:

1. No condensation of steam to water occurs within the vessel during a transient.
2. All energy given up by the liquid goes directly to the steam phase.
3. The heat transferred to the interface is that given up by the liquid phase.

A mass balance for the interface yields

$$\dot{M}_{\ell} = \dot{M}_{V} \tag{VI-23}$$

that is, the material that leaves the water as water enters the vapor phase as steam. This requires the addition of a considerable amount of energy which must come from the liquid phase. For the interface region which does no kinetic work and possesses no mass or volume, the energy balance becomes simply

$$_{\ell}\dot{Q}_{V} + h_{\ell}\dot{M}_{\ell} - h_{V}\dot{M}_{V} = 0 \tag{VI-24}$$

If Eq. (VI-23) is sustituted into Eq. (VI-24), there is obtained

$$_{\ell}\dot{Q}_{V} = \dot{M}_{V}h_{\ell V} \tag{VI-25}$$

which shows that the heat transferred to the interface comes from the liquid phase and is used to flash the liquid into vapor.

Initial and Boundary Conditions

Initial conditions in the vessel are known for both the liquid and the vapor in the saturated state. These known quantities include the mass, specific volume, pressure, temperature, enthalpy, and internal

energy of each phase which are monitored through appropriate temperature, pressure, and weight measurements. The assumption is made that the vessel walls are perfectly insulated and there is no heat loss to the environment through the walls during a transient. Also, since there is no heat addition from the walls to the steam, the steam expansion may be considered as isentropic. The total heat transferred to the liquid phase may be measured and is considered as a known boundary condition. The heat transfer consists of three terms: heat transfer from the specimen, preheaters, and container walls to the liquid. All energy required to flash liquid into vapor is derived from these three sources.

The vessel is initially in a saturated state at some elevated pressure. When the system is suddenly exposed to a reduced pressure condition (simulating a steam line break), the saturated liquid becomes superheated for a brief period of time. The water relieves its superheat by flashing a portion of its mass to vapor, which is continuously discharging through the orifice. The assumption will be made that the system remains close to a saturated state throughout the discharge (this will be verified experimentally). Thus, the saturated vapor and water properties will remain functions of pressure.

B. Solution for Flow Rates

Once the system equations have been obtained, one may obtain the solutions for the four unknowns $\dot{M}$, $\dot{M}_v$, $\dot{M}_e$, and $\dot{P}$. First, the equations for the various flow rates are obtained. From Eq. (VI-4), one has

$$\dot{M}_v = - \frac{M_g \dot{P} + v_\ell \dot{M}_\ell}{v_v} \qquad \text{(VI-26)}$$

and from combining Eqs. (VI-10), (VI-1), and (VI-25), one obtains

$$\dot{M}_V h_{\ell V} + h_V(\dot{M}_\ell + \dot{M}_V) = u_\ell \dot{M}_\ell + u_V \dot{M}_V + M_u \dot{P} \qquad \text{(VI-27)}$$

which may be written as

$$\dot{M}_V(h_{\ell V} + h_V - u_V) - M_u \dot{P} = \dot{M}_\ell(u_\ell - h_V) \qquad \text{(VI-28)}$$

Equation (VI-26) may now be substituted into Eq. (VI-28), and $\dot{M}_\ell$ may be solved for in terms of $\dot{P}$

$$\dot{M}_\ell = -\frac{\dot{P}\left[M_g\left(\frac{h_\ell - u_V}{v_V}\right) - M_u\right]}{\frac{v_\ell}{v_V}(h_\ell + u_V) + h_V - u_\ell} \qquad \text{(VI-29)}$$

A similar relation for $\dot{M}_V$ in terms of $\dot{P}$ can be found by equating (VI-16) with (VI-25).

$$\dot{M}_V = \frac{M_\ell \dot{P}}{h_{\ell V}}(h_\ell - v_\ell) \qquad \text{(VI-30)}$$

The relation for the exit mass flow rate is then given by Eq. (VI-1).

C. Solution for Pressure Rate

It is necessary now to obtain a relation for the rate of pressure drop during a transient which is independent of the other variables. One problem remains before this can be accomplished, however, and this concerns the type of discharge to be considered. The additional assumption will be made that the discharge at the throat of the outlet pipe is choked or critical. The most widely known critical flow models are those of Fauske [66], Moody [72], and Levy [71]. The model developed by Moody

is incorporated into the present analysis to calculate the critical flow rate. A discussion of his model is given in Appendix D.

Once the assumption of critical discharge is made, the exit mass flow rate, $\dot{M}_e$, is determined from

$$\dot{M}_e = GA_o \tag{VI-31}$$

where G, the critical mass velocity in Moody's model, is found as discussed in Appendix D and A_o is the area of the outlet orifice. Thus, with G and $\dot{M}_e$ known, the system pressure rate can be found as follows.

Equation (VI-1) may now be written as

$$\dot{M}_\ell + \dot{M}_V = \dot{M}_e = GA_o \tag{VI-32}$$

or

$$\dot{M}_\ell = GA_o - \dot{M}_V \tag{VI-33}$$

Now, if Eqs. (VI-4), (VI-30), and (VI-33) are combined, the following relation is obtained

$$\dot{P} = - \frac{GA_o v_\ell}{\frac{M_\ell v_{\ell V}}{h_{\ell V}}\left(h_\ell' - v_\ell\right) + M_g} \tag{VI-34}$$

where

$$M_g = M_\ell v_\ell' + M_V v_V'$$

and the relation for $\dot{P}$ is now independent of the other derivatives. A solution can, therefore, be obtained for the pressure rate by choosing a suitable time increment and employing the critical mass velocity predicted by Moody's model. The other variables can then be calculated from Eqs. (VI-29), (VI-30), and (VI-1).

D. Solution Procedure

A Fortran program was developed for the solution of the equations. This program consists of four main parts:

1. Generation of saturated liquid/vapor properties and their derivatives.
2. Prediction of critical mass velocity from Moody's model.
3. Solution of predictive equations for $\dot{P}$, $\dot{M}_\ell$, $\dot{M}_v$, and $\dot{M}_e$.
4. Calculation of subsidiary variables from the auxiliary equations in Appendix E.

The main program equations are (VI-1), (VI-29), (VI-30), and (VI-34).

Data from the depressurization tests are presented in the next chapter. These results are compared with the present model and with those of other investigators.

VII. DISCHARGE DATA AND ANALYSIS

A. Procedure and System Calibration

Care was taken during testing to be sure that the entire system is clean. All interior surfaces of the boiler were cleaned before each test. Alternate cleaning with acetone and distilled water was employed. The 3 kilowatt immersion heater--used to maintain saturated conditions within the boiler--was cleaned with steel wool, acetone, and distilled water before each test.

When the instrumentation was installed and connected, the boiler was sealed to the atmosphere, and pump down of the system was started. The dry system was exposed to a 29-inch Hg. vacuum for one-half hour; then, the boiler was filled with distilled, deionized water from the purification loop to a level approximately 6 inches above the support block assembly. A vacuum of 29-inch Hg. was again applied for one-half hour--during this time, the system was checked carefully for leaks.

The water admitted to the boiler was circulated previously in the purification loop for a minimum of three hours. Prior resistance measurements compare favorably with the value of 0.5×10^6 ohm centimeters at 68 degrees Fahrenheit reported in [47].

When the boiler was filled and degassed, it was vented slowly to the atmosphere, and the system was again sealed. At this point, full power was initiated to the preheaters, and the system was allowed to self-pressurize to the desired level of discharge--usually 100 psia.

The appropriate pressures and temperatures were checked periodically during pressure buildup. When the system reached the desired pressure, power to the preheaters was adjusted to maintain constant pressure. A period of approximately one-half hour was then allowed for the system to attain steady state saturated conditions at the elevated pressure.

The steady state pressures and temperatures were tabulated, and the signals were then switched to calibrated, automatic recorders for the transient portion of the test. Recorder speed and time settings were selected; whereupon, the recorders were started, and the quick opening valve was opened manually, discharging the boiler. The opening time for the valve is estimated at 0.3 second. Various discharge times were obtained by varying the orifice diameter size. The discharge process could be studied visually during a transient through the various windows in the boiler. After steady state conditions were again obtained, following blowdown, the various readings were tabulated, and the test was concluded.

An initial series of tests were necessary to calibrate the various transducers and recorders associated with the facility. Also, the calibration tests served to check the system response to blowdown through various sized orifices. The test specimen was not mounted on the support block for the calibration tests. It was added, however, before subsequent testing, in order to monitor the dynamic wall temperature response as a function of depressurization time.

Initial results obtained from the load cell are shown in Fig. 37 for a 0.25 inch discharge. These data have been smoothed to obtain a

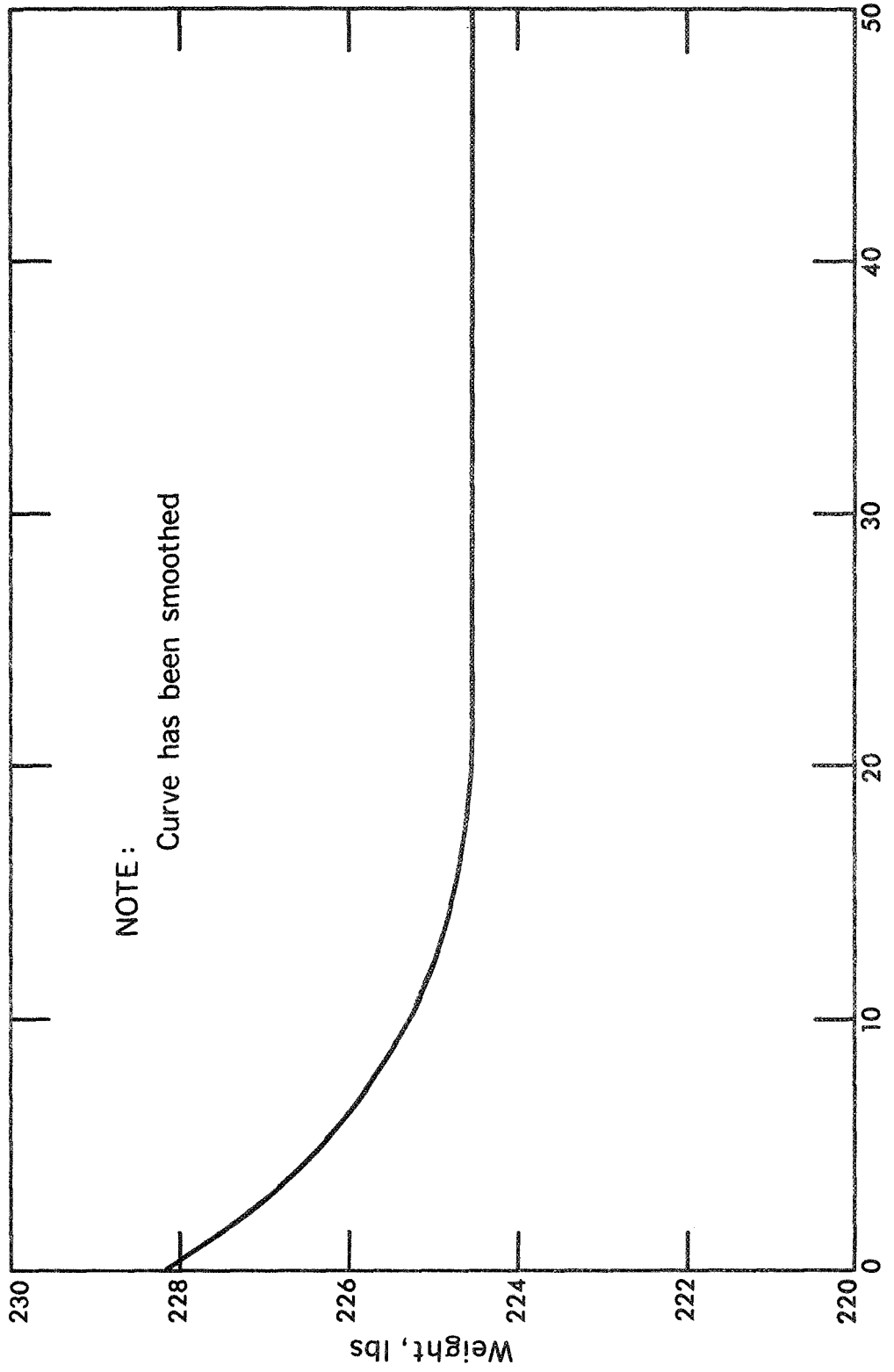

FIG. 37 WEIGHT VERSUS TIME FOR 1/4 INCH DEPRESSURIZATION TEST

continuous trace of weight versus time. System vibrations hampered somewhat the obtaining of useful data from the load cell. In subsequent tests, the cell was found to be faulty, and it was not used during the course of the investigation.

A total of twenty-two saturated discharge tests were attempted. A listing of these tests is given in Appendix F. In addition, four data runs were conducted for initially subcooled conditions in the vessel. These are also summarized in Appendix F. In the discussion to follow, each discharge test will be referred to by its run number.

Break sizes (orifice diameters) from 0.25 to 1.0 inch were simulated during the study. Several phenomena have been observed in the system pressures and temperatures during discharge. These will be discussed as a function of break size. All of the saturated tests were initiated for saturated boiler conditions at a pressure of 100 psia (T = 327.8 degrees Fahrenheit).

Consider the pressure-versus-time trace shown in Fig. 38 for discharge through a 0.25 inch orifice. There is a characteristic spike in the trace which occurs during the first second of depressurization. During this initial period, the pressure drops off rapidly, recovers momentarily, and then continues decreasing less rapidly throughout the rest of the venting period. This feature has been apparent in all the blowdown tests of this investigation. The spike is similar to that observed by other investigators [5,7,85]. Moody [85] explains the phenomenon as a combination of two effects: initial discharge of slightly subcooled liquid, which is not restricted by a two-phase mechanism, and the delay time for vapor bubbles to form and expand in

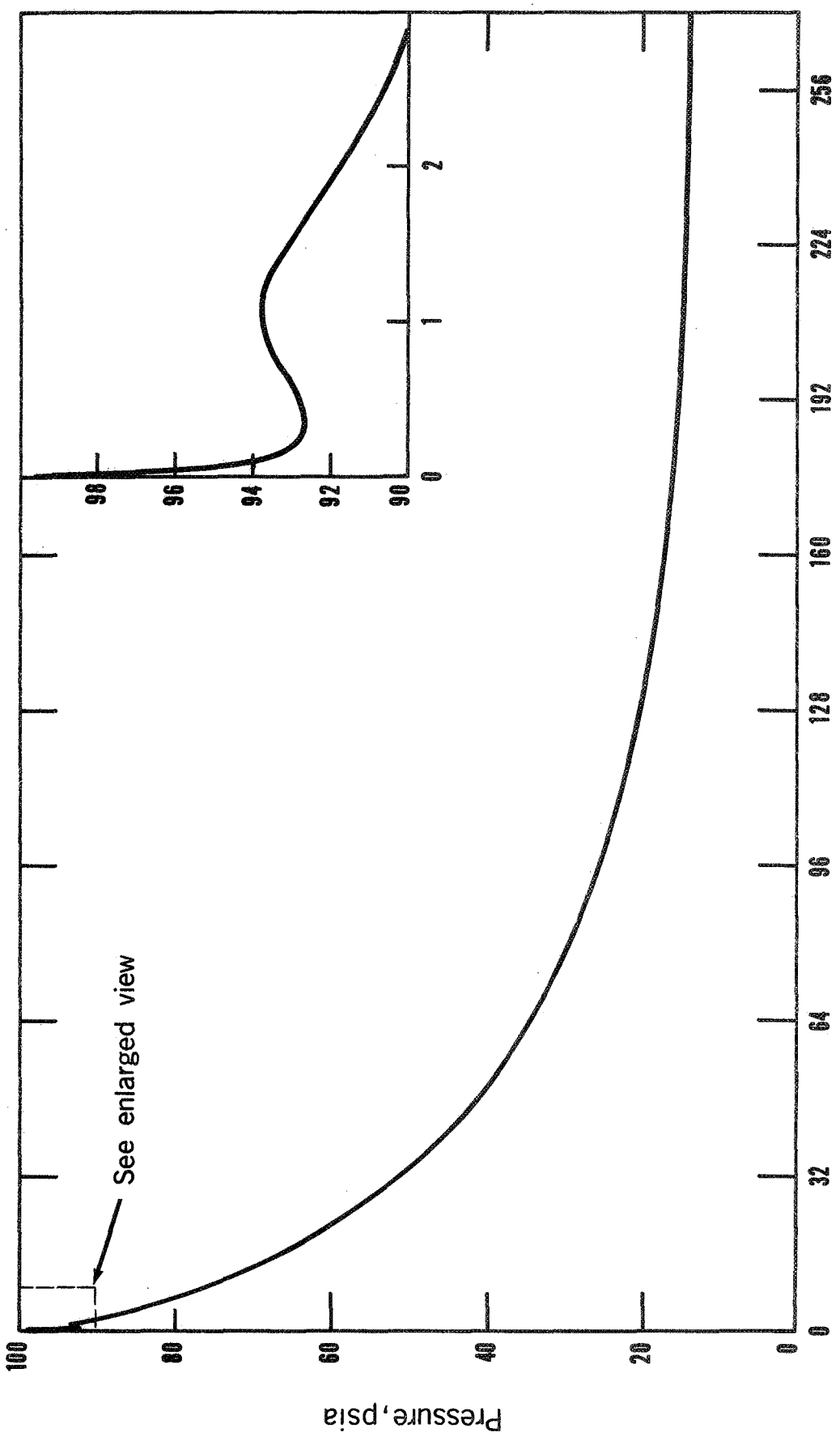

FIG. 38 PRESSURE VERSUS TIME FOR DISCHARGE THROUGH A 1/4 INCH ORIFICE

the liquid. A more detailed explanation can be offered and supported by the following results.

B. Experimental Results

The information given in Appendix F indicates that the system is usually in a slightly subcooled state prior to blowdown. However, the system remained close to saturated conditions throughout the vent period for the 0.25 inch discharge runs. This is not the case for the discharge through a 0.5 or a 1 inch orifice, as evidenced by Figs. 39 and 40. Figure 39 represents the degree of liquid bulk superheat occuring during test 22 for discharge through a 1 inch orifice. The bulk liquid became superheated during the initial phases of discharge and remained thus throughout most of the test period. Similar results obtained in test 18 through a 0.5 inch orifice are shown in Fig. 40.

In some instances, the liquid reached a slightly subcooled state at the end of the discharge, as shown by the data in Appendix F. Head [104] noted that a similar condition of subcooling occurred when saturated liquid oxygen was allowed to discharge from rocket propellant tanks. The subcooled condition is a result of the dynamic effects caused by the rapid expansion and the convective currents associated with the nucleation from the boiler and within the bulk liquid. Also, during a discharge, the water within the boiler is repeatedly lifted up and dropped, thus creating a cooling tower effect. The liquid bulk increased rapidly back to saturated conditions following conclusion of the discharge.

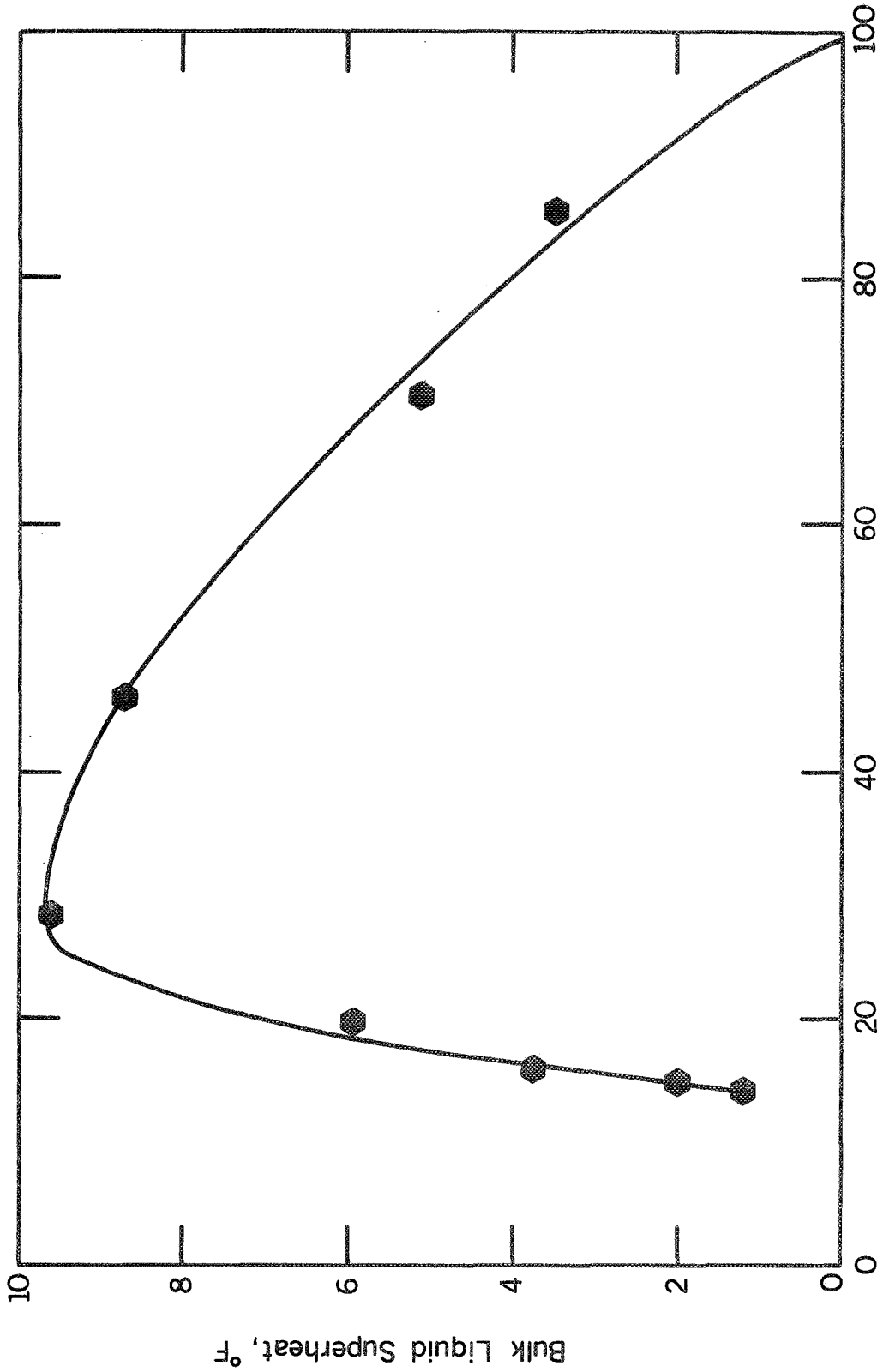

FIG. 39 BULK LIQUID SUPERHEAT VERSUS PRESSURE FOR DISCHARGE THROUGH ONE INCH ORIFICE

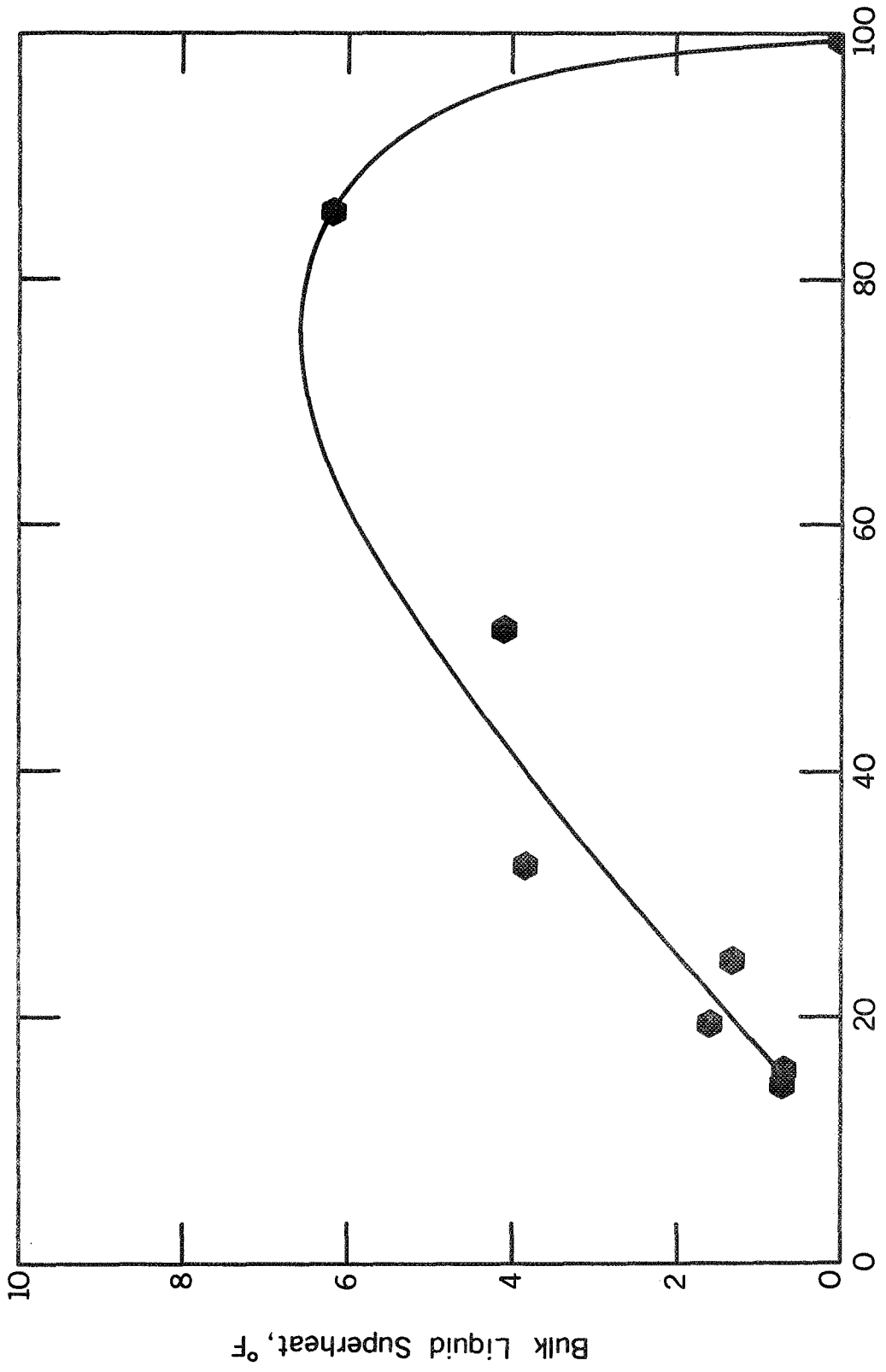

FIG. 40 BULK LIQUID SUPERHEAT VERSUS PRESSURE FOR DISCHARGE THROUGH ONE-HALF INCH ORIFICE

Figure 41 represents the initial phase of discharge through a 1 inch orifice. The test was performed on the present apparatus with the thrust reversers in place. However, in this test, the specimen was not installed and heated so that there was less power added to the system than that necessary to sustain a steady (fully choked) discharge. The test trace in Fig. 41 indicates that the flow was at first unchoked (evidenced by the rapid initial outflow of subcooled liquid), became choked, and then oscillated between choked and unchoked conditions. Unusual acoustics accompanied the oscillations shown in Fig. 41. At first the "tuned exhaust" phenomenon was suspected. However, further tests with different length exhausts ruled out the possibility of the tuned exhaust. Further, in additional tests with the specimen heated, no oscillations were observed. This indicates that the additional heat flux supplied by the test specimen provided enough power to sustain a fully choked condition throughout the discharge, after the initial rapid outflow (pressure spike).

Thus, it is believed that the delay time for vapor bubbles to form and expand in the liquid constitutes a major reason that the initial flow is not restricted by the two-phase mechanism. Shortly after venting is begun, the flow is thought to be fully choked (as a result of the two-phase mechanism); thus, the mass flow is reduced. During the fully choked period, the pressure decreases less rapidly with time. Consideration must be given to the relationship between geometry and the available power to determine whether a fully choked condition can be sustained throughout the discharge. The discharge

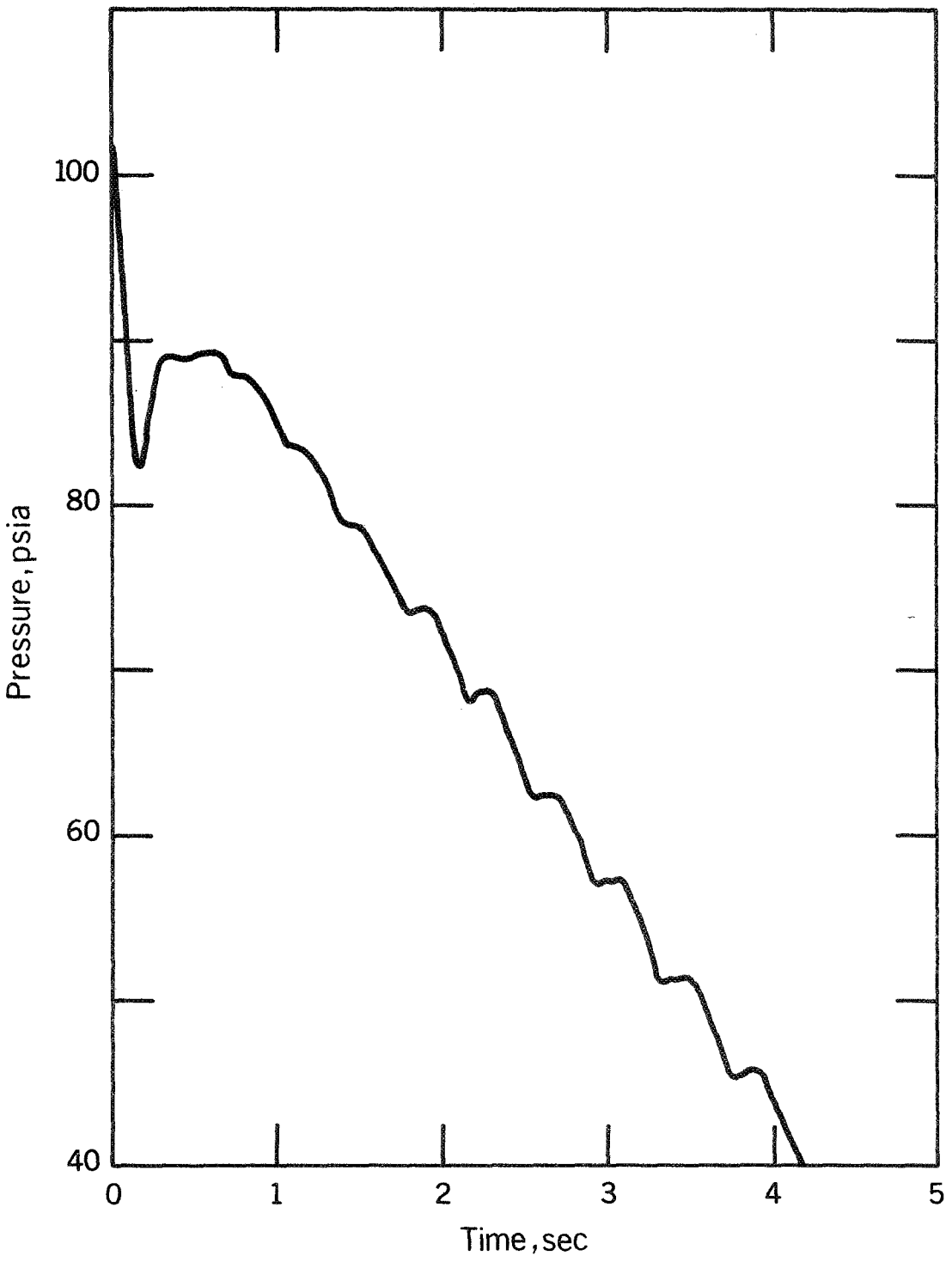

FIG. 41 PRESSURE OSCILLATIONS OBTAINED DURING INITIAL PHASE OF DISCHARGE THROUGH A ONE INCH ORIFICE

remained fully choked for all tests performed with a 0.25 inch orifice while oscillations have occurred during the 1 inch discharge with the specimen unheated.

As a result of the nature of the discharge, the analysis in Chapter VI will be applied only to the discharge through small orifices. One reason for this can be found in Appendix F and Figs. 39 and 40. It is assumed in the analysis that the system remains saturated during blowdown. The liquid and vapor temperatures in Appendix F for a 0.25 inch discharge remain close to saturation during the entire test. On the other hand, the data in Figs. 39 and 40 represent typical results obtained for discharge through larger orifices under conditions where no oscillations occur. Also, the rapidity of discharge from larger orifices would make analysis quite complicated.

Moody [85], in his analysis of blowdown, stressed the importance of liquid-vapor action in the vessel. In his test configuration, the blowdown nozzle was located at the bottom of the tank, in the liquid section. The blowdown consisted first of saturated water blowdown, followed by saturated vapor blowdown as shown in Figs. 10 and 11. A characteristic of his results is the "knee" in the pressure drop curve which occurs when the system is depleted of liquid and saturated vapor blowdown begins. Moody points out that vapor entrainment in the liquid yields a higher stagnation enthalpy near the break, or outlet, the effect of which is two fold at a given stagnation pressure: maximum flow rate is decreased, and initial pressure drop rate is increased.

For the present case of blowdown through the top of the vessel, it might be surmised that the opposite of Moody's conclusion would be

true. That is, liquid entrained in the vapor should give a lower stagnation enthalpy near the outlet. This, in turn, would increase the maximum flow rate and decrease the rate of initial pressure drop. Some evidence is available to support this contention if the pressure rates and length of discharge in the two studies are compared. However, the lack of similarity between the two types of discharge prevent any substantial comparison on this basis.

The test conditions for all blowdown tests are summarized in Tables 14 and 15. All significant parameters for both the saturated and subcooled discharge runs have been listed. The tests conducted to determine wall heat transfer and temperature response, tests 9-12, are not included in the tables. Also, those tests in which an equipment malfunction or power failure was incurred have been excluded.

All the data are plotted in Figs. 42, 43, and 44. The figures include both saturated and subcooled data. The dimensional time parameter t*, as used by Moody [85], has been used in the graphs. Some interesting points may be found in the representation of the pressure data. First, the dimensional time parameter enables all of the saturated data to be plotted on the same graph. Due to the large number of curves, they have been plotted separately. However, comparison of points for the three different orifice diameters yields the fact that all of the data points seem to fall along a single curve. This indicates a very consistent pressure behavior for all saturated blowdown tests. The difference in the figures may be attributed to the variation and location of heat input, as shown in Table 14. The heat flux

TABLE 14

CONDITIONS FOR SATURATED DISCHARGE TESTS

Run No.	Vessel Initial Pressure (psia)	Saturation Temperature (°F)	Orifice Throat Area (in^2)	Back Pressure (atm)	Upstream Pipe Area (in^2)	Strip Heat Flux (Btu/hr)	Preheater Power (Btu/hr)	Initial Water Mass (lb_m)	Final Water Mass (lb_m)	Length of Run (sec)
1)	100.9	328.5	0.196	1	7.07	-	10,200	25.35	21.73	75
3)	99.6	327.6	0.049	1	7.07	-	10,200	25.35	-	210
4)	99.5	327.5	0.049	1	7.07	-	10,200	25.35	-	250
5)	99.4	327.4	0.196	1	7.07	-	10,200	25.35	19.25	80
6)	99.1	327.2	0.049	1	7.07	-	10,200	25.35	20.25	350
7)	97.7	326.1	0.049	1	7.07	3,451	4,573	25.35	-	-
8)	100.1	327.9	0.196	1	7.07	3,495	3,959	25.35	-	-
14)	99.5	327.4	0.196	1	7.07	5,352	628	25.35	19.00	80
15)	100.8	328.4	0.196	1	7.07	-	3,823	25.35	20.75	80
16)	100.1	327.9	0.196	1	7.07	4,992	-	25.35	19.25	80
17)	100.8	328.4	0.196	1	7.07	4,027	-	25.35	-	70
18)	99.5	327.4	0.196	1	7.07	-	-	25.35	-	80
19)	99.6	327.5	0.049	1	7.07	6,665	-	25.35	19.25	280
20)	99.6	237.5	0.049	1	7.07	5,903	-	25.35	20.50	300
21)	99.7	327.6	0.785	1	7.07	8,956	-	25.35	10.25	17
22)	99.9	327.7	0.785	1	7.07	7,358	-	25.35	9.25	16

TABLE 15

CONDITIONS FOR SUBCOOLED DISCHARGE TESTS

Test	23	24	25	26
Vessel Initial Pressure (psia)	99.0	99.0	99.5	100.0
Saturation Temperature (°F)	327.1	327.1	327.4	327.8
Saturation Enthalpy (Btu/lbm)	297.7	297.7	298.0	298.4
Initial Water Temperature (°F)	275.0	301.0	279.0	307.0
Initial Water Enthalpy (Btu/lbm)	243.9	270.6	248.0	276.8
Initial Water Subcooling (Btu/lbm)	53.8	27.1	50.0	21.6
Flashing Pressure (psia)	45.5	68.0	48.5	74.5
Orifice Throat Area (in^2)	.785	.785	.049	.049
Back Pressure (atm.)	1	1	1	1
Upstream Pipe Area (in^2)	7.07	7.07	7.07	7.07
Strip Heat Flux (Btu/hr)	3386	5939	4329	4969
Preheater Power (Btu/hr)	-	-	-	-
Initial Water Mass (lbm)	25.35	25.35	25.35	25.35
Final Water Mass (lbm)	13.1	12.25	21.4	20.1
Length of run (sec)	16	16	210	260

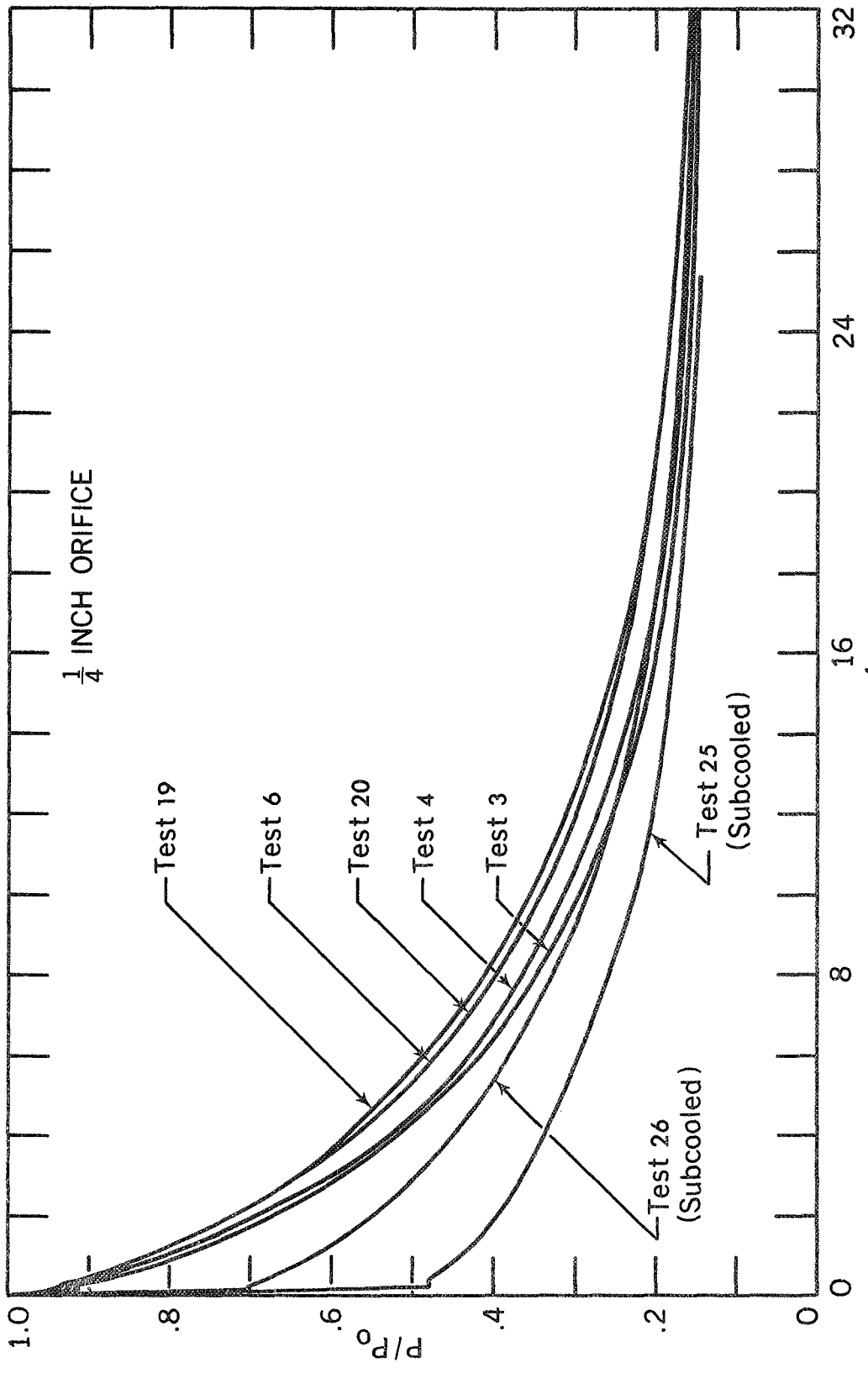

FIG. 42 PRESSURE HISTORY FOR BLOWDOWN THROUGH A ONE-QUARTER INCH ORIFICE

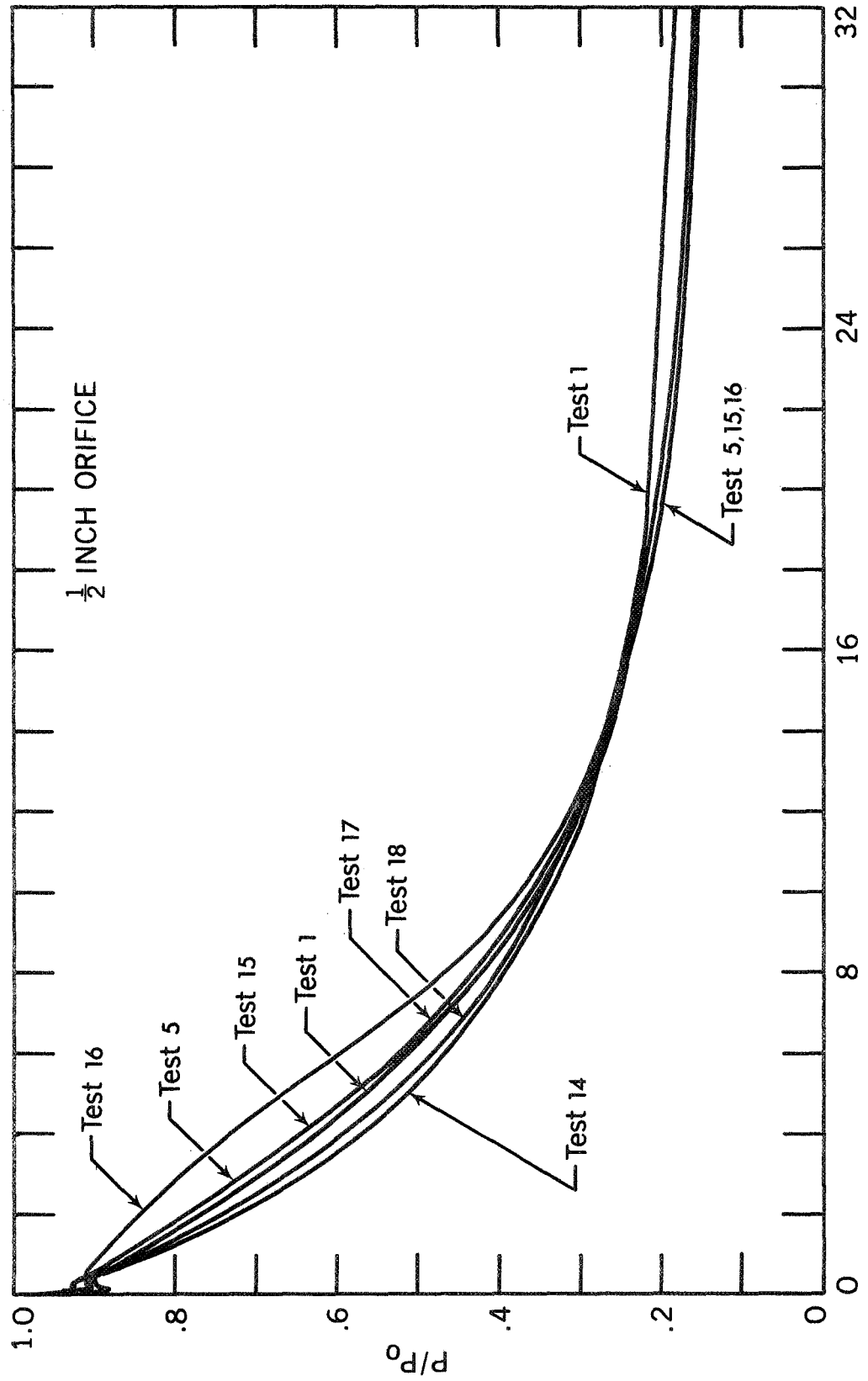

FIG. 43 PRESSURE HISTORY FOR BLOWDOWN THROUGH A ONE-HALF INCH ORIFICE

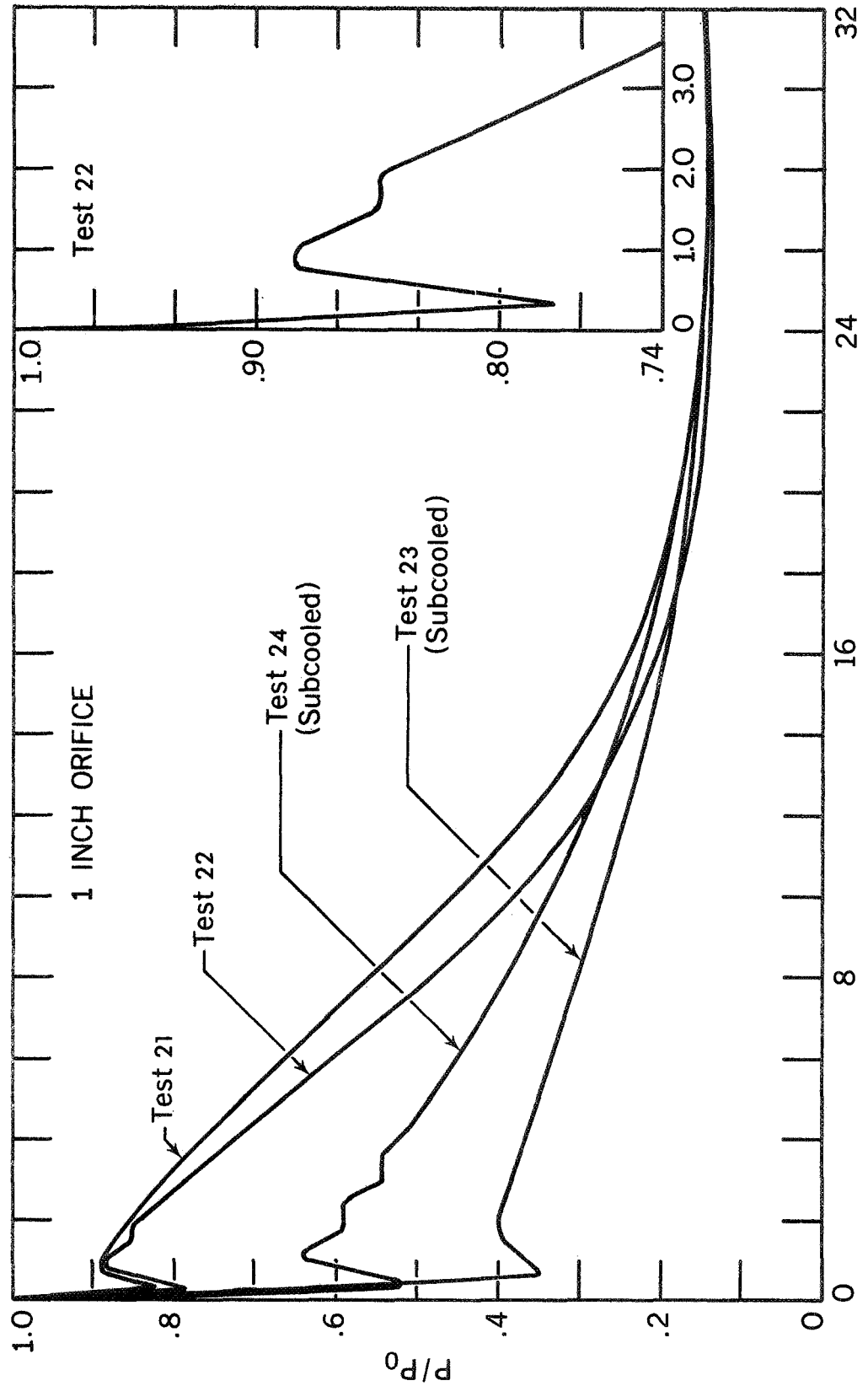

FIG.44 PRESSURE HISTORY FOR BLOWDOWN THROUGH A ONE INCH ORIFICE

in each test was supplied from a combination of the strip heater and/or the preheaters. It was impossible to control strictly the amount of heat input, since this is dependent, in part, on ambient conditions. Another feature apparent in Figs. 42 and 44 is the subcooled blowdown behavior. The initial conditions for these tests varied widely and explain the varied behavior. The amount of subcooling accounts for the extent of initial rapid pressure drop. Thereafter the rate of pressure drop stabilizes into a smooth steady decrease. It can be seen that the total time of discharge is approximately the same as for the saturated data. No explanation is offered for this behavior at present.

Measurements were made to determine the dependency of residual water in the vessel after blowdown on orifice, or simulated break size. These measurements are indicated in Table 14 and are shown graphically in Fig. 45. The residual water is about the same for both the 0.25 and 0.5 inch orifice blowdowns, indicating a similarity of behavior between the two sizes. Residual water for the 1 inch blowdown is only about one-half that for the other sizes. Also represented in Fig. 45 are prior measurements [80] conducted with and without hydraulic restrictions. The residual water tests in [80] were conducted from 520°F and 2330 psig, conditions far removed from the present case. The present system is also much smaller, containing less than one percent of the mass of the large-scale system [80].

Four tests (9-12) were devoted to measuring the wall temperature of the vessel during discharge. The data for these tests are given in Appendix F. Three iron-constantan thermocouples were used in both the large and small wall of the boiler to determine the interior, middle

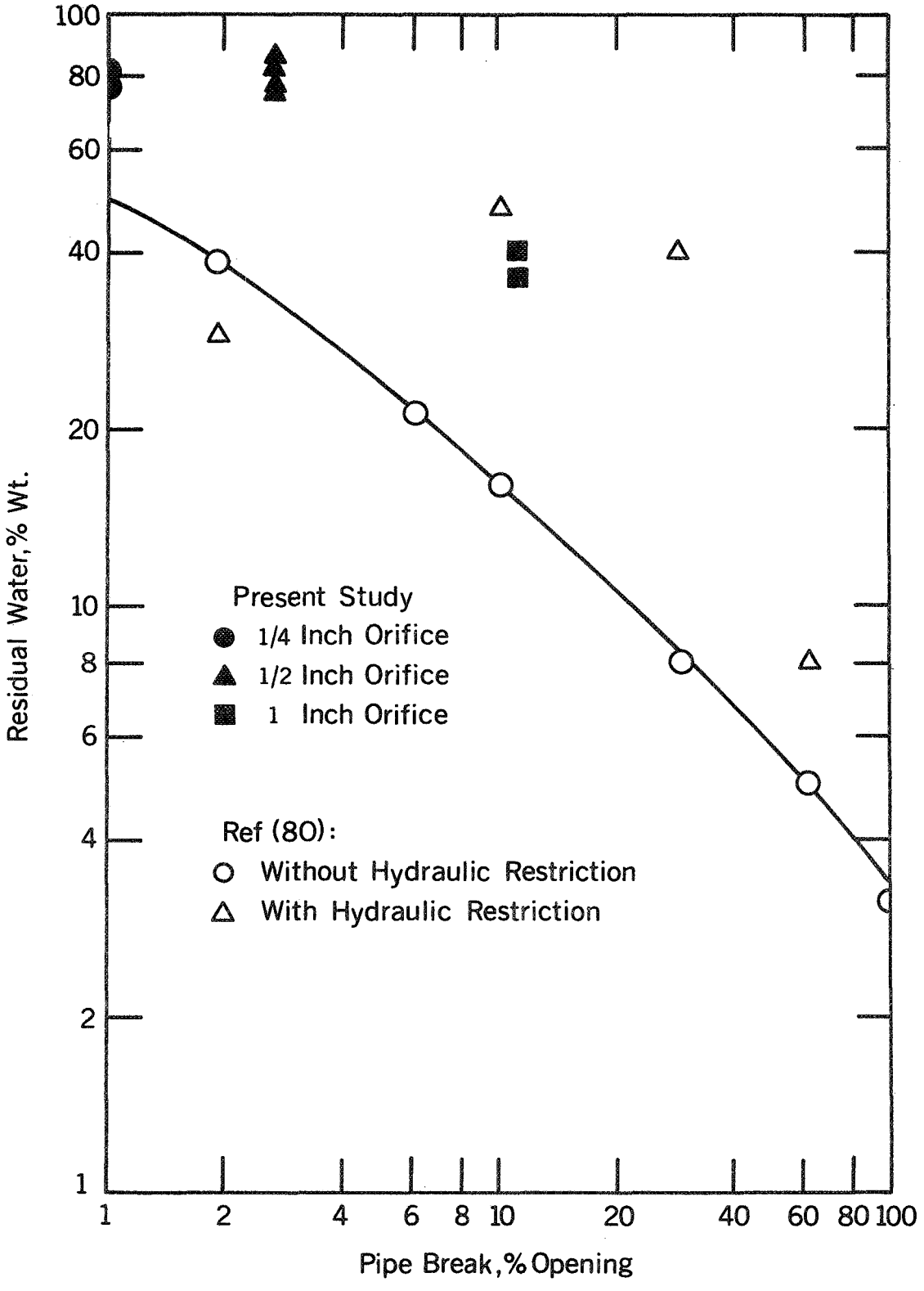

FIG. 45 RESIDUAL WATER FOR BLOWDOWN THROUGH VARIOUS ORIFICE SIZES

and exterior temperature response of the stainless-steel wall. Essentially linear traces were obtained in each case, with the temperature of the wall decreasing linearly with pressure, after a small initial time lapse.

C. Comparison With Model Developed in This Study

The analysis presented in the previous chapter may be used to simulate vapor discharge through a small opening. The appropriate equations have been programmed for digital computation. An important item in the generation of a solution for flow rates and pressure drop is the calculation of critical mass velocity. The model chosen for determining the critical mass velocity, G, is that of Moody [72].

Moody has presented a flow model which determines the parameter G as a function of vessel stagnation pressure and stagnation enthalpy. The vessel stagnation pressure is a known function in each successive increment of blowdown. However, during blowdown, the stagnation enthalpy is unknown. Since the system remains saturated and no provision exists for determining velocity, stagnation enthalpy must be considered as an additional parameter. The value is essentially constant during blowdown and is very nearly that of the saturated liquid, due to the low quality and small velocity of the mixture in the vessel.

The enthalpy of the liquid/vapor mixture prior to blowdown was 303 Btu/lbm. This value was used for the initial stagnation enthalpy in Moody's model for calculating the critical mass velocity. However, due to the structure of his model, the calculations diverge for small values of quality, i.e., values of enthalpy close to that of saturated

liquid. Then, a range of solutions for various initial values of stagnation enthalpy were determined. The results of the calculations are presented in Figs. 46 and 47. The predicted pressure versus time curves in Fig. 46 are compared with experimental data from tests 4, 6, and 19. All of the discharge tests were conducted with a 0.25 inch orifice. Good agreement is shown between the experimental and predicted traces. Both the rate of pressure drop and the length of discharge are in agreement with all observed data which have been obtained with the small opening. As stated earlier, the predictions are not applicable to discharge through large openings, or rapid blowdown. In this case, the liquid/vapor mixture does not remain close enough to saturation conditions to satisfy the approximations made in the analysis. The entire nature of the discharge is changed during a rapid depressurization. The interface is continually lifted and dropped, and considerable mixing of liquid and vapor occurs. In addition, slugs of liquid are thrown out through the discharge port.

During a controlled depressurization, by comparison, the liquid/vapor interface is disturbed to a much lesser extent. No liquid is detected being blown from the vessel, as determined by visual observation. The analysis applies only to this type of blowdown.

It is difficult to distinguish between what constitutes a large or small opening, or a rapid from a controlled depressurization. The distinction in this investigation was determined from visual observations of a number of discharge tests. Further study is needed to define the complex inter-relationships between vessel size and geometry and the diameter of the blowdown orifice or nozzle size.

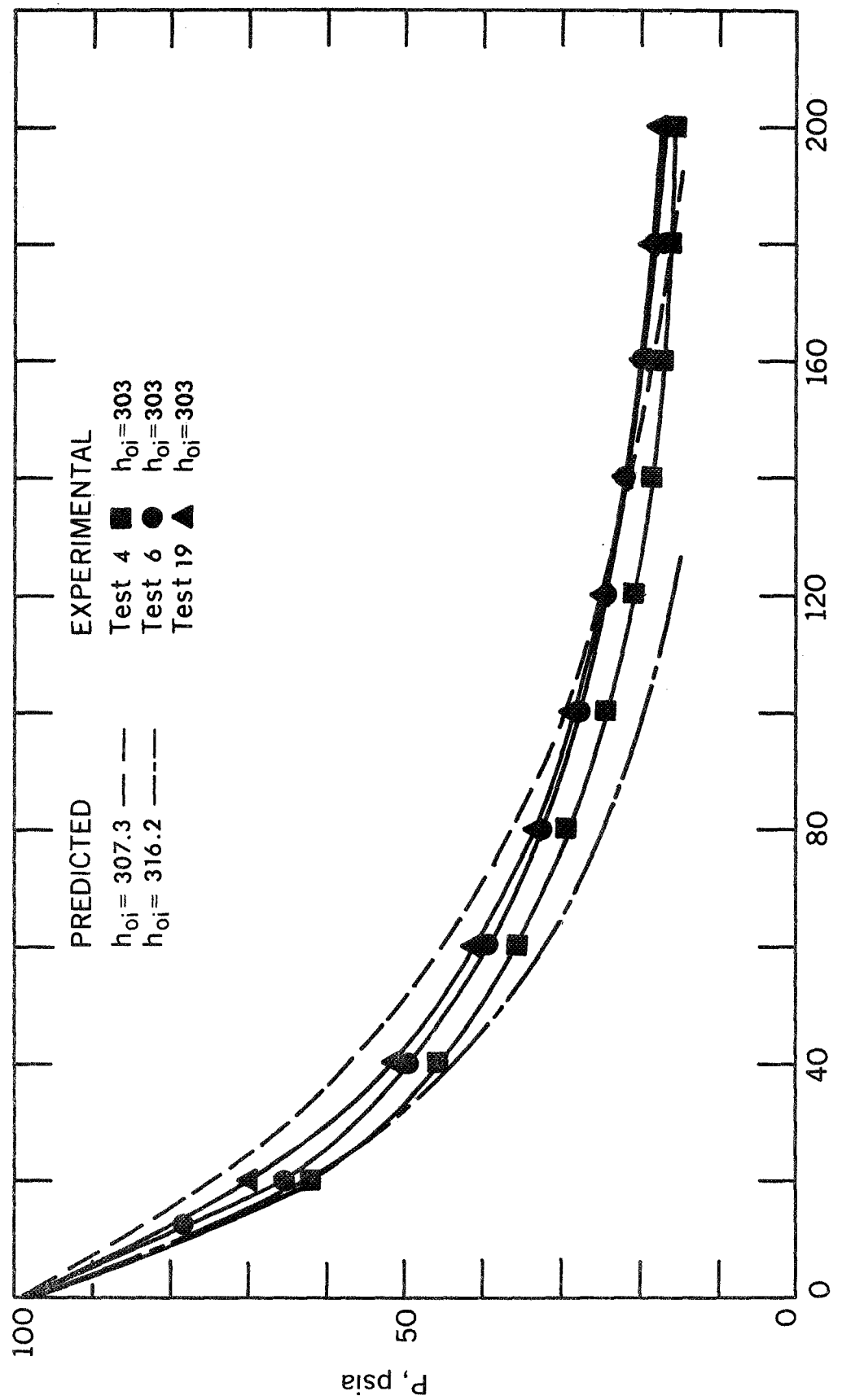

FIG. 46 COMPARISON OF PREDICTED AND EXPERIMENTAL PRESSURE HISTORY

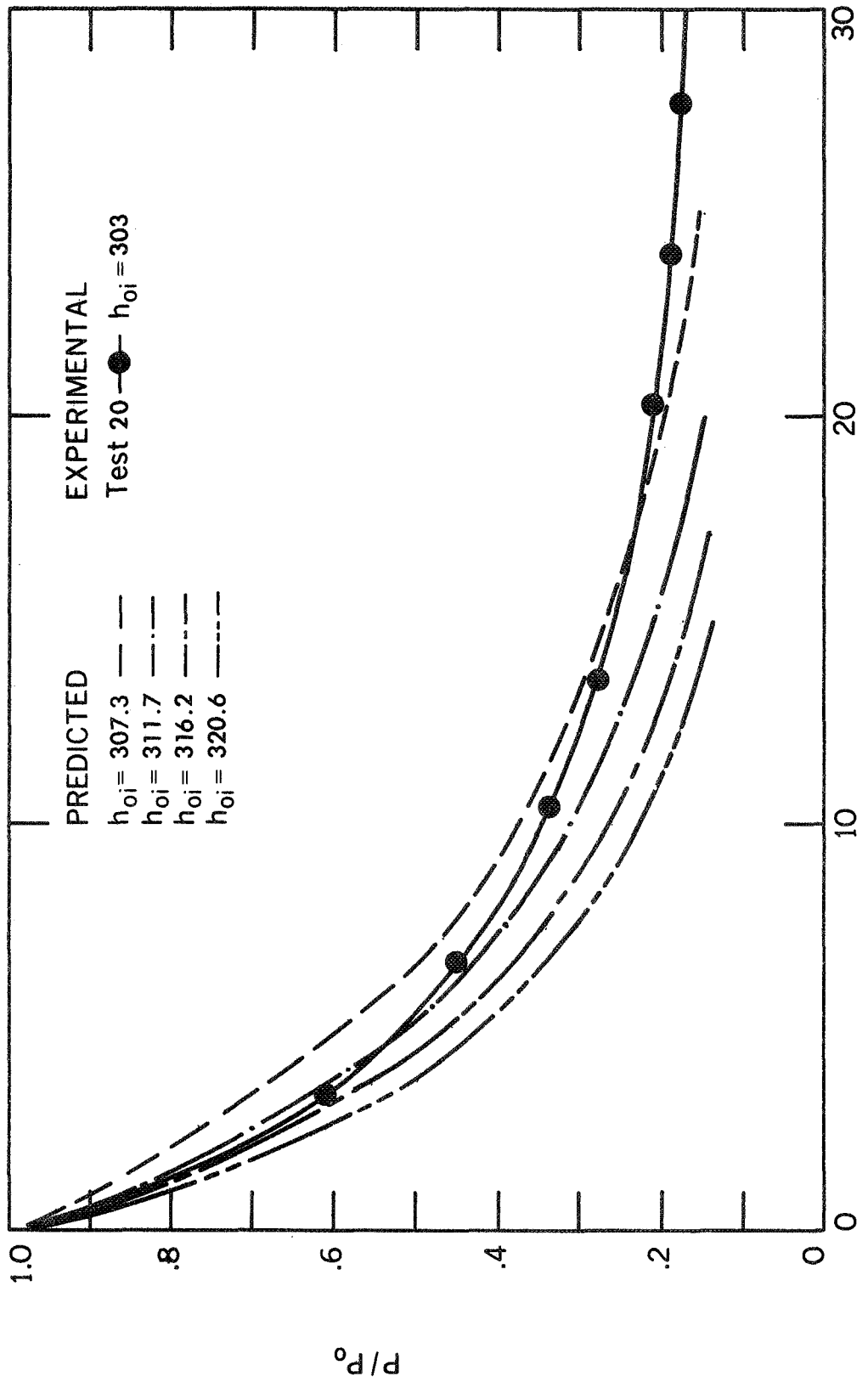

FIG. 47 PRESSURE VERSUS DIMENSIONAL TIME: COMPARISON WITH EXPERIMENTAL RESULTS

The predicted pressure-drop results are repeated in Fig. 47. In the figure, pressure has been non-dimensionalized by dividing by the initial vessel pressure and the dimensional time has been introduced, as used by Moody [85]. Also, included in the figure are experimental data from test 20 for a 0.25 inch diameter orifice. Again, the agreement between theory and experiment is pointed out.

The residual water remaining in the vessel after blowdown is dependent on break size (orifice size) and on the location of the break. As observed during top blowdown tests [79], the steam exiting the blowdown nozzle was of higher quality than the steam of comparable bottom blowdown tests. The difference in quality of the steam for top and bottom blowdowns was the result of the different elevations of the blowdown nozzle.

In the top blowdown configuration, the enthalpy stored in the fluid was dissipated by an expanding or flashing of the fluid in the vessel to high quality steam which was allowed to escape through the blowdown nozzle. In the bottom blowdown configuration, the expanding fluid in the vessel maintained a fluid pressure which forced a fluid mixture out the bottom of the blowdown nozzle. The results of the blowdown tests performed with the vessel in the top configuration and with small simulated pipe breaks indicate that pipe breaks near the top of a reactor vessel will result in an appreciable amount of residual water in the vessel at the conclusion of blowdown.

The same conclusion is valid in the present case, as has been seen in Fig. 45. Data for the 0.25 inch orifice blowdown indicate that

approximately 20 percent of the fluid mass is discharged. A comparison with the theory may be drawn in the following way. Once the pertinent mass flow rates have been computed, the incremental mass change is determined for a known increment of time by taking appropriate balances. A balance between the liquid/vapor system masses and the mass discharged through the orifice in the top of the vessel yields the present value of total system mass. An appropriate system of accounting which has been incorporated into the computer program continually updates the values of liquid, vapor, and total system mass. The procedure also permits the calculation of residual mass for comparison with the experimental value.

A plot of system mass fraction versus dimensionless pressure change is presented in Fig. 48. As expected, the theory predicts a continuous decrease in total mass as a function of time, or incremental pressure decrease. If the experimental values of Fig. 45 are compared with the predicted curve, it is found that the theory of this study slightly underpredicts the discharge whereas the application of Moody's analysis results in a large error. The underprediction is to be expected. During the actual discharge, a certain amount of liquid will be entrained in the vapor being discharged from the vessel. The equations which were derived account only for vapor discharge. Any liquid discharged during the blowdown will account for differences such as those observed in Fig. 48. The theory of this study predicts the residual mass-fraction within 10 percent deviation.

A close account of liquid/vapor action during discharge is important in determining the nature of the blowdown. In full scale systems

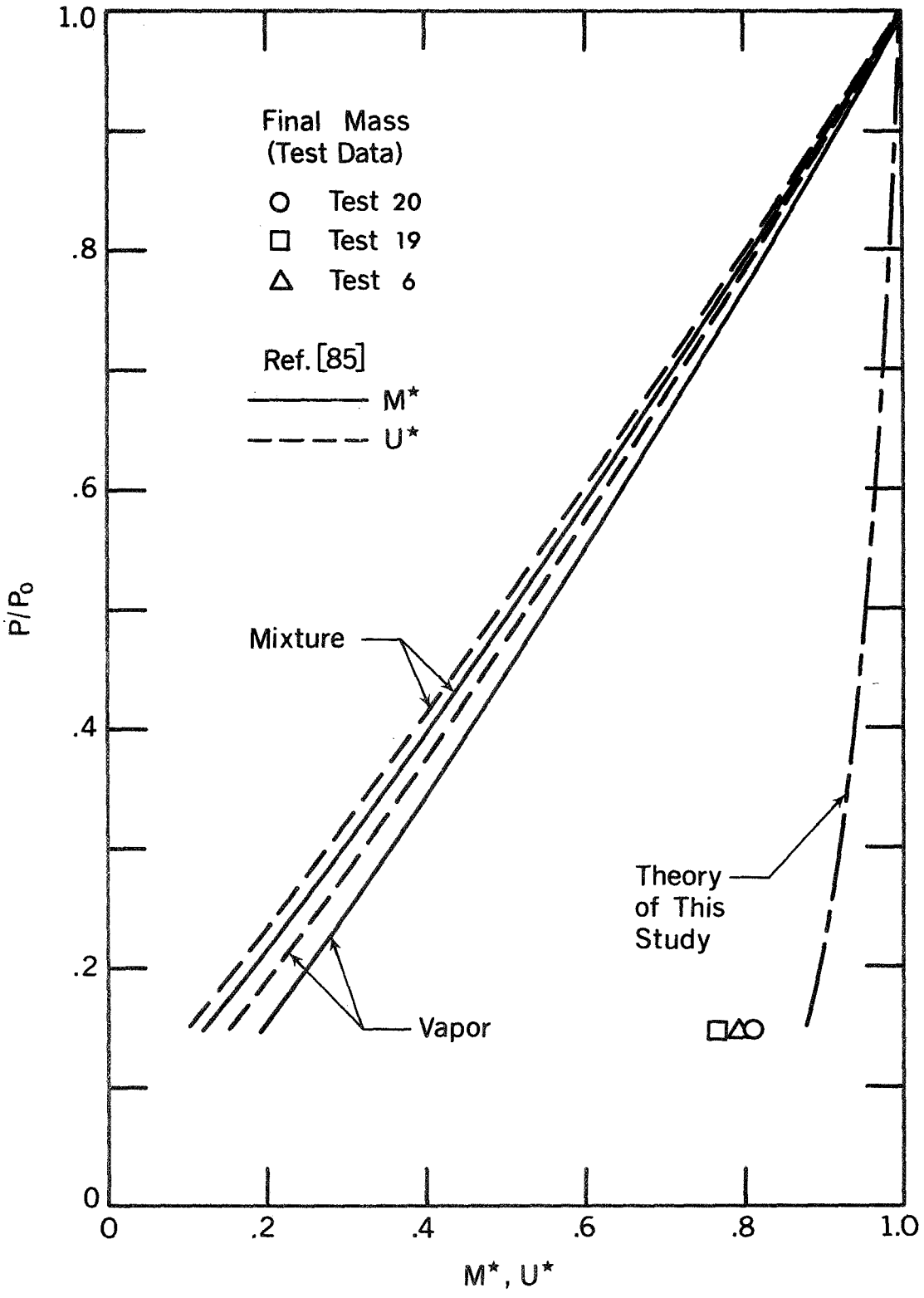

FIG. 48 SYSTEM MASS-FRACTION VERSUS DIMENSIONLESS PRESSURE CHANGE

such knowledge may be essential in determining core heat-transfer environment and transient forces on vessel internals. The blowdown rate depends upon local time-dependent fluid properties in the vessel. The present model yields system masses and mixture quality as a function of pressure or blowdown time. The continuous decrease in total mass and increase in vapor system mass during discharge would perhaps lead one to expect an increase in mixture quality as a function of time. This is not the case. Although total vapor volume increases and total liquid volume decreases with decreasing pressure, this serves only to increase the specific volume of the vapor fraction. Thus, system quality is essentially constant, exhibiting a slight decrease with pressure decrease. The model developed in this study also yields local time-dependent liquid and vapor properties within the vessel.

D. Comparison with Other Investigations

Moody [85] developed a general blowdown formulation to predict maximum flow rate in terms of vessel stagnation properties. The model also yields time-dependent pressure, mass and energy in a vessel for various saturated-water reference systems. He presented graphs that can be used to estimate system pressure, mass and energy at various times during a vessel blowdown from 1000 psia and 2000 psia steam/water reference systems. For comparison with the theory of this study it was necessary to generate the required data for a 100 psia reference system. The appropriate model equations were used along with realistic input conditions for the present system to calculate comparison graphs for both saturated-vapor and homogenized mixture characteristic blowdowns.

The results of these calculations are presented in Figs. 48 and 49.

Time-dependent system pressure for both vapor and mixture blowdown is plotted versus dimensional time in Fig. 49. Also included in the graph are the theory of this investigation and data from test 3. The model of Moody does not predict blowdown time adequately for the current system. The writer's theory agrees well with the experimental pressure drop curve.

The model developed in this study does not account for the system energy as a function of blowdown time as does the Moody theory. However, the experimental system studied is not the same from the viewpoint of energy addition. Energy is constantly being added to the current experimental blowdown facility through the preheaters and/or the heated strip. This would account for some of the error exhibited by the Moody predictions. This is seen in Fig. 48 where Moody's values for system mass-and energy-fraction are plotted versus pressure. The data points are measured values of final mass for a number of blowdown tests. The prediction of the present study is shown for comparison. Moody's prediction does not agree with the data or theory of this study. This is true for both the saturated vapor and homogenized mixture characteristic blowdown curves. The predicted energy fraction curves would be expected to exhibit the same general disagreement. However, as explained, no data are available for suitable comparison.

Fauske [82] has examined the current status of model studies and empirical evaluations of the critical coolant loss rates through various apertures. A comparison was given of the Fauske [2], Levy [71] and

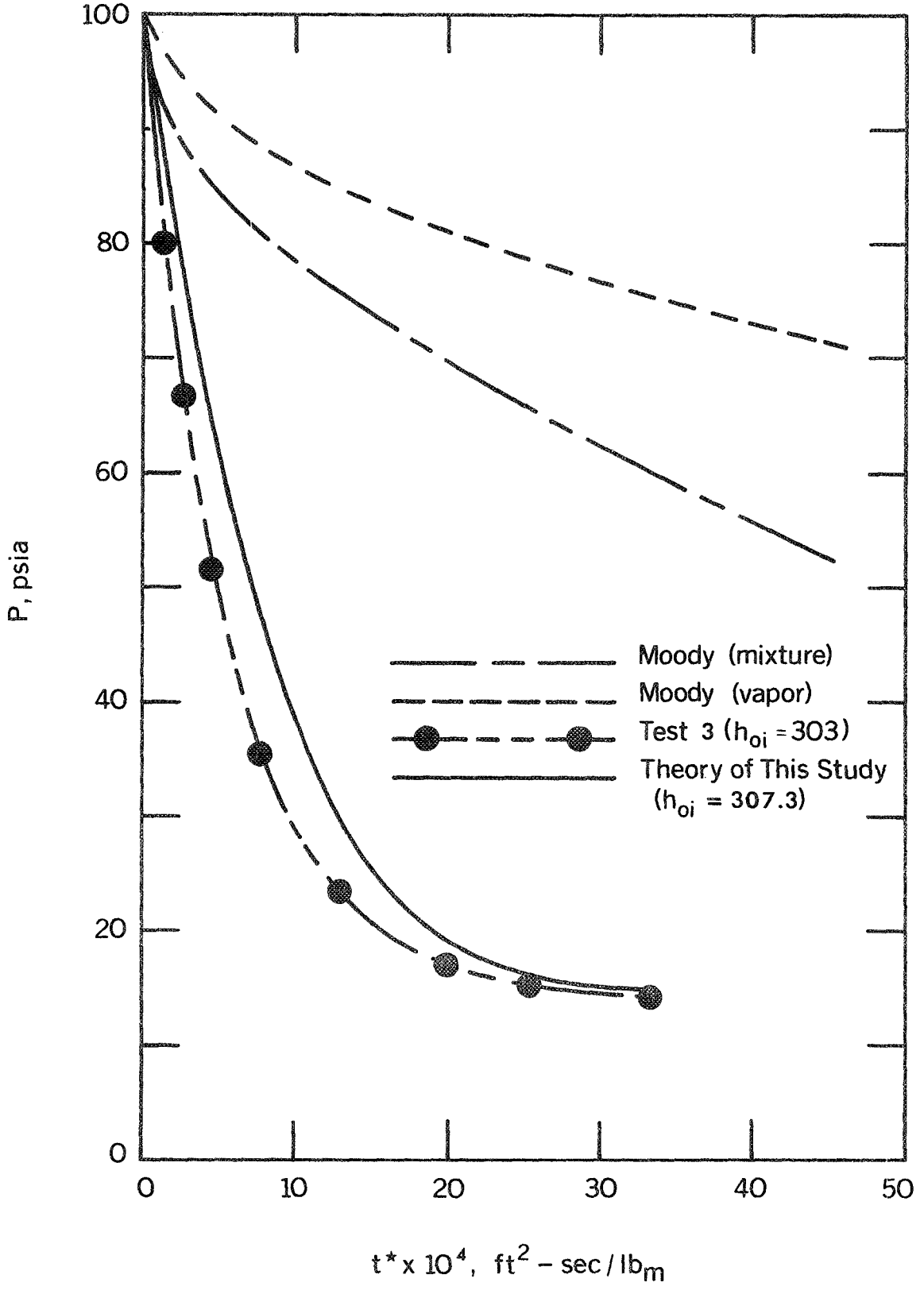

FIG. 49 COMPARISON OF THEORETICAL PRESSURE HISTORY WITH MOODY'S [85] PREDICTION FOR VAPOR & MIXTURE BLOWDOWN

Moody [72] models for critical flow rate. The differences between models are surprisingly small and all three methods correlate experimental data well. The Moody model yields mass flow values which are consistently higher than the Fauske results except for low qualities. In regions of low and decreasing quality, the Levy and Moody models yield maximum flow rates, whereas the Fauske model leads to increasing flow rates.

The results that have been obtained should be examined in relation to blowdown studies on full-scale systems. The size of the orifice or nozzle relative to the pressure vessel diameter is thought to have an important effect on the flow rate during blowdown. Blowdown behavior of the Humboldt and Bodega vessels, Figs. 10 and 11, was very similar although one system was about fifty percent larger in diameter and volume than the other. This behavior may be compared with the information from the current facility presented in Figs. 38, 42-44, and 46-47. It is seen that similar characteristics are evident for the various facilities. This tends to indicate that reduced scale tests can be used to predict loss of coolant from large reactor vessels, providing the information on orifice size to vessel diameter is available for a sufficient range of conditions, including effects of initial pressure.

VIII. SUMMARY AND CONCLUSIONS

A. Surface and Pressure Effects in Nucleate Pool Boiling

The desired end result of studies concerning surface effects on boiling is a method of surface characterization which would describe an increase in nucleation sites by an increase in the descriptor index. The numerous parameters involved with boiling heat transfer make this a complicated, if not impossible, task. A number of basic investigations on the boiling phenomenon will be required to progress in this direction. The surface studies of the present investigation were oriented to this end.

The present study has been concerned with pool boiling at various pressures from chemically etched 304 stainless-steel surfaces in contact with distilled water. The surfaces were prepared in this manner to produce variations in nucleation sites and surface roughness. Results show the changes in heat transfer with varying rms surface roughness and preparation technique. The Rohsenow pool boiling correlation was used to correlate the data successfully. Conclusions of this phase of the study include the following:

1. Additional Data on Surface Effects

Data have been added to the literature on surface effects on boiling. These data show that surface preparation technique affects

the boiling heat transfer mechanism and emphasize the statement that rms surface roughness alone is not adequate to describe a boiling heat transfer surface.

2. Applicability of Rohsenow Equation

The study has shown the applicability of the Rohsenow equation for correlating pool boiling heat transfer. New values of C_{sf} and the exponent, r, are presented for chemically etched stainless-steel surfaces. In this respect, it has been demonstrated that the exponent of the Rohsenow equation varies and accounts for surface preparation technique.

3. Extended Range of Rohsenow Correlation

This study has shown the desirability of extending the use of the Rohsenow correlation. The extension of the information for the exponent, r, and the coefficient, C_{sf}, of the Rohsenow correlation is recommended for other surface preparation techniques as well as for other surface-liquid combinations. It is suggested that the equation be applied to cryogenic pool boiling data.

4. Wall Superheat Change With Pressure

Several correlations which have appeared in the literature are compared with the present elevated pressure pool boiling data. The correlations of Rohsenow and Borishansky are restrictive to certain types of surfaces. However, these correlations have been shown to be applicable for a variety of boiling conditions by a simple adjustment of the exponents

and coefficients. The correlation presented by Lienhard and Schrock does not contain a surface characterization term and is more restrictive.

Based on available data, the backshift found for wall superheat of a pool boiling system with increased pressure is not a direct function of system pressure but is due in large extent to aging of the test surface. The backshift was encountered for chemically etched specimens tested in a low to high pressure sequence, with the atmospheric pressure test conducted first. The phenomenon was not noticeable in the reverse sequence of testing. This might indicate some inhibition of the vapor formation process from the combined pressure and surface aging effects.

The slope of the heat-flux-versus-wall-superheat curve (for a chemically etched surface) is a function of pressure and decreases as system pressure increases. This indicates that for Rohsenow's correlation, the exponent r of the heat flux term may be a function of system pressure.

At present, there is no pool boiling correlation which sufficiently describes the various surface parameters. Caution should be used when any general correlation for pool boiling is applied which does not adequately characterize the test surface.

B. Saturated Discharge

A basic analytical and experimental study has been conducted on transient fluid behavior during saturated blowdown. Data were collected on pressure, temperature and heat flux before, during and after depressurization of a saturated pool-boiling vessel. Parameters examined include

wall superheat response and liquid/vapor action during both rapid and controlled depressurization. Some of the conclusions of this phase of the investigation are:

1. Pressure Fluctuations in Saturated Depressurization

A basic explanation has been given for pressure fluctuations observed in discharging saturated systems. No satisfactory previous explanation had existed for pressure spikes observed in the pressure versus time charts for such systems. Considerable experimental evidence has been obtained and presented to support the explanation.

2. Role of Operational Parameters on Discharge

The role of the parameters, heat flux, surface superheat, system geometry, operating pressure, method of pressure release and type of fluid on depressurization has been studied. In this regard, the effect of the type of depressurization on the residual mass in the system has been determined. The type of discharge has been controlled by using various sized orifices ranging from one-fourth to one inch diameters. Certain characteristics are common to all type discharges studied. Heat flux and orifice size have both been found to influence the bulk liquid superheat and the strength of the discharge.

3. Model Studies

Results of previous investigations were reviewed and correlated with the present study as far as was possible. The predictive model developed by Moody was found to be the best model currently appearing

in the literature. His model was adapted and compared to the results obtained. However, the comparison was found to be unsatisfactory. The basic phenomena involved were studied and an analytical model was formulated to describe the system.

The writer's model appears to be satisfactory in predicting the experimental results that have been obtained. The model yields system pressures and temperatures, along with various system masses as a function of discharge time. Also, the model may be used to obtain local time-dependent liquid and vapor properties within the vessel. Certain restrictions of the model should be pointed out. The analysis has been formulated for the current experimental facility; no attempt has been made to orient the model toward large-scale reactor systems in current use. Also, the analysis applies to a controlled discharge in which vapor only is discharged from the system.

However, it is believed that the experimental results that have been obtained may permit certain conclusions about large-scale systems. Similarities in blowdown behavior have been pointed out. This indicates that reduced-scale tests can be effective in predicting pressure behavior and loss of coolant from large reactor vessels, provided certain information is made available.

The study has added basic information on transient fluid behavior for the design engineer who must consider overall system performance. Although the study was conducted with a non-cryogenic fluid, the general approach appears to be compatible with cryogenic analysis.

REFERENCES

1. J. W. Westwater, "Nucleate Pool Boiling II," Petro Chemical Engineering, Vol. 33, No. 10 (1961), p. 53-60.

2. J. W. Westwater, "Things We Don't Know About Boiling," Research in Heat Transfer, Pergamon Press, New York, (1963), pp. 61-73.

3. W. M. Rohsenow, "A Method of Correlating Heat Transfer Data for Surface Boiling of Liquids," ASME Transactions, Vol. 74 (1952).

4. J. H. Lienhard and V. E. Schrock, "Generalized Displacement of the Nucleate Boiling Heat-Flux Curve, with Pressure Change," International Journal of Heat and Mass Transfer, Vol. 9, No. 4 (April, 1966), pp. 355-363.

5. V. M. Borishansky, I. I. Novikov, and S. S. Kutateladze, "Use of Thermodynamic Similarity in Generalized Experimental Data of Heat Transfer," International Developments in Heat Transfer, Part II (1961), pp. 475-482.

6. N. M. Kuznetsov and V. N. Oleinik, "Application of the Thermodynamic Similarity Theory to Correlation of Experimental Data on Heat Transfer of Boiling Organic Heat-Transfer Fluids," Journal of Engineering Physics, Vol. 10, No. 1 (1966), p. 64.

7. R. C. Progelhof and J. A. Owczarek, "The Rapid Discharge of a Gas from a Cylindrical Vessel Through an Orifice," Winter Annual Meeting, ASME, Philadelphia, November 17-22, (1963).

8. H. K. Fauske, "The Discharge of Saturated Water Through Tubes," Chemical Engineering Progress Symposium Series, Vol. 59, No. 61 (1965), pp. 210-216.

9. F. J. Moody, "Maximum Two-Phase Vessel Blowdown from Pipes," ASME Transactions--Journal of Heat Transfer, Vol. 88, Series C, No. 3 (August, 1966), pp. 285-295.

10. W. D. Ward, Calculations of Mass-Flow and Thrust Produced for a Two-Phase Fluid Mixture Passing Through a Choked Nozzle, NASA Technical Memorandum, TM X-53269, (August, 1965).

11. J. R. Howell and K. J. Bell, "An Experimental Investigation on the Effects of Pressure Transients on Pool Boiling Burnout," Chemical Engineering Progress Symposium Series, Vol. 59 (1963), pp. 88-94.

12. G. E. Tanger, R. I. Vachon, and R. B. Pollard, "Pool Boiling Response to Pressure Decay," Proceedings of the Third International Heat Transfer Conference, Vol. IV (May, 1966), pp. 38-43.

13. P. M. Ordin, S. Weiss, and H. Christenson, "Pressure-Temperature Histories of Liquid Hydrogen Under Pressurization and Venting Conditions," Advances in Cryogenic Engineering, New York: Plenum Press, Inc., (1960), Vol. 5, pp. 481-486.

14. M. Jakob and W. Fritz, Forschung a. d. Geb. d. Ingenieurwes, Vol. 2, (1931), p. 435.

15. H. B. Clark, P. S. Strenge, and J. W. Westwater, "Active Sites of Nucleate Boiling," Chemical Engineering Progress Symposium Series, Vol. 55, No. 29, (1959), pp. 103-110.

16. C. Corty and A. S. Foust, "Surface Variables in Nucleate Boiling," Chemical Engineering Progress Symposium Series, Vol. 51, No. 17, (1955), pp. 1-12.

17. K. Nishikawa, "Nucleate Boiling Heat Transfer of Water on the Horizontal Roughened Surface," Memoirs of the Faculty of Engineering, Kyushu University, Vol. 17, No. 2, (1958), pp. 85-103.

18. R. F. Gaertner and J. W. Westwater, "Population of Active Sites in Nucleate Boiling Heat Transfer," Chemical Engineering Progress Symposium Series, Vol. 56, No. 30, (1960), pp. 39-48.

19. P. Griffith and J. D. Wallis, "The Role of Surface Conditions in Nucleate Boiling," Chemical Engineering Progress Symposium Series, Vol. 56, No. 30, (1960), pp. 49-63.

20. P. J. Berenson, "Experiments on Pool Boiling Heat Transfer," International Journal of Heat and Mass Transfer, Vol. 5, (1962), pp. 985-999.

21. C. F. Bonilla, J. J. Grady, and G. W. Avery, "Pool Boiling Heat Transfer from Scored Surfaces," AIChE Preprint 32, Sixth National Heat Transfer Conference, (August, 1963).

22. Y. Y. Hsu and R. W. Graham, "An Analytical and Experimental Study of the Thermal Boundary Layer and the Ebullition Cycle in Nucleate Boiling," NASA TN-D-594, (1961).

23. B. Otterman, "Photographic Study of Bubble Dimensions and Boiling Action on Mercury and Standard Engineering Surfaces," Proceedings Heat Transfer and Fluid Mechanics Institute, (1962), pp. 185-196.

24. J. W. Westwater, "Boiling Heat Transfer," American Scientist, Vol. 47, (1959), pp. 427-446.

25. P. A. Lottes and R. Viskanta, "Nucleation and Boiling from a Liquid-Liquid Interface," Proceedings Heat Transfer and Fluid Mechanics Institute, (1962), pp. 171-184.

26. F. K. Gordon, T. Singh, and E. Y. Weissman, "Boiling Heat Transfer between Immiscible Liquids," International Journal of Heat and Mass Transfer, Vol. 3, (1961), pp. 90-93.

27. B. R. Mead, F. E. Romie, and A. G. Guibert, "Liquid Superheat and Boiling Heat Transfer," Proceedings Heat Transfer and Fluid Mechanics Institute, (1951), pp. 209-216.

28. Y. Y. Hsu, "On the Size of Active Nucleation Cavities on a Heating Surface," Journal of Heat Transfer, ASME Transactions, Series C, Vol. 84, No. 3, (August, 1962), pp. 207-216.

29. H. M. Kurihara and J. E. Myers, "The Effects of Superheat and Surface Roughness on Boiling Coefficients," AIChE Journal, Vol. 6, No. 1, (1960), pp. 83-86.

30. J. Frenkel, Kinetic Theory of Liquids, Oxford Press, (1946), Dover Publications, New York, (1955).

31. M. Jakob, "Local Temperature Differences Occurring in Evaporation, Condensation, and Catalytic Reaction," Temperature, Its Measurement and Control in Science and Industry, Reinhold Publishing Corporation, New York, (1941), p. 834.

32. R. F. Gaertner, "Photographic Study of Nucleate Pool Boiling on a Horizontal Surface," Journal of Heat Transfer, ASME Transactions, Series C, Vol. 87, No. 1, (1965), pp. 17-29.

33. W. M. Rohsenow and J. A. Clark, "A Study of the Mechanism of Boiling Heat Transfer," ASME Transactions, (July, 1951), pp. 609-620.

34. M. Jakob, Heat Transfer, Vol. 1, John Wiley & Sons, Inc., New York, (1949), p. 614.

35. K. Forster and R. Grief, "Heat Transfer to a Boiling Liquid-Mechanisms and Correlations," Journal of Heat Transfer, ASME Transactions, Series C, Vol. 81, (1959), pp. 43-53.

36. J. D. Moore and R. B. Mesler, "Measurements of Rapid Surface Temperature Fluctuations During Nucleate Boiling of Water," AIChE Journal, Vol. 7, (1961), pp. 620-624.

37. W. Fritz, "Berechnung des Maximal Volumens Von Dampfblasen," Physik Z., Vol. 36, (1935), p. 379.

38. R. Moissis and P. J. Berenson, "On the Hydrodynamic Transitions in Nucleate Boiling," Journal of Heat Transfer, ASME Transactions, Series C, Vol. 85, No. 3, (1963), p. 221.

39. Y. P. Chang and N. W. Snyder, "Heat Transfer in Saturated Boiling," Chemical Engineering Progress Symposium Series, Vol. 56, No. 30, (1960), pp. 25-38.

40. M. T. Cichelli and C. F. Bonilla, "Heat Transfer to Liquids Boiling Under Pressure," AIChE Transactions, Vol. 41 (1945), pp. 755-787.

41. S. G. Bankoff, "Prediction of Surface Temperatures at Incipient Boiling," Chemical Engineering Progress Symposium Series, Vol. 55, No. 29, (1959), pp. 87-94.

42. S. G. Bankoff, "A Note on Latent Heat Transport in Nucleate Boiling," AIChE Journal, Vol. 8, No. 1, (1962), pp. 63-65.

43. D. S. Cryder and A. C. Finalborgo, "Heat Transmission from Metal Surfaces to Boiling Liquids: Effects of Temperature of the Liquid on Film Coefficient," AIChE Transactions, Vol. 33, (1937), p. 346.

44. F. Kreith and M. J. Summerfield, "Heat Transfer to Water at High Flux Densities," ASME Transactions, Vol. 71, (1949), pp. 805-815.

45. I. A. Raben, R. T. Beaubouef, and G. E. Commerford, "A Study of Heat Transfer in Nucleate Pool Boiling of Water at Low Pressure," Chemical Engineering Progress Symposium Series, Vol. 61, No. 57, (1965), pp. 249-257.

46. D. A. Huber and J. C. Hoehne, "Pool Boiling of Benzene, Diphenyl, and Benzene-Diphenyl Mixtures Under Pressure," ASME Transactions, Journal of Heat Transfer, Series C, Vol. 85, (1963), pp. 215-220.

47. J. H. Lienhard and V. E. Schrock, "The Effect of Pressure, Geometry , and the Equation of State upon the Peak and Minimum Boiling Heat Flux," Journal of Heat Transfer, ASME Transactions, Series C, Vol. 85, No. 3, (1963), 261-272.

48. J. H. Lienhard and K. Watanabe, "On Correlating the Peak and Minimum Boiling Heat Fluxes with Pressure and Heater Configuration," Journal of Heat Transfer, ASME Transactions, Series C, Vol. 88, No. 1, (1966), pp. 94-100.

49. P. J. Marto, J. A. Moulson and M. D. Maynard, "Nucleate Pool Boiling of Nitrogen with Different Surface Conditions," Journal of Heat Transfer, ASME Transactions, Series C, Vol. 90, No. 4, (November, 1968), pp. 437-444.

50. P. J. Marto and W. M. Rohsenow, "Effects of Surface Conditions on Nucleate Pool Boiling of Sodium," Journal of Heat Transfer, ASME Transactions, Series C, Vol. 88, No. 2 (1966), pp. 196-204.

51. W. C. Elrod, J. A. Clark, E. R. Lady and H. Merte, "Boiling Heat-Transfer Data at Low Heat Flux," Journal of Heat Transfer, ASME Transactions, Series C, Vol. 89, No. 3 (August, 1967), pp. 235-243.

52. S. T. Hsu and F. W. Schmidt, "Measured Variations in Local Surface Temperatures in Pool Boiling of Water," Journal of Heat Transfer, ASME Transactions, Series C, Vol. 83, (1961), p. 254.

53. J. Madejski, "Theory of Nucleate Pool Boiling," International Journal of Heat and Mass Transfer, Vol. 8, (1965), pp. 155-171.

54. C. W. Cowley, W. J. Timson, and J. A. Sawdye, "A Method for Improving Heat Transfer to a Boiling Fluid," I and EC Progress Design and Development, Vol. 1, No. 2 (1962), pp. 81-84.

55. R. I. Vachon, G. E. Tanger, D. L. Davis, and G. H. Nix, "Pool Boiling on Polished and Chemically Etched Stainless Steel Surfaces," Journal of Heat Transfer, ASME Transactions, Series C, Vol. 90, No. 2, (May, 1968), pp. 231-238.

56. L. S. Tong, Boiling Heat Transfer and Two-Phase Flow, John Wiley & Sons, New York, (1965).

57. R. R. Kepple and T. V. Tung, Two-Phase (Gas-Liquid) System: Heat Transfer and Hydraulics--An Annotated Bibliography, ANL-6734, USAEC Report, (1963).

58. E. Giffen, "Rapid Discharge of Gas from a Vessel into the Atmosphere," Engineering, Vol. 150, (1940), pp. 134-136, 154-155, 181-183.

59. J. Kestin and J. S. Glass, "The Rapid Discharge of a Gas from a Cylindrical Vessel," Aircraft Engineering, Vol. 23, (1951), pp. 300-304.

60. R. Progelhof and J. A. Owczarek, "The Rapid Discharge of a Gas from a Cylindrical Vessel Through a Nozzle," AIAA Journal, Vol. 1, (1963), pp. 2182-2184.

61. J. Kestin and J. S. Glass, "Application of the Method of Characteristics to the Transient Flow of Gases," Proceedings, Institute of Mechanical Engineers, Vol. 161, (1949), pp. 250-258.

62. R. C. Progelhof, "Determination of the Mass of Gas in a Rapidly Discharging Vessel," AIAA Journal, Vol. 2, (1964), pp. 137-139.

63. H. S. Isbin and G. R. Gavalas, "Two-Phase Flow Through an Aperture," Proceedings of the 1962 Heat Transfer and Fluid Mechanics Institute (June, 1962), 126-140.

64. J. K. Ferrell and J. W. McGee, Two-Phase Flow Through Abrupt Expansions and Contractions, Final Report Volume III on USAEC Contract At-(40-1)-2950, North Carolina State University, Raleigh, North Carolina, (June, 1966).

65. H. K. Fauske, Contribution to the Theory of Two-Phase, One-Component Critical Flow, ANL-6633, Argonne National Laboratory, Argonne, Illinois, (October, 1962).

66. H. K. Fauske, Two-Phase Critical Flow with Application to Liquid-Metal Systems (Mercury, Cesium, Rubidium, Potassium, Sodium, and Lithium), ANL-6779, Argonne National Laboratory, Argonne, Illinois, (October, 1963).

67. W. Bornhorst and A. Shavit, Study of the Boundary Conditions at a Liquid-Vapor Interface Through Irreversible Thermodynamics, Quarterly Progress Report, Massachusetts Institute of Technology, Cambridge, (September, 1965).

68. P. Griffith and G. Snyder, The Mechanism of Void Formation in Initially Subcooled Systems, Report 9041-26 on Contract Nonr-1841 (39), Massachusetts Institute of Technology, Cambridge, (September, 1963).

69. W. A. Olsen, Experimental and Analytical Investigation of Interfacial Heat and Mass Transfer in a Pressurized Tank Containing Liquid Hydrogen, NASA TN D-3219, (March, 1966).

70. K. D. Coughren, Pressurizing Vessel Performance Equations, BNWL-116, Battelle-Northwest, Richland, Washington, (August, 1965).

71. S. Levy, "Prediction of Two-Phase Critical Flow Rate," Journal of Heat Transfer, ASME Transactions, Series C, Vol. 87, No. 1, (February, 1965), pp. 53-58.

72. F. J. Moody, "Maximum Flow Rate of a Single Component, Two-Phase Mixture," Journal of Heat Transfer, ASME Transactions, Series C, Vol. 87, No. 1, (February, 1965), pp. 134-142.

73. L. S. Tong, "The Heat Transfer Mechanisms During a Loss-of Coolant Accident," Proceedings, Fourth Annual Symposium on Heat Transfer, Idaho Falls, Idaho, (May, 1967).

74. F. W. Albaugh, J. J. Fuquay, H. Harty, E. E. Voiland, and D. C. Worlton, Nuclear Safety Quarterly Report, BNWL-433, Battelle-Northwest, Richland, Washington, (July, 1967).

75. R. T. Allemann, Reactor Safeguards Experimental Unit, Battelle-Northwest, Richland, Washington, Personal Correspondence, (August 23, 1967).

76. K. A. Dietz (Editor), Quarterly Technical Report STEP Project: (October, 1965 - December, 1965), IDO-17167, (September, 1966).

77. K. A. Dietz (Editor), Quarterly Technical Report STEP Project: (January, 1966 - March, 1966), IDO-17186, (November, 1966).

78. K. A. Dietz (Editor), Quarterly Technical Report STEP Project: (April, 1966 - June, 1966), IDO-17187, (January, 1967).

79. K. A. Dietz (Editor), Quarterly Technical Report STEP Project: (July, 1966 - September, 1966), ID)-17213, (April, 1967).

80. K. A. Dietz (Editor), Quarterly Technical Report STEP Project: (October, 1966 - December, 1966), IDO-17214, (April, 1967).

81. R. B. Pollard, "The Effect of Pressure and Pressure Decay on Pool Boiling from Stainless Steel Surfaces," Unpublished Master's Thesis, Auburn University, Auburn, Alabama, (August, 1965).

82. H. K. Fauske, Reactor Engineering Division, Argonne National Laboratory, Argonne, Illinois, Personal Correspondence, (September, 1967).

83. T. R. Wilson, Manager, Engineering and Test Branch, Atomic Energy Division, Phillips Petroleum Company, Idaho Falls, Idaho, Personal Correspondence, (September, 1967).

84. B. M. Johnson, Containment Systems Experiment, Part III, BNW-233, Battelle-Northwest, Richland, Washington, (May, 1966).

85. F. J. Moody, Maximum Two-Phase Vessel Blowdown from Pipes, APED-4827, 65APE4, General Electric Company, (April, 1965).

86. Preliminary Hazards Summary Report, Bodega Bay Atomic Park Unit No. 1, Pacific Gas and Electric Company, (December, 1962).

87. C. H. Robbins, Tests of a Full Scale 1/48 Segment of the Humboldt Bay Pressure Suppression Containment, GEAP-3596, (November, 1960).

88. W. M. Rohsenow, Personal Communication, Oak Ridge, Tennessee, (July 26, 1966).

89. R. I. Vachon, G. H. Nix, and G. E. Tanger, "Evaluation of Constants for the Rohsenow Pool Boiling Correlation," Journal of Heat Transfer, ASME Transactions, Series C, Vol. 90, No. 2, (May, 1968), pp. 239-247.

90. R. I. Vachon, G. E. Tanger, G. H. Nix, and L. H. Goree, "Pool Boiling of Water on 304 Stainless Steel Etched with Hydrochloric Acid," Report VI, Contract NAS8-11234, Auburn Research Foundation, (August, 1966).

91. R. I. Vachon, G. E. Tanger, G. H. Nix, and D. L. Davis, "Pool Boiling of Water from Mechanically Polished and Chemically Etched Stainless Steel Surfaces," Report IV, Contract NAS8-11234, Auburn Research Foundation, (December, 1965).

92. Personal Communication, S. T. Hsu, (July 17, 1965).

93. R. K. Young and R. L. Hummel, "Higher Coefficients for Heat Transfer with Nucleate Boiling," Chemical Engineering Progress Symposium Series, Vol. 61, No. 59, (1965), pp. 264-270.

94. R. I. Vachon, G. H. Nix, J. F. Hare, and W. C. Anderson, "The Rohsenow Pool Boiling Correlation - Examination of the Equation and a Tabulation of Data," Report VII, Contract NAS8-11234, Auburn Research Foundation, (December, 1966).

95. C. F. Bonilla and C. W. Perry, "Heat Transmission to Binary Liquid Mixtures," AIChE Transactions, Vol. 37, (1941), p. 685.

96. C. F. Bonilla, Y. S. Bush, A. Stalder, N. S. Shaikamahmud, and A. Ramachandran, "Pool Boiling Heat Transfer with Mercury," Chemical Engineering Progress Symposium Series, Liquid Metals Technology, Part I, Vol. 53, No. 20, (1957).

97. J. N. Addoms, Doctor of Science Thesis, Chemical Engineering Department, Massachusetts Institute of Technology, (1948).

98. A. N. Nahavandi, "The Loss of Coolant Accident Analysis in Pressurized Water Reactors," Presented at Loss-of-Coolant Heat Transfer Panel, 10th National Heat Transfer Conference, Philadelphia, Pennsylvania, (August 11-14, 1968).

99. Battelle Northwest, Nuclear Safety Quarterly Report, BNWL-816, Richland Washington, (September, 1968).

100. F. J. Moody, "Liquid/Vapor Action in a Vessel During Blowdown," APED-5177, General Electric Company, (June, 1966).

101. D. H. Brown, Transient Thermodynamics Analysis of Thermal Systems, Report 62 GL 36, General Electric Company, Schenectady, New York, (1962).

102. D. H. Brown, Transient Thermodynamics of Reactors and Process Apparatus, Report DF-r56 GL 316, General Electric Company, Schenectady, New York, (1956).

103. C. D. Hodgman, R. C. Weast, and S. M. Selby, Handbook of Chemistry and Physics, Chemical Rubber Publishing Company, New York, 38th Edition, (1956), p. 2338.

104. Personal Communication with R. R. Head, Chief, Applied Mechanical Research Branch, Propulsion and Vehicle Engineering Laboratory, Marshall Space Flight Center, Huntsville, Alabama, (May 21, 1965).

APPENDIX A

PREPARATION AND TEST PROCEDURE FOR CHEMICALLY ETCHED SURFACES

The specimens were cut from type 304 cold-rolled, bright, annealed sheet material. The long dimension coincides with the rolling direction. The specimens (4.6 inches x 0.996 inch x 0.030 inch) were examined carefully with a microscope and metallograph for any visible scratches and discarded if scratches were found. Profilometer measurements of seven as-received specimens indicated a surface roughness of approximately 4.3 rms, parallel to the mill marks. Roughness perpendicular to the rolling direction was approximately 4.8 rms. The specimens were assumed to be uniform on a macroscopic basis prior to surface preparation as a result of these measurements.

The specimens were immersed in a 37 percent hydrochloric acid solution to produce pitted surfaces. Specimens were placed in a flat pyrex dish containing 300 ml of acid which was changed every two hours. The bottom side and edges of the specimens were coated with vacuum grease to isolate the chemical reaction to the top side. No surfaces were used with visible scratches prior to etching. The specimens are characterized only by total etching time. Surface conditions vary with etching time, but it has been found [55] that etching time and method of etching characterize a surface.

The etched specimens were cleaned with distilled water. No change in surface roughness was evident from the cleaning procedures. The chemical nature of the surfaces was unaltered by the etching process as determined by spectrographic analysis using a Phillips Vacuum X-Ray Spectrograph with a Wolfram target x-ray tube.

Three 30-gage, iron-constantan thermocouples were butt welded to the bottom of the test specimen on the major axis. The specimen was then mounted on the glass phenolic support block with an epoxy seal. The temperature of the top surface was calculated using the measured bottom surface temperatures and the unidirectional steady state heat conduction equation. Bulk fluid temperature was monitored with 30-gage, iron-constantan couples. Appropriate shielding and filters prevented A. C. pickup by the thermocouple leads.

The water was deionized with a cation and anion deionizer. Average water resistivity was maintained at 55,000 ($\pm$ 10 percent) ohm-centimeters at 60°F.

The dry system was subjected to a vacuum of 30 inches Hg for 30 minutes. Deionized degassed water was admitted into the chamber until the free surface was five inches above the test strip. Again, the system was subjected to a 30-inch vacuum for 30 minutes. The boiler was vented to the atmosphere, and the water was brought to saturation temperature by a preheater. Power to the test strip was then initiated. At this point, the system was isolated if the run was to be conducted at an elevated pressure. As soon as equilibrium was reached for a certain power input, the temperature, pressure,

and power were recorded. This procedure was repeated over a range of increasing power levels. After each test, the boiler was drained, and the procedure was repeated for each of the test surfaces.

APPENDIX B

ANALYSIS OF ERRORS FOR POOL BOILING DATA

Usually, in conducting an error analysis, the types of errors must be classified. A general classification may be made as follows:

1. Systematic Errors
2. Personal Errors
3. Mistakes
4. Random Errors

Mistakes and personal errors may be reduced to a minimum through proper design of the experiment. Systematic errors, on the other hand, are those which always affect the experiment in one direction. Random errors may occur in either direction, and these, along with the systematic errors, are to be estimated in the error analysis.

The usual procedure in an error analysis is to give both an external and an internal estimate of the error involved in any experiment. The external error is based on the experimenter's knowledge of the individual errors which contribute to the final compounded error while the results actually obtained during the experiment determine the internal estimate. Since the external estimate of error is based on the general conditions associated with the experimental apparatus, it will usually not change from one specimen type to another.

Primarily, the data utilized in the pool boiling analysis have consisted of heat flux and temperature-difference measurements. The equation used for calculating heat flux is

$$q'' = 3.413\ I^2R \tag{B-1}$$

Test-strip resistance may be represented as

$$R = \frac{\rho L}{A_1} \tag{B-2}$$

The combining of Eqs. (B-1) and (B-2) yields

$$q'' = 3.413\ \frac{I^2\rho L}{A_1} \tag{B-3}$$

Current, length, and area are directly measurable quantities, whereas the resistivity is taken from a graph at the appropriate temperature. The equation of the graph was found for use in automatic computation procedures.

Temperature difference is calculated from

$$\Delta T = T_w - T_{sat} \tag{B-4}$$

Test strip temperature is measured at three locations beneath the surface and the following relation is used to calculate the upper surface temperature [81]:

$$T_w = T_u - \frac{3.413\ I^2\rho Ly}{2A_1k_sA} \tag{B-5}$$

Thus, the temperature difference is given as

$$\Delta T = T_u - T_{sat} - \frac{3.413\ I^2\rho Ly}{2A_1k_sA} \tag{B-6}$$

or

$$\Delta T = T_u - T_{sat} - \frac{3.413\ I^2\rho}{2W^2k_s} \tag{B-7}$$

Current and test-strip width are the directly measured quantities while resistivity and conductivity are taken from graphs which have known equations. Equations (B-3) and (B-7) are the final equations to be used in conducting the external analysis.

Consider the function relationship

$$q'' = F(I,\rho,L,A_1) \tag{B-8}$$

as given by Eq. (B-3). Here, q'' is the measured heat flux and I, ρ, L, and A_1 are the separate measured quantities which are likely to be in error. Then,

$$dq'' = \sum_{n=a}^{d} \left(\frac{\partial F}{\partial n}\right) dn \tag{B-9}$$

The variation in q'' is considered to be produced by errors in the variables, Eq. (B-8), which have error magnitudes designated as e_a to e_d. Thus,

$$e_E = \sum_{n=a}^{d} \left(\frac{\partial F}{\partial n}\right) e_n \tag{B-10}$$

where

e_E = total magnitude of error involved

e_n = magnitude of separate errors

Equation (B-10) cannot be solved directly since it is not known how the error terms were added. However, e_E^2 may be evaluated:

$$e_E^2 = \sum_{n=a}^{d}\left(\frac{\partial F}{\partial n}\right)^2 e_n^2 + \sum_{\substack{n=a \\ m=a}}^{d}\left(\frac{\partial F}{\partial n}\right)\left(\frac{\partial F}{\partial m}\right)dndm \qquad \text{(B-11)}$$

where $m \neq n$. When the errors are independent and symmetrical with regard to the positive and negative values, the cross products in the second term of Eq. (B-11) disappear, giving

$$e_E^2 = \sum_{n=a}^{d}\left(\frac{\partial F}{\partial n}\right)^2 e_n^2 \qquad \text{(B-12)}$$

This equation is the general form for the resultant error in terms of its components. To obtain the total proportional error, divide Eq. (B-12) by $(q'')^2$, the quantity squared, and take the square root. For the case $F(a,b,c,d) = abcd = q$, there is obtained

$$\varepsilon_E = \left(\varepsilon_a^2 + \varepsilon_b^2 + \varepsilon_c^2 + \varepsilon_d^2\right)^{\frac{1}{2}}$$

where ε_n, $n = a, b, \ldots$ is the proportional error associated with the quantities a, b, . . . and ε_E is the total proportional error.

The functional form for the heat flux is

$$q'' = F(I,\rho,L,A_1) = 3.413\,\frac{I^2\rho L}{A_1} \qquad \text{(B-13)}$$

Following the foregoing analysis, the equation for the total proportional error involved in heat-flux measurements becomes

$$\varepsilon_q = \left(4\varepsilon_I^2 + \varepsilon_\rho^2 + \varepsilon_L^2 + \varepsilon_A^2\right)^{\frac{1}{2}} \qquad \text{(B-14)}$$

It is estimated that the following proportional errors affect the end result.

Current:	2 parts in 100 =	ε_I
Resistivity:	5 parts in 100 =	ε_ρ
Length:	1 part in 72 =	ε_L
Area:	10 parts in 100 =	ε_A

Use of Eq. (B-14) yields $\varepsilon_q = \pm 12\%$ as the external estimate of error for heat flux from any of the types of specimens mentioned as possible heat-transfer surfaces.

The functional form for temperature difference is

$$\Delta T = F(T_w, T_{sat}, I, , W, k_s)$$

$$= T_w - T_{sat} - \frac{3.413\ I^2 \rho L y}{2 A_1 k_s A} \qquad \text{(B-15)}$$

and the estimate of proportional error is

Wall Temperature:	2 parts in 100 =	ε_{T_w}
Saturation Temperature:	1 part in 100 =	ε_{T_s}
Current:	2 parts in 100 =	ε_I
Resistivity:	5 parts in 100 =	ε_ρ
Width:	3 parts in 100 =	ε_w
Conductivity:	10 parts in 100 =	ε_k

Application of the foregoing analysis yields $\varepsilon_{\Delta T} = \pm 13.2\%$ as the external estimate of error for the temperature difference between the upper wall and the contacting fluid.

It should be pointed out that the external estimate does not include personal errors and mistakes which might occur. Also, this

estimate is based on external effects associated with instrumentation and measurement errors. Thus, it is tacitly assumed that the specimen undergoing the test is ideal; that is, it is assumed that each type of specimen tested is free from indeterminate effects. Obviously, this is not the case for boiling heat transfer experiments. Such adverse effects as specimen aging, small barometric changes, liquid contamination, and specimen variance affect the reproducibility of boiling data. Of these effects, specimen variance is the most serious.

The application of the external estimate of error calculated herein, along with the data, shows that the internal error is consistent with the estimated error. Thus, the error analysis gives some assurance as to the accuracy of the study.

APPENDIX C

SUMMARY OF DATA INCLUDED IN ADJUSTED ROHSENOW CORRELATION

The data for this study were obtained from the literature on pool boiling heat transfer. Data have been collected from the original source when possible. Also, data collected by the writer and reported previously [90,91] are included in the analysis. Variation of surface conditions was the main parameter investigated. The results of twelve separate investigations on various liquid-surface combinations have been correlated with the Rohsenow equation. Results of the correlations show that r values do vary. Information on each study is summarized in the following paragraphs.

The effect of varying surface conditions on pool boiling has been the object of numerous investigations [15,16,18-21,29,32,52,93]. Corty and Foust [16] measured nucleate boiling coefficients of ether, n-pentane and freon 113 from copper and nickel surfaces. Surface roughness and contact angle were varied by polishing with different grades of emery cloth. Profilometer rms roughness was measured and found to vary from 2.2 to 23 micro-inches.

A quantitative method for predicting the heat transfer coefficient versus superheat relation for various surfaces and liquids was presented by Kurihara and Myers [29]. Various grades of emery were used to obtain a range of roughness values for the copper heating

surfaces. The liquids investigated were water, acetone, n-hexane, carbon disulfide and carbon tetrachloride. The authors measured surface roughness before and after test runs; however, no roughness values were reported in the study.

Clark, Strenge and Westwater [15], in a microscopic study of surfaces, identified photographically 20 separate nucleation sites during boiling of ether and pentane on zinc and aluminum alloy surfaces. The size of the active pits ranged from 0.0003 to 0.003 in. Surface roughness values were not given.

Other attempts at surface preparation have consisted of mechanical polishing, artificial scoring, and lapping. Polished surfaces were used by Gaertner and Westwater [18] and Griffith and Wallis [19]. Gaertner and Westwater conducted 51 experimental runs with an aqueous solution of nickel salts on copper in an attempt to determine the relationship between q/A, $T_w - T_s$, and the site density, n/A. A 2 in. diameter surface polished with 7 grades of emery through 4/0, with all visible scratches removed from the surface, was employed in the tests.

Methanol, ethanol, and water solutions were boiled on copper in the investigation of Griffith and Wallis [19]. Surfaces were prepared with 3/0 emery, always stroking in the same direction. The authors prepared a special surface for their studies by pricking 37 holes of uniform shape and size in the 3/0 surface. Comparative tests were conducted on a similar surface without the holes to demonstrate the increase in heat flux for increased roughness.

Lapped surfaces were used by Berenson [20]. Mechanical polishing of the copper surface with various grades of emery cloth was also employed as a means of preparation.

Artificial scoring was employed by Bonilla, Grady, and Avery [21]. Copper surfaces were prepared with parallel scratches of known depth, geometry, and length. The scratches were spaced at distances of 1, 1/2, 1/4, and 1/8 inch on four plates. A Brush Surface Analyzer was used to measure surface roughness.

Hsu and Schmidt [52] investigated "ground' and polished surfaces of 304 stainless steel. Surfaces [92] of 19, 21, and 40 rms were produced by grinding with an Al_2O_3 grinding wheel. A 5.2 rms surface was produced using a polishing machine and emery powder.

Young and Hummel [93] investigated the effect of poorly wetted randomly positioned spots on a wetted surface during pool boiling. Water was boiled from 304 stainless steel surfaces. Data were obtained for milled, pitted,,and Teflon-spotted surfaces. No mention was given of surface roughness.

Platinum and copper surfaces in nucleate pool boiling were used by Gaertner [32]. Numerous photographs and motion pictures were taken in order to identify the various regions which exist in nucleate boiling. The surfaces were prepared by polishing with 2/0 and 4/0 emery, respectively. A transverse measurement of the copper surface with a Talysurf profilometer indicated an arithmetic average roughness of 9.5 micro-inch.

The data from the investigations mentioned in the preceding paragraphs were used, along with data obtained by the writer [90,91] on mechanically polished and chemically etched stainless steel surfaces. Rohsenow's [3] equation was applied to the data in an attempt to obtain a cross-correlation of the diverse data on pool boiling.

TABLE 16

SURFACE-LIQUID COMBINATION AND SURFACE FINISHES

USED BY CORTY AND FOUST [16]

Run Number	Liquid	Surface Material	Surface Finish	Profilometer Roughness RMS
10 to 13	n-Pentane	Copper	Polished with 4/0 emery paper	6
14 to 15	n-Pentane	Copper	Polished with 4/0 emery paper	6
1	n-Pentane	Nickel	Polished with 4/0 emery paper	2.2
2	n-Pentane	Nickel	Polished with 2/0 emery paper	3
3	n-Pentane	Nickel	Polished with 0 emery paper	10
4	n-Pentane	Nickel	Polished with 1 emery paper	12
5	n-Pentane	Nickel	Polished with 2 emery paper	23

*All specimens prepared by hand polishing techniques

TABLE 17

SURFACE-LIQUID COMBINATION AND SURFACE FINISHES

USED BY KURIHARA AND MYERS [29]

Run Number	Liquid	Surface Material	Surface Finish
I-1, I-2 I-3	Water	Copper	Polished with 4/0 emery paper
II-1	Water	Copper	Polished with 3/0 emery paper
III-1, III-2	Water	Copper	Polished with 2/0 emery paper
IV-1, IV-2	Water	Copper	Polished with 0 emery paper
V-1	Water	Copper	Polished with 1 emery paper
VI-1, VI-2	Water	Copper	Polished with 2 emery paper
VII-1	Water	Copper	Polished with 140 mesh carborundum
I	Carbon Tetrachloride	Copper	Polished with 4/0 emery paper
IV	Carbon Tetrachloride	Copper	Polished with 0 emery paper
VI	Carbon Tetrachloride	Copper	Polished with 2 emery paper

*All specimens prepared by hand polishing techniques

TABLE 18

SURFACE-LIQUID COMBINATION AND SURFACE FINISHES

USED BY BERENSON [20]

Run Number	Liquid	Surface Material	Surface Finish	Surface Condition Before Test
38	n-Pentane	Nickel	Mirror Finish	Cleaned with CCl_4
39	n-Pentane	Nickel	Lapped circularly with Grit D, No. 160	Cleaned with CCl_4
2, 3	n-Pentane	Copper	Mirror Finish	Cleaned with CCl_4
33, 36	n-Pentane	Inconel	Mirror Finish	Cleaned with CCl_4
34	n-Pentane	Inconel	Lapped circularly with Grit D, No. 160	Cleaned with CCl_4
16, 17	n-Pentane	Copper	Lapped circularly with Grit E, No. 120	Cleaned with CCl_4
7, 8, 9	n-Pentane	Copper	Lapped in one direction with Grit E, No. 120	Oxidized (Not Cleaned)
10	n-Pentane	Copper	Lapped in one direction with Grit E, No. 120	Cleaned with CCl_4
31	n-Pentane	Copper	No. 320 emery rubbed in one direction	Cleaned with CCl_4
32	n-Pentane	Copper	No. 60 emery rubbed in one direction	Cleaned with CCl_4
19, 20	Carbon Tetrachloride	Copper	Lapped circularly with Grit E, No. 120	Cleaned with CCl_4

*All specimens prepared by hand polishing techniques

TABLE 19

SURFACE-LIQUID COMBINATION AND SURFACE FINISHES

USED BY BONILLA, GRADY, AND AVERY [21]

Run Number	Liquid	Surface Material	Surface Finish	Surface Condition
A	Water	Copper	Mirror Finish	
B	Water	Copper	Mirror Finish	Scored by Steel, scratches 1 in. apart
C	Water	Copper	Mirror Finish	Scored by Steel, scratches ½ in. apart
D	Water	Copper	Mirror Finish	Scored by Steel, scratches ¼ in. apart
E	Water	Copper	Mirror Finish	Scored by Steel, scratches 1/8 in. apart (deep)

*Specimens hand polished with various grades of emery, final polished with jeweler's rouge, and scored with steel scriber

TABLE 20

SURFACE-LIQUID COMBINATIONS AND SURFACE FINISHES

USED BY HSU AND SCHMIDT [52]

Run Number	Liquid	Surface Material	Surface Finish	Roughness RMS
108, 110, 111	Water	Stainless Steel	Ground	40
119, 120	Water	Stainless Steel	Ground	21
101, 102 103, 104	Water	Stainless Steel	Ground	19
112, 113, 114	Water	Stainless Steel	Polished	5.2

*Specimens were machine prepared

TABLE 21

SURFACE-LIQUID COMBINATIONS AND SURFACE FINISHES

USED BY YOUNG AND HUMMEL [93]

Run Number	Liquid	Surface Material	Surface Finish	Surface Condition
1	Water	Stainless Steel	Milled	
3-P	Water	Stainless Steel	Pitted	
7 ST	Water	Stainless Steel	Milled	Spots of Teflon on the surface
3 PT	Water	Stainless Steel	Pitted	Teflon in the pits
2 PT	Water	Stainless Steel	Pitted	Teflon in the pits

*Specimens pitted mechanically, spotted with Teflon

TABLE 22

OTHER SURFACE-LIQUID COMBINATIONS AND SURFACE FINISHES

Run Number	Liquid	Surface Material	Surface Finish	Reference
1	n-Pentane	zinc-crystals	polished*	[15]
1	Water	paraffin treated copper	polished with 3/0 emery paper with cavities**	[19]
2	Water	paraffin treated copper	polished with 3/0 emery paper without cavities**	[19]
1	Water	Copper	polished with 4/0 emery paper**	[32]

*Hand polished, final polished by machine technique

**Hand polished

TABLE 23

SUMMARY OF SPECIMEN AND TEST CONDITIONS: MECHANICALLY POLISHED SPECIMENS [91]

Run Number	Liquid	Surface Material	Surface Finish	Roughness RMS
1-A,B,C	Water	Stainless Steel	600 emery	2.6
2-A,B,C	Water	Stainless Steel	600 emery	2.6
3-A	Water	Stainless Steel	600 emery	2.6
4-A,B,C	Water	Stainless Steel	320 emery	10
5-A,B,C	Water	Stainless Steel	320 emery	10
6-A,B,C	Water	Stainless Steel	320 emery	10
7-A,B,C	Water	Stainless Steel	80 emery	40
8-B,C	Water	Stainless Steel	80 emery	40
9-A,B,C	Water	Stainless Steel	36 emery	61
10-A,B,C	Water	Stainless Steel	36 emery	61

*All specimens hand polished in one direction with different grades of emery

TABLE 24

SUMMARY OF SPECIMEN AND TEST CONDITIONS: CHEMICALLY ETCHED SPECIMENS [90]

Run Number	Liquid	Surface Material	Surface Finish	Roughness RMS
76-A,B	Water	Stainless Steel	Etched 6 hr.	32
77-A,B	Water	Stainless Steel	Etched 4 hr.	27
78-A,B	Water	Stainless Steel	Etched 5 hr.	30
79-A,B	Water	Stainless Steel	Etched 7 hr.	42
80-A,B	Water	Stainless Steel	Etched 2 hr.	16
82-A,B	Water	Stainless Steel	Etched 7 hr.	42
83-A	Water	Stainless Steel	Etched 5 hr.	30
84-A,B	Water	Stainless Steel	Etched 4 hr.	27

*All specimens etched for different times in 37% solution of hydrochloric acid

APPENDIX D

SUMMARY OF MOODY'S MODEL FOR CRITICAL MASS FLOW RATE

Moody [72] made the following assumptions in the development of his model: Both phases are at the same static pressure and in local equilibrium at the exit; the flow is annular with a uniform exit velocity; and the slip ratio is an independent variable. The continuity and energy equations are

$$G = \frac{M}{A} = \frac{\alpha}{x}\frac{u_v}{v_v} = \frac{1 - \alpha}{1 - x}\frac{u_\ell}{v_\ell} \tag{D-1}$$

$$h_o = x\left(h_v + \frac{v_v^2}{2g_c J}\right) + \left(1 - x\right)\left(h_\ell + \frac{v_\ell^2}{2g_c J}\right) \tag{D-2}$$

where

$$x = \frac{M_v}{M}; \qquad 1 - x = \frac{M_\ell}{M} \tag{D-3}$$

$$\alpha = \frac{A_v}{A}; \qquad 1 - \alpha = \frac{A_\ell}{A} \tag{D-4}$$

If the slip ratio

$$K = \frac{v_v}{v_\ell} \tag{D-5}$$

is introduced, Eqs (D-4) and (D-5) yield

$$\alpha = \frac{1}{1 + K\,\frac{1 - x}{x}\,\frac{v_\ell}{v_v}} \tag{D-6}$$

Properties along the saturation line are functions of pressure only and are given by:

$$
\begin{aligned}
v_\ell &= v_\ell\,(P) & h_V &= h_V\,(P)\\
v_V &= v_V\,(P) & s_\ell &= s_\ell\,(P)\\
h_\ell &= h_\ell\,(P) & s_V &= s_V\,(P)\\
h_{\ell V} &= h_{\ell V}(P) & s_{\ell V} &= s_{\ell V}(P)
\end{aligned}
\qquad \text{(D-7)}
$$

and s_o is given by

$$s_o = s_\ell + x s_{\ell V} \qquad \text{(D-8)}$$

Equations (D-1) through (D-8) are combined to give the relation for mass flow rate

$$G = \frac{2g_c J\left[h_o - h_\ell - \frac{h_{\ell V}}{s_{\ell V}}(s_o - s_\ell)\right]}{\left[\frac{K(s_V - s_o)v_\ell}{s_{\ell V}} + \frac{(s_o - s_\ell)v_V}{s_{\ell V}}\right]^2\left[\frac{s_o - s_\ell}{s_{\ell V}} + \frac{s_V - s_o}{K\, s_{\ell V}}\right]} \qquad \text{(D-9)}$$

Moody obtained the following for K at maximum flow rate

$$K = K_M = \left(\frac{v_V}{v_\ell}\right)^{1/3} \qquad \text{(D-10)}$$

and showed that G has a single maximum value for known P_o and h_o. When the stagnation enthalpy is unknown, as in the present case, then h_o is an additional parameter in the solution procedure.

APPENDIX E

AUXILIARY PROGRAM EQUATIONS

The quality of liquid/vapor in the system at any time is given by

$$x = \frac{M_V}{M_\ell + M_V} \tag{E-1}$$

The mixture's specific volume, internal energy, enthalpy, and entropy are calculated with the following equations:

$$v = v_\ell + x v_{\ell V} \tag{E-2}$$

$$u = u_\ell + x u_{\ell V} \tag{E-3}$$

$$h = h_\ell + x h_{\ell V} \tag{E-4}$$

$$s = s_\ell + x s_{\ell V} \tag{E-5}$$

These were entered into the computer program along with the saturated liquid/vapor properties. An interpolation scheme was used to calculate the various properties for any pressure of interest. The program keeps a running account of each variable, and these may be output as a function of the blowdown time. The expressions given by Nahavandi [98] for a void fraction

$$\alpha = \frac{(0.8333 + 0.167x)xv_V}{xv_V + (1 - x)v_\ell} \tag{E-6}$$

and the momentum-averaged specific volume

$$v^* = \frac{x^2}{\alpha} v_v + \frac{(1 - x)^2}{1 - x} v_\ell \qquad \text{(E-7)}$$

were included in the program to permit possible further comparisons with other investigators.

APPENDIX F

SUMMARY OF DISCHARGE DATA

A. Saturated Discharge Tests

Time, Seconds	Pressure, psia	Liquid Temperature, °F	Vapor Temperature, °F	Saturation Temperature, °F
Run Number 1: ½ Inch Orifice				
0.0	100.9	326.8	326.6	328.5
0.1	88.3	326.8	326.6	318.9
0.5	92.8	323.5	326.6	322.4
1.0	92.1	323.5	320.5	321.9
2.0	87.7	320.2	317.3	318.5
10.0	55.4	287.5	286.2	287.6
20.0	35.0	256.2	255.7	259.3
30.0	24.9	236.2	235.6	239.9
40.0	23.2	226.2	225.0	235.9
50.0	19.5	217.8	218.6	226.7
60.0	17.1	214.5	214.6	219.7
70.0	16.2	212.8	212.0	216.9
75.0	15.5	212.6	212.0	214.7
Run Number 2: (Equipment Malfunction)				
Run Number 3: ¼ Inch Orifice				
0.0	99.6	327.3	327.3	327.6
0.2	92.5	327.3	327.3	322.6
0.5	--	327.3	321.5	--
0.75	93.1	326.7	321.9	322.7
1.0	92.9	324.0	322.3	323.3
5.0	84.7	317.7	316.0	316.0
10.0	74.3	307.7	306.8	307.0
20.0	60.6	294.0	293.0	293.4
30.0	51.3	281.7	281.8	282.6
40.0	44.0	272.7	273.3	273.0
50.0	38.5	265.3	265.3	264.9
60.0	34.2	258.0	258.5	257.9
70.0	30.8	251.7	252.0	251.8
80.0	27.9	245.7	247.0	246.2
90.0	25.4	240.7	242.0	240.9
100.0	23.1	235.7	237.3	235.7
110.0	22.1	232.3	233.8	233.3

APPENDIX 6 (Cont.)

Time, Seconds	Pressure, PSIA	Liquid Temperature, °F	Vapor Temperature, °F	Saturation Temperature, °F
120.0	20.5	229.0	230.0	228.0
130.0	19.3	225.7	227.0	226.0
140.0	18.1	222.3	224.0	222.7
150.0	17.5	219.3	222.0	219.6
160.0	16.7	218.7	219.7	218.5
180.0	15.8	215.0	217.3	215.7
190.0	15.4	212.7	216.0	214.3
200.0	15.1	212.3	215.3	213.3
210.0	14.9	212.3	214.3	212.7
Run Number 4:	1/4 inch orifice			
0.0	99.5	327.0	326.8	327.5
0.2	92.8	327.0	326.8	322.5
0.5	-	-	322.0	-
0.75	93.2	327.0	322.0	322.8
0.8	-	327.0	-	-
1.0	93.1	324.3	322.0	322.8
5.0	85.6	317.7	315.3	316.8
10.0	76.4	309.0	308.2	308.9
20.0	62.3	294.3	294.3	295.2
30.0	52.9	284.0	284.3	284.7
40.0	45.6	274.0	275.0	275.3
50.0	40.2	265.0	267.2	268.0
60.0	35.8	258.3	260.3	260.6
70.0	32.1	251.3	254.2	254.2
80.0	29.2	245.0	249.0	248.8
90.0	26.6	241.7	243.7	243.5
100.0	24.7	235.3	240.0	239.4
110.0	23.2	232.0	235.7	235.9
120.0	21.4	228.3	232.0	231.6
130.0	20.3	223.7	228.7	228.7
140.0	19.1	222.0	225.7	225.5
150.0	18.4	218.7	223.7	223.5
160.0	17.6	215.3	221.7	221.2
170.0	16.9	212.7	219.7	219.1
180.0	16.4	212.0	218.0	217.6
190.0	16.2	210.0	217.0	216.9
200.0	15.9	208.7	215.3	215.9
210.0	15.7	207.0	215.0	215.3
220.0	15.4	205.3	214.3	214.3

APPENDIX 6 (Cont.)

Time, Seconds	Pressure, PSIA	Liquid Temperature, °F	Vapor Temperature, °F	Saturation Temperature, °F
230.0	15.1	205.3	213.7	213.4
240.0	14.9	205.3	213.3	213.0
250.0	14.8	205.3	213.3	212.3
Run Number 5:	1/2 inch orifice			
0.0	99.4	327.7	328.3	327.4
0.10	-	323.0	-	-
0.25	87.6	321.6	-	318.1
0.60	-	321.9	320.8	-
0.75	91.7	321.9	322.0	321.7
1.0	90.6	321.9	321.7	320.8
5.0	73.3	306.3	306.7	306.1
10.0	54.3	286.5	286.8	286.3
20.0	32.5	255.6	255.3	254.8
30.0	23.5	237.4	236.7	235.6
40.0	19.1	226.4	225.3	225.5
50.0	16.9	219.5	218.3	219.1
60.0	15.8	216.3	215.0	215.7
70.0	15.2	214.3	213.3	213.7
80.0	14.7	213.3	213.3	211.9
Run Number 6:	1/4 inch orifice			
0.0	99.1	326.7	-	327.2
1.0	91.5	326.7	-	321.4
1.4	91.8	326.7	-	321.6
1.8	92.0	326.7	-	321.8
2.2	-	326.7	-	-
2.4	91.5	326.4	-	321.4
5.4	86.5	323.7	-	317.4
10.0	78.3	315.3	-	310.5
20.0	65.6	303.7	-	298.5
30.0	56.4	293.7	-	288.6
40.0	49.4	285.0	-	280.3
50.0	44.0	277.7	-	273.1
60.0	39.2	271.3	-	266.2
70.0	35.8	265.0	-	260.7
80.0	32.7	260.7	-	255.4
90.0	30.3	255.0	-	250.9
100.0	27.7	251.0	-	245.8
110.0	26.2	247.5	-	242.7

APPENDIX 6 (Cont.)

Time, Seconds	Pressure, PSIA	Liquid Temperature, °F	Vapor Temperature, °F	Saturation Temperature, °F
120.0	24.3	243.3	-	238.5
130.0	22.9	240.0	-	235.4
140.0	22.0	237.5	-	233.1
150.0	20.9	234.5	-	230.3
160.0	19.7	231.5	-	227.1
170.0	19.0	229.7	-	225.2
180.0	18.2	228.0	-	222.9
190.0	17.7	225.7	-	221.4
200.0	16.9	224.7	-	219.3
210.0	16.7	222.7	-	218.5
220.0	16.2	221.7	-	216.8
230.0	15.7	221.0	-	215.5
250.0	15.3	218.3	-	214.2
270.0	15.2	217.7	-	213.7
290.0	14.8	217.0	-	211.9
310.0	14.4	215.3	-	210.9
330.0	14.3	214.8	-	210.4
350.0	14.1	214.8	-	209.9
Run Number 7: (Equipment Malfunction)				
Run Number 8: (Equipment Malfunction)				
Runs 9-12: (See Section C)				
Run Number 13: (Power Failure)				
Run Number 14: 1/2 inch orifice				
0.0	99.5	326.7	327.0	327.4
0.1	87.3	326.7	-	318.1
0.6	89.6	324.8	-	319.9
1.1	-	320.9	-	-
5.0	65.5	300.0	-	298.3
10.0	48.6	281.1	282.9	279.1
20.0	31.9	256.3	257.9	253.8
30.0	23.9	242.2	242.0	237.6
40.0	19.7	230.6	232.1	227.2
50.0	17.2	223.6	224.0	219.9
60.0	15.8	218.9	219.4	215.7
70.0	14.6	215.9	216.6	211.6
80.0	14.5	214.3	215.1	211.2

APPENDIX 6 (Cont.)

Time, Seconds	Pressure, PSIA	Liquid Temperature, °F	Vapor Temperature, °F	Saturation Temperature, °F
Run Number 15: 1/2 inch orifice				
0.0	100.8	328.0	-	328.4
0.17	91.7	327.3	-	321.6
0.2	91.4	327.1	-	321.4
0.4	-	330.5	-	-
0.7	-	327.1	-	-
0.9	-	325.9	-	-
1.0	90.1	324.9	-	320.3
1.4	-	322.8	-	-
1.7	-	324.7	-	-
10.0	56.3	293.2	-	288.5
20.0	34.0	260.8	-	257.7
30.0	24.6	241.7	-	239.3
40.0	19.5	228.8	-	226.5
50.0	16.5	220.5	-	217.8
60.0	15.1	215.5	-	213.4
70.0	14.4	212.2	-	211.0
80.0	14.4	211.0	-	211.0
Run Number 16: 1/2 inch orifice				
0.0	99.5	325.3	327.7	327.4
0.1	91.6	320.4	-	321.5
0.2	-	317.9	332.7	-
0.3	92.4	320.4	-	322.1
0.5	-	323.4	327.7	-
0.6	91.6	322.9	-	321.5
1.0	90.9	321.6	325.2	320.9
10.0	63.3	297.6	298.9	296.2
20.0	34.9	273.7	260.5	259.1
30.0	23.3	250.5	238.9	236.3
40.0	18.4	226.2	225.4	223.6
50.0	15.8	217.5	215.6	215.8
60.0	14.5	213.3	212.4	211.2
70.0	14.5	211.3	210.7	211.2
80.0	14.5	210.8	211.5	211.2
Run Number 17: 1/2 inch orifice				
0.0	100.8	328.0	327.4	328.4
0.1	88.6	326.8	-	319.2
0.2	88.6	325.5	328.5	319.2

APPENDIX 6 (Cont.)

Time, Seconds	Pressure, PSIA	Liquid Temperature, °F	Vapor Temperature, °F	Saturation Temperature, °F
0.3	89.9	326.8	-	320.3
0.4	90.5	328.0	323.8	320.7
0.6	90.8	327.3	-	320.9
1.0	88.6	326.5	-	319.2
1.2	88.6	325.5	-	319.2
1.5	87.3	325.5	-	318.1
1.7	86.6	324.3	-	317.6
2.1	84.9	319.4	-	316.1
10.0	56.9	290.4	289.6	289.3
20.0	34.2	258.9	258.1	257.9
30.0	24.5	239.3	239.5	238.9
40.0	19.8	225.9	226.8	227.4
50.0	17.2	218.6	218.8	220.1
60.0	15.8	213.1	213.4	215.5
70.0	14.5	210.7	211.0	211.4
Run Number 18: 1/2 inch orifice				
0.0	99.5	327.3	328.0	327.4
0.2	85.9	327.3	326.1	317.0
0.4	88.4	327.8	323.2	318.9
0.6	89.7	329.9	319.6	320.1
1.0	87.9	329.9	-	318.6
1.4	85.5	322.9	-	316.7
10.0	51.4	286.9	283.3	282.8
20.0	32.6	258.9	255.5	255.1
30.0	24.4	239.9	238.8	238.6
40.0	19.6	228.5	227.5	226.9
50.0	17.1	220.5	220.3	219.6
60.0	15.6	215.6	214.9	214.9
70.0	15.2	212.7	211.9	213.6
80.0	14.5	212.0	210.7	211.3
Run Number 19: 1/4 inch orifice				
0.0	99.6	327.7	-	327.5
0.25	94.8	327.7	-	327.0
0.75	94.8	327.7	-	324.0
1.0	-	328.8	-	-
3.0	-	327.3	-	-
10.0	79.0	314.2	-	311.2
20.0	66.9	302.9	-	299.8
30.0	57.7	288.0	-	290.2
40.0	-	285.2	-	-

APPENDIX 6 (Cont.)

Time, Seconds	Pressure, PSIA	Liquid Temperature, °F	Vapor Temperature, °F	Saturation Temperature, °F
50.0	45.5	277.9	-	275.0
60.0	41.1	272.2	-	268.9
70.0	37.2	267.1	-	262.9
80.0	33.6	260.9	-	256.8
90.0	30.7	255.2	-	251.7
100.0	28.5	250.6	-	247.3
110.0	26.6	247.2	-	243.4
120.0	24.7	243.3	-	239.3
130.0	23.3	240.2	-	236.3
140.0	21.9	236.7	-	233.0
150.0	20.6	233.7	-	229.6
160.0	19.8	230.9	-	227.5
170.0	19.0	224.9	-	225.3
180.0	18.5	223.4	-	223.7
190.0	17.3	221.4	-	220.2
210.0	17.1	218.4	-	219.8
220.0	16.6	217.9	-	218.1
230.0	16.0	219.4	-	216.4
240.0	15.9	217.5	-	216.0
250.0	15.8	216.7	-	215.6
260.0	15.5	216.4	-	214.7
270.0	14.9	215.5	-	212.9
280.0	14.7	215.2	-	211.9
290.0	14.6	214.0	-	211.5
Run Number 20: 1/4 inch orifice				
0.0	99.6	327.0	326.0	327.5
0.3	93.9	-	-	323.3
1.3	93.5	-	-	322.9
3.0	-	326.5	-	-
5.0	-	322.2	-	-
10.0	78.7	314.1	310.2	310.9
20.0	66.3	300.9	297.1	299.3
40.0	50.1	283.3	279.7	281.1
60.0	40.2	269.2	265.1	267.5
80.0	32.9	257.0	253.4	255.5
100.0	28.2	246.4	243.1	246.9
120.0	24.3	240.5	235.6	238.5
140.0	21.6	233.2	229.4	232.1
160.0	19.9	228.4	223.2	227.9
180.0	17.8	223.6	219.4	221.8

APPENDIX 6 (Cont.)

Time, Seconds	Pressure, PSIA	Liquid Temperature, °F	Vapor Temperature, °F	Saturation Temperature, °F
200.0	16.9	219.9	215.7	218.9
220.0	16.2	217.1	212.9	216.9
240.0	15.9	215.1	210.7	216.0
260.0	15.1	213.7	208.7	213.3
280.0	14.8	212.7	208.0	212.4
300.0	14.6	211.5	207.0	211.5
Run Number 21: 1 inch orifice				
0.0	99.7	326.9	327.0	327.6
0.15	82.2	326.2	-	313.9
0.29	-	326.0	-	-
0.30	88.9	325.9	-	319.4
0.45	89.1	324.1	-	319.5
0.70	87.6	322.6	-	318.3
0.90	86.9	321.4	-	317.8
1.0	84.9	316.0	320.9	316.1
2.0	74.7	312.1	312.3	307.3
3.0	63.4	-	-	296.9
4.0	52.4	291.3	290.7	284.0
5.0	41.6	265.0	263.3	269.6
6.0	33.5	-	-	256.7
7.0	26.7	-	-	243.7
8.0	21.4	238.4	238.7	231.7
9.0	18.6	-	-	224.1
10.0	17.1	221.1	221.4	219.7
11.0	15.9	-	-	215.9
12.0	15.8	213.0	214.4	215.5
13.0	15.3	-	-	214.2
14.0	15.2	211.5	213.7	213.7
15.0	14.9	-	-	212.8
16.0	14.8	-	-	212.4
17.0	14.7	211.5	213.7	211.9
Run Number 22: 1 inch orifice				
0.0	100.0	327.0	327.0	327.7
0.15	78.1	324.3	-	310.4
0.35	88.1	323.2	-	318.7
0.50	88.2	321.8	-	318.8
0.70	85.2	319.9	-	316.4
0.90	85.1	318.6	-	316.3
1.0	83.6	317.4	-	315.1

APPENDIX 6 (Cont.)

Time, Seconds	Pressure, PSIA	Liquid Temperature, °F	Vapor Temperature, °F	Saturation Temperature, °F
1.1	81.5	317.1	-	313.3
1.2	81.3	315.7	-	313.1
2.0	70.4	308.9	307.8	303.3
4.0	45.9	284.4	281.7	275.7
6.0	28.5	257.0	253.0	247.4
8.0	19.8	233.3	231.5	227.4
10.0	16.1	220.4	219.4	216.7
12.0	14.9	214.9	214.5	212.7
14.0	14.6	213.0	214.2	211.7
15.0	14.5	212.8	214.2	211.3
16.0	14.5	212.5	214.2	211.3

B. Subcooled Discharge Tests

Time, Seconds	Pressure, PSIA	Liquid Temperature, °F	Vapor Temperature, °F	Saturation Temperature, °F
Run Number 23: 1 inch orifice				
0.0	99.0	273.3	262.0	327.1
0.22	34.0	-	-	257.7
0.3	34.0	-	-	257.7
0.7	40.5	-	270.9	267.9
1.0	39.1	273.3	272.2	265.9
1.6	-	274.1	-	-
2.0	35.8	269.2	267.4	260.6
4.0	28.9	251.4	253.3	248.2
6.0	22.9	238.4	239.5	235.1
8.0	18.4	225.1	225.4	223.4
10.0	16.9	215.4	216.4	219.4
12.0	14.7	211.5	212.5	211.9
14.0	14.4	210.6	212.3	210.9
16.0	14.4	210.3	212.0	210.9

APPENDIX 6 (Cont.)

Time, Seconds	Pressure, PSIA	Liquid Temperature, °F	Vapor Temperature, °F	Saturation Temperature, °F
Run Number 24: 1 inch orifice				
0.0	98.6	299.3	291.0	326.8
0.15	51.3	299.3	-	282.7
0.24	51.3	298.2	-	282.7
0.55	63.3	297.3	-	296.2
0.85	58.3	294.8	-	290.8
1.00	-	292.8	291.9	-
1.15	57.9	291.5	-	290.3
1.35	53.8	290.3	-	285.7
1.70	53.1	286.7	-	284.9
2.0	50.4	284.1	284.1	281.5
4.0	37.6	266.5	266.6	263.6
6.0	27.7	250.4	248.3	245.8
8.0	20.5	232.9	231.4	229.3
10.0	16.9	220.5	219.5	219.4
12.0	15.1	213.7	213.7	213.3
14.0	14.5	211.5	211.6	211.4
16.0	14.4	210.3	210.7	210.9
Run Number 25: 1/4 inch orifice				
0.0	99.5	278.7	273.5	327.4
2.0	47.3	-	-	277.5
3.0	47.3	-	241.6	277.5
5.0	-	281.1	272.2	-
10.0	41.8	273.7	270.9	269.9
20.0	37.1	265.4	263.4	262.8
30.0	33.4	259.2	257.4	256.6
40.0	30.6	252.5	250.4	251.4
50.0	27.9	248.1	245.4	246.3
60.0	25.5	242.9	241.6	241.1
70.0	23.9	238.7	237.7	237.7
80.0	22.4	234.8	233.2	234.2
90.0	21.2	232.3	230.1	231.1
100.0	19.9	228.8	227.2	227.9
110.0	19.3	226.1	224.6	226.0
120.0	18.3	223.1	221.8	223.3
130.0	17.5	221.1	218.1	220.9
140.0	17.1	218.7	216.8	219.7
150.0	16.3	217.4	214.9	217.2

APPENDIX 6 (Cont.)

Time, Seconds	Pressure, PSIA	Liquid Temperature, °F	Vapor Temperature, °F	Saturation Temperature, °F
160.0	15.9	216.4	214.2	215.9
170.0	15.6	214.7	211.6	214.9
180.0	15.2	213.2	210.3	213.6
190.0	14.5	212.2	209.2	211.3
200.0	14.5	210.9	209.2	211.3
210.0	14.5	210.0	207.7	211.3
Run Number 26: 1/4 inch orifice				
0.0	99.9	307.0	297.3	327.7
1.0	70.0	-	284.1	302.9
1.5	-	-	294.9	302.9
3.2	-	307.0	299.8	-
10.0	59.6	293.1	293.6	292.3
20.0	51.0	283.9	284.1	282.3
30.0	44.6	274.4	274.9	273.9
40.0	40.2	267.1	267.2	267.5
50.0	36.1	260.7	260.9	261.1
60.0	32.7	255.7	256.1	255.3
70.0	29.6	250.5	249.9	249.5
80.0	27.4	246.2	246.2	245.2
90.0	25.5	241.8	241.6	241.2
100.0	23.9	238.2	238.6	237.5
110.0	22.5	234.6	234.2	234.3
120.0	21.2	231.5	230.9	230.9
130.0	20.1	229.6	228.0	228.1
140.0	19.7	226.3	225.6	227.1
150.0	18.4	224.4	224.3	223.7
160.0	17.8	221.3	221.6	221.7
170.0	17.1	219.2	219.4	219.7
180.0	16.8	217.9	216.9	218.9
190.0	15.9	216.8	216.9	216.3
200.0	15.7	215.6	214.5	215.4
210.0	15.6	213.9	213.7	214.9
220.0	14.9	213.2	212.7	212.7
230.0	14.5	211.3	211.9	211.3
240.0	14.5	211.1	211.5	211.3
250.0	14.5	210.8	210.8	211.3
260.0	14.5	210.8	210.5	211.3

C. Wall Temperature Data

Time, Seconds	System		Large Plate			Small Plate		
	Liquid Temp. °F	Vapor Temp. °F	Inside Temp. °F	Middle Temp. °F	Outer Temp. °F	Inside Temp. °F	Middle Temp. °F	Outer Temp. °F
Run Number 9: 1/4 inch orifice								
0	327.2	328.3	314.7	314.7	313.9	311.8	312.5	312.5
10	311.3	309.9	305.8	309.5	310.1	304.1	306.9	309.0
20	299.2	296.9	298.5	303.5	303.3	294.5	298.3	297.1
30	290.4	287.6	290.7	296.1	295.7	287.0	290.9	289.7
40	280.8	278.9	283.3	288.3	287.3	278.2	282.9	281.3
50	272.1	271.8	274.5	280.1	280.1	269.3	273.9	273.9
60	264.9	265.4	268.2	272.9	272.1	261.9	266.9	266.1
70	258.7	260.0	260.9	265.9	265.6	255.7	259.8	259.6
80	252.5	253.4	255.0	259.9	259.9	249.7	254.2	253.4
90	248.7	249.3	249.5	253.3	253.1	244.2	247.4	247.6
100	243.8	245.3	244.4	247.0	247.8	239.4	242.6	242.6
110	239.6	241.6	240.3	243.4	243.5	234.6	238.1	237.5
120	235.4	237.6	235.9	237.9	238.6	230.6	233.7	233.4
130	234.1	233.6	232.2	234.6	235.2	227.3	229.9	229.9
140	230.4	229.6	228.9	231.3	231.8	223.9	226.5	226.5
150	227.9	224.2	225.6	226.8	227.2	220.6	224.7	222.9
160	224.6	226.9	223.3	223.9	223.8	217.9	220.9	220.2
170	222.1	221.5	220.0	221.3	221.5	215.7	218.7	217.9
180	220.4	219.4	218.3	219.0	219.2	213.5	216.4	215.6
190	217.9	217.5	216.7	215.7	216.9	211.3	213.5	213.3
200	215.9	216.2	214.5	213.6	214.7	209.5	211.9	211.4

Time, Seconds	System		Large Plate			Small Plate		
	Liquid Temp. °F	Vapor Temp. °F	Inside Temp. °F	Middle Temp. °F	Outer Temp. °F	Inside Temp. °F	Middle Temp. °F	Outer Temp. °F
210	215.4	214.9	213.4	212.8	212.9	207.9	209.7	209.8
220	214.2	213.5	211.2	211.2	211.3	20619	208.6	208.7
230	212.9	212.7	210.1	210.1	210.1	205.8	207.5	207.5
240	212.2	210.8	209.0	209.0	209.0	204.7	206.3	206.3
Run Number 10: 1/4 inch orifice								
0	327.0	328.0	313.5	313.7	313.3	307.0	309.0	309.0
10	309.4	309.8	305.8	308.1	309.9	298.8	303.5	302.9
20	300.8	296.9	299.1	302.7	303.1	289.6	295.1	294.6
30	293.5	287.7	291.5	295.1	295.5	281.3	287.6	286.9
40	287.1	278.7	283.5	287.5	287.6	272.3	278.9	278.5
50	279.9	272.1	275.8	279.5	279.9	265.2	272.4	270.6
60	273.7	265.8	268.8	272.2	273.1	258.8	265.1	264.1
70	268.0	260.5	262.5	265.8	266.6	252.3	258.5	257.3
80	263.6	255.2	257.0	259.2	259.8	246.9	253.0	251.6
90	258.0	249.9	251.1	253.6	254.1	241.9	247.6	245.9
100	252.4	244.6	246.1	248.1	249.6	237.7	242.4	241.7
110	249.1	242.3	243.1	243.7	243.9	233.4	238.0	237.1
120	240.9	237.5	238.3	239.5	239.7	231.0	235.2	234.6
130	236.0	235.7	234.3	235.5	236.3	227.6	231.5	230.9
140	229.3	231.7	231.7	232.2	232.8	224.8	229.3	228.0
150	228.2	229.0	228.2	228.4	228.3	222.3	225.9	225.3
160	224.9	226.4	225.6	225.1	226.0	220.1	223.8	223.0
170	222.7	224.3	222.9	222.9	223.5	217.3	220.5	220.1

APPENDIX 6 (Cont.)

Time, Seconds	System		Large Plate			Small Plate		
	Liquid Temp. °F	Vapor Temp. °F	Inside Temp. °F	Middle Temp. °F	Outer Temp. °F	Inside Temp. °F	Middle Temp. °F	Outer Temp. °F
180	220.4	221.6	220.1	220.7	220.3	215.2	218.3	217.8
190	219.3	218.9	218.3	217.3	218.1	213.0	216.1	215.5
200	218.2	217.1	216.8	216.2	215.8	211.3	213.9	213.7
210	215.9	215.8	214.6	213.9	214.2	208.8	211.7	210.9
220	214.9	214.5	213.5	212.9	212.4	207.7	210.6	209.9
230	213.9	213.7	211.7	210.7	211.2	205.9	209.6	208.0
240	212.6	213.2	210.2	209.6	210.1	204.5	207.4	206.4
250	211.9	211.8	209.8	208.4	208.9	203.4	206.3	205.3
260	211.5	210.5	208.0	207.3	207.8	202.3	205.2	204.2
Run Number 11: 1/4 inch orifice								
0	326.3	327.3	315.8	315.8	315.8	309.7	312.7	312.7
10	310.6	309.8	310.4	311.6	311.9	302.3	308.1	307.9
20	298.6	298.4	302.7	304.9	305.9	293.8	300.5	301.2
30	288.7	288.7	294.1	298.7	298.5	285.4	292.5	291.8
40	281.7	279.8	287.1	289.9	290.6	278.9	283.7	283.9
50	273.0	273.3	279.9	282.5	283.1	270.3	278.0	275.7
60	267.2	266.2	272.6	275.3	276.4	263.0	269.4	269.8
70	261.0	260.5	266.3	268.4	269.7	255.5	262.4	261.9
80	254.9	255.2	260.2	263.0	263.4	250.0	256.7	255.9
90	249.9	251.3	254.7	256.9	257.8	244.6	251.0	250.1
100	246.2	246.0	250.2	250.9	252.2	240.6	245.8	245.4
110	241.6	242.9	245.8	246.5	247.7	235.7	241.1	240.3
120	238.4	238.5	240.9	242.4	242.9	233.1	236.6	237.5
130	235.5	235.9	237.2	239.1	239.6	228.7	233.2	232.8

Time, Seconds	System		Large Plate			Small Plate		
	Liquid Temp. °F	Vapor Temp. °F	Inside Temp. °F	Middle Temp. °F	Outer Temp. °F	Inside Temp. °F	Middle Temp. °F	Outer Temp. °F
140	231.7	232.5	233.9	235.8	235.8	225.5	229.7	229.2
150	229.3	229.3	230.5	232.5	232.4	223.3	227.5	226.9
160	226.8	226.7	228.3	229.2	229.5	220.1	224.5	223.3
170	224.3	224.1	224.9	225.9	226.8	216.8	221.8	219.8
180	223.4	221.5	223.2	223.1	224.6	215.7	219.5	218.6
190	220.6	220.1	221.6	221.5	222.4	213.6	217.2	216.3
200	218.2	218.0	219.4	219.3	220.1	211.4	214.9	213.9
210	216.9	216.2	217.2	217.1	217.9	209.3	212.7	211.6
220	214.9	214.9	214.9	216.0	215.6	208.2	210.8	210.4
230	214.5	213.6	214.3	213.8	214.5	207.1	209.3	209.2
240	213.2	212.3	212.7	212.7	213.4	206.0	208.1	208.0
250	212.5	211.5	211.6	211.6	212.3	204.9	206.9	206.8
260	212.0	210.2	210.5	210.5	210.5	203.8	205.8	205.7
Run Number 12: 1/4 inch orifice								
0	325.7	327.5	310.8	311.2	310.5	300.0	300.3	300.3
10	298.4	309.5	304.2	308.9	307.1	302.4	293.8	294.7
20	289.4	296.8	297.9	302.4	300.7	283.8	287.5	289.0
30	279.6	286.6	289.1	293.7	293.9	275.8	279.9	281.4
40	272.8	277.5	282.8	287.2	]86.3	]68.5	272.8	272.4
50	267.5	270.9	275.1	277.9	278.4	261.9	266.2	265.9
60	259.5	263.4	267.7	277.7	270.5	254.5	258.5	259.1
70	253.8	258.2	261.1	265.4	264.5	248.2	253.1	252.6
80	248.1	252.9	255.6	258.2	258.4	243.9	247.7	247.4
90	243.7	247.7	250.1	251.9	252.7	238.9	242.9	242.5
100	238.2	243.9	245.7	247.5	247.1	234.7	238.2	236.8

APPENDIX 6 (Cont.)

Time, Seconds	System		Large Plate			Small Plate		
	Liquid Temp. °F	Vapor Temp. °F	Inside Temp. °F	Middle Temp. °F	Outer Temp. °F	Inside Temp. °F	Middle Temp. °F	Outer Temp. °F
110	235.9	240.2	240.5	243.3	242.9	229.0	231.7	231.8
120	233.7	235.8	237.2	238.9	238.8	225.2	227.7	227.8
130	229.1	231.0	232.8	234.5	234.9	222.0	225.1	224.4
140	226.9	229.7	229.5	231.1	231.6	218.8	221.9	222.1
150	224.6	227.1	226.6	227.8	229.3	216.7	218.6	218.7
160	223.5	223.2	221.8	224.5	224.8	213.6	215.8	215.3
170	222.3	221.9	221.8	222.2	222.5	211.4	213.2	214.9
180	220.0	219.3	219.6	219.9	220.3	209.3	210.9	210.8
190	217.8	216.7	217.4	216.7	217.9	207.2	209.2	208.5
200	215.5	215.4	215.2	214.4	215.7	206.1	207.7	207.4
210	214.4	214.0	212.9	213.3	213.5	204.0	205.5	205.1
220	212.5	212.7	211.9	211.1	212.3	202.3	204.4	203.3
230	212.1	211.4	210.7	210.4	210.5	201.5	202.7	202.4
240	209.8	210.1	209.6	208.8	208.9	200.2	201.2	201.7
250	209.1	208.8	207.9	207.7	207.8	199.4	200.1	200.6
260	208.7	208.0	206.9	205.9	206.7	198.1	199.2	199.5
270	208.7	207.5	206.3	205.5	206.0	197.7	199.0	198.3